Abstract

Numerous forest fires occurred during the summer of 2004 in the Klondike Goldfields region of the Yukon Territory, an area of extensive discontinuous permafrost. More than 35 shallow detachment failure landslides developed in subsequent weeks in Steele Creek, a small drainage basin located about 60 km south of Dawson City.

Preliminary observations of the failures and near-surface thermal regime were made through freeze-up of 2004 and continued in the summers of 2005 and 2006. Detachment failures were mapped and individual sites were surveyed. Air and ground temperatures were measured in burned and unburned areas. In addition, two-dimensional DC resistivity transects were used to examine subsurface conditions in the area.

Forest fire contributed to detachment failure activity on permafrost slopes by destroying the surface organic mat, causing burned surface temperatures to rise, thawing active layers by up to 20 cm (+31%) deeper than unburned slopes and weakening the surface root structures. Deeper thaw melted transient layer ground ice, raising soil porewater pressures. The thermal differences between burned and unburned sites were greater at the north-facing than south-facing sites, and active layer freezing and thawing processes varied according to both aspect and burned status. More southerly-facing and/ or burned sites generally thawed earlier, refroze later and had warmer temperatures than more northerly and/or unburned sites. Thaw of burned areas with high ground surface temperatures can be expected to continue, depending on climatic conditions, until sufficient revegetation occurs to shade the surface and rebuild the insulating organic mat.

The detachment failures occurred from a few weeks to two years after forest fire, and only on slopes where permafrost was extensive. They were not similar to others in the literature in that almost all occurred in coarse-gained soils and had failure planes elevated above the permafrost table. These landslides were flow-type failures that rafted portions of the organic mat on top of deforming, non-cohesive sediment. They occurred in areas of deeper thaw but their distribution and the resistivity data suggest that they were associated with supra-permafrost taliks which concentrated groundwater flow.

In an unglaciated area like the Klondike region this landsliding process has likely occurred thousands of times during the Pleistocene and may be responsible for elements of the form of the region's slopes. Predicted increases in the frequency and magnitude of forest fire in the boreal forest due to warming climates may increase incidence of these types of failures.

Acknowledgments

The author acknowledges financial support from the National Science and Engineering Research Council through its Northern Internship Program and Discovery Grant (to A. Lewkowicz), the Yukon Geological Survey, Northern Scientific Training Program (Indian and Northern Affairs Canada) and the University of Ottawa (To A. Lewkowicz).

Material support and assistance with fieldwork was provided by Klondike Star, the Indian River Farm, EBA Engineering Consultants Ltd., Cam Arkinstal, Yukon Client Services and Inspections Mining Inspectors (Mark Novosad, Jim Leary, Al Rothwell), Gimlex Mining (Tara and Jim Christie), Aurora Geosciences (Mike Schultz), Geoff Hodgeson, Yukon Geological Survey (Panya Lipovsky, Bill LeBarge, Jeff Bond) and Don, Vibeke and Aren Coates. The resistivity imaging was conducted by Dr Bernd Etzelmüller of the University of Oslo, with assistance from Phil Bonaventure and Emily Schultz.

This project would not have occurred without guidance, assistance and inspiration of my supervisor, Dr. Antoni Lewkowicz. I would also like to thank Dr. Luke Copland and Dr. Peter johnson, the members of the thesis jury. I am extremely grateful for the tireless assistance of Martina Knopp, who helped with all field aspects of the study and provided unwavering support and assistance throughout the duration of this project.

Chapter 1: Overview and Objectives

Introduction

This thesis is an examination of landslides that occurred following a fire in northern boreal forest underlain by discontinuous permafrost. The study area includes the Steele and Bishop Creek drainages near Dawson City in the western-central plateau of the Yukon Territory (Figure 1.1). Fieldwork was conducted to characterize the landslides of Steele Creek as well as to quantify physical and thermal disturbance to permafrost affected by the 2004 forest fire in the Indian River Valley.

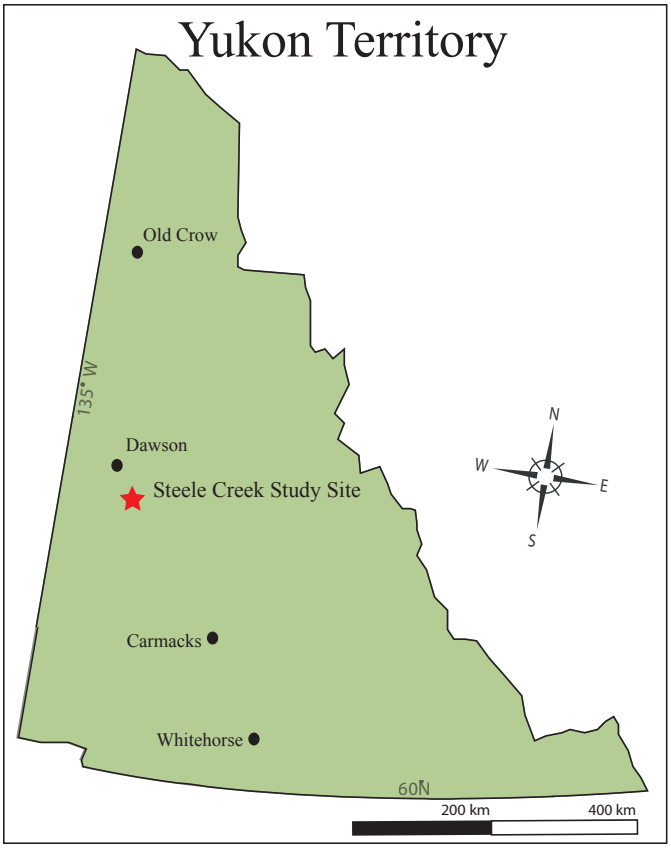

Figure 1.1 Map of Yukon Territory with Steele Creek study area starred.

Context of this Project

The Steele Creek valley is located at the southern edge of the Klondike Goldfields, a placer mining area that has been home to dozens of small mines since the 1898 Klondike Gold Rush. Placer mining involves the separation through gravity of gold from riverbed gravels. This requires creek water to be used in sluice boxes, and then discharged into settling ponds along with suspended sediment and tailings before being reintroduced to the watercourse. This effluent is strictly monitored by regulatory agencies to ensure that the water turbidity does not exceed limits harmful to aquatic wildlife (Yukon Client Services and Inspections, 2006; Yukon Watersheds Strategy, 2006). When landslides such as those seen in Steele Creek dump debris into creeks, suspended sediment concentrations may be elevated, causing water quality problems for miners and regulatory agencies, as well as affecting aquatic ecosystems. The large number of detachment failures along Steele Creek was first noticed on August 22, 2004 by Jim Leary of Yukon Client Services and Inspections (Mining Inspectors). He expressed concern about possible riparian impacts, and suggested study of the slides (Leary personal communication September 20, 2004).

Active layer detachment slides are a geotechnical challenge to infrastructure development in areas of permafrost, as they can be triggered by any surface thermal disturbance (e.g. Morgenstern & Nixon, 1971; Smith, 1975; Viereck, 1982; Williams & Burn, 1996; Hanna et al., 1998; Yoshikawa et al., 2003). Road and pipeline developments in periglacial environments may be susceptible to these mass movements, particularly when adjacent areas are affected by forest fire (Huscroft et al., 2004a; Hana et al., 1998). Due to the cyclical nature and short recurrence inter-

val of forest fire (50-200 years), most developments in the boreal forest may expect to be impacted by fire at some point during the lifespan of infrastructure (Dyke, 2004). Understanding the process of permafrost-related detachment sliding and identifying those slopes prone to catastrophic mass movement is an important design consideration in northern engineering projects (Heginbottom & Radburn, 1992; Heginbottom et al., 1995).

The evolution of slopes in the unglaciated regions of the central Yukon Territory has produced a landscape of steep, v-shaped valleys terminating in small, underfit creeks (Lipovsky et al., 2006; Smith et. al., 2004). Slopes are blanketed in bedrock-derived colluvium, while valley bottoms are filled with silty "muck" deposits. This region is home to rich deposits of placer gold (Fraser & Burn, 1997; Lowey, 2004; LeBarge & Coates, 2005). The mechanism by which mineral-bearing bedrock weathers into colluvium that subsequently is eroded and transported downslope and concentrated in creek bottoms has not been extensively studied (Bond & Sanborn, 2006).

As detachment failures in the study area appear to be largely related to forest fire (McRoberts & Morgenstern, 1974a, 1974b; Lewkowicz and Harris, 2005a, 2005b), changes in vegetation cover or fire recurrence interval could have had a profound impact on the rate of slope evolution. Climatic conditions determine permafrost characteristics (Shur & Jorgensen, 2007) and frequency of fire (McCoy & Burn, 2005). Climate change in the past may have impacted the rate of slope evolution through these factors, and detachment failures may be responsible, at least in part, for the current morphology of the region's slopes. Future climate changes may affect the rate and

extent of forest fire (McCoy & Burn, 2005) and subsequent detachment failure activity (Lewkowicz & Harris 2005a).

Summary of Research Questions

Preliminary observations at the research sites coupled with a literature review revealed several questions related to the detachment failures which occurred after the 2004 fires.

1. Are these failures similar to others described in the literature?
2. What factors lead to post-fire slope instability?
3. What is the relationship between the failure plane and the permafrost table?
4. What are the thermal differences between burned and unburned permafrost terrain with differing aspects?

Organization of the Thesis

Chapter 1 contains the introduction, context of the project and summary of research questions. Chapter 2 reviews the literature on forest fire impacts on permafrost and slope stability in permafrost areas. Chapter 3 presents the study area and Chapter 4 describes the methodology used. The results section, which constitutes the body of the thesis, is divided into three parts. Chapter 5 examines detachment failures in the Steele Creek valley, their distribution and morphology, and includes limited geotechnical analyses. This section also examines the geomorphologic significance of the slides and their causal factors. Chapter 6 deals with the thermal impacts of forest

fire on permafrost in the Steele and Bishop Creek valleys. This includes results from air and ground temperature monitoring stations, as well as qualitative observations on the permafrost in the area. Chapter 7 presents the results and interpretation of a resistivity geophysics study of the Steele Creek Valley conducted in collaboration with Dr. Bernd Etzelmüller of the University of Oslo. Chapter 8 is a conclusion which synthesizes the results relating to the geomorphologic response of the Steele Creek valley to forest fire.

References are presented in Chapter 9. Morphological details of all the Steele Creek failures are found in Appendix A, and geotechnical information is found in Appendix B.

Chapter 2: Literature Review - Forest Fire, Permafrost and Slope Stability

The complex interaction between forests, climate and permafrost is one of the defining features of the taiga, the great boreal forest that rings the northern hemisphere (Geertsema, 2005). The thermal buffer of the forest and the underlying organic layer maintains the permafrost in areas where it is out of climatic equilibrium. The climate controls the presence, and in some cases persistence, of permafrost as a thermal feature (Shur & Jorgensen, 2007), as well as the occurrence of fire (Yoshikawa et al., 2003; McCoy & Burn, 2005). The disturbance to permafrost brought on by forest fire is thought to be responsible for various forms of short and long-term slope instability (McRoberts & Morgenstern 1974a, 1974b; Lewkowicz & Harris 2005a, 2005b). These impacts can be due to hydrological, biological or geotechnical changes to slopes wrought by the fire. Climate change is expected to increase the frequency of forest fire (McCoy & Burn, 2005), which along with permafrost thaw caused by warmer temperatures, may result in increased rates of slope failure (Lyle, 2005; Huscroft et al., 2004b; Lipovsky et al., 2006). The literature review in this chapter examines the potential responses of permafrost to forest fire, and describes previous research on active layer detachments and other landslides in the Yukon.

Permafrost

Permafrost is ground material that remains in a cryotic state (at or below 0ºC) for more than two consecutive years (ACGR, 1988). It is present in regions where the air temperatures are cold enough that soil which freezes during the winter does not thaw completely in subsequent summers (Henry & Smith, 2001). This layer of frozen ground can range in thickness from a few meters at its southern limit to hundreds of meters thick in the Canadian High Arctic (Heginbottom et al., 1995). The active layer experiences seasonal thawing and freezing and is the region in which most hydrological processes take place (Carlson, 1952). Permafrost in the northern hemisphere rings the Arctic Ocean due to reduced insolation, and is also present in high mountain chains at mid-latitudes due to adiabatic cooling. Mean annual air temperatures vary from very close to 0ºC near the southern limits of permafrost to -8ºC near the northern tree line (Smith & Riseborough, 2002). Canada has approximately 40% of its land mass underlain by permafrost (See Figure 2.1) (French, 1996).

Figure 2.1: Canada Permafrost Distribution (From Geological Survey of Canada 2007).

Permafrost distribution in the discontinuous permafrost zone (<50% permafrost by area) is dictated by the thermal relationship between the ground and the atmosphere (Smith & Riseborough, 2002). These may be separated into surface offset effects, including vegetation shading and snow cover, and thermal offset effects, including soil type, thermal properties and the thickness of the organic mat (Smith, 1975; Williams & Burn, 1996 Viereck, 1982; Haugen et al., 1982; Yoshikawa et al., 2003).

Forest Fire

Forest fires typically burn locations in the boreal forest every 50-300 years (Yarie, 1981; Dyrness et al., 1986; Yoshikawa et al., 2003). The severity of the fire determines the degree of damage to the trees and the organic mat. This modification of the ground surface conditions leads to changes in the thermal regime, and often to a deepening of the active layer and thaw of near-surface permafrost (Burn, 1998; Harry & MacInnes, 1988; Mackay 1995, 1977; Racine et al., 1983; Savigny et al., 1995 and others). Permafrost areas that are affected by a thermal disturbance such as forest fire react to varying degrees. Some locations will experience extensive thaw and subsidence while others will not be affected at all (Viereck, 1982; Swanson, 1996; Yoshikawa et al., 2003). Generalizations regarding responses are therefore difficult to make, as the effects are site- and time-specific (Mackay, 1995). Permafrost varies from climate-driven in the continuous permafrost zone to climate-driven, ecosystem-protected in the discontinuous zone to ecosystem-protected at the edge of the sporadic zone (Shur & Jorgensen, 2007). These classifications refer to the varying effects of climate and ecosystem in creating the conditions for permafrost to form, and on maintaining an environment in which it can persist. The response of permafrost once the ecosystem has been altered by fire is determined by the role of the ecosystem in protecting that permafrost.

Destruction of the Organic Layer

Fire history is an important control on the thickness of the organic layer in the boreal forest (Yoshikawa et al., 2003). A fast-moving fire can skip over and miss patches of the organic layer while low-intensity fires may not entirely destroy the organic layer, and saturated areas may not burn at all (Swanson, 1996). However, if the fire is intense and the organic layer is desiccated, it may be completely destroyed, exposing mineral soil (Rouse, 1976). During a forest fire, surface temperatures may increase rapidly up to 800ºC with no significant rise in temperature at depths as shallow as 15 cm. The heat from the fire itself does not directly transfer to deeper soil layers (Yoshikawa et al., 2003).

Permafrost thaw and active layer deepening is mainly dependent upon the degree of organic mat destruction. Greater destruction leads to an increase in heat flux into the ground. In some sites where the organic mat has been slightly burned, the thermal impact on underlying soil is minimal, despite a lower albedo due to surface charring. A threshold thickness of around 10 cm of organic materials remaining after fire was found to be necessary to reduce the thermal impact on permafrost in central Alaska (Yoshikawa et al., 2003).

Thermal Conductivity of Soil and Organic Layer

Changes in the thermal conductivity of soils and vegetation after fire affect heat fluxes between the permafrost and the atmosphere. The thermal conductivity of intact moss is extremely low (about the same as air) and is the reason for the high insulating capacity of the organic mat (Yoshikawa et al., 2003). Mineral soils are much more conductive than the organic mat even when dry, but the thermal conductivities of both increase sharply with water content. Post-fire increases in soil moisture content and hence the soil thermal conductivity make this an important factor in affecting post-fire heat transfer within the ground and result in active layer deepening due to thaw of permafrost (Yoshikawa et al., 2003).

Soil Moisture

During the actual fire, moisture contents decrease, but increase almost immediately afterwards (Yoshikawa et al., 2003). Evapotranspiration is reduced due to the death of most of the vegetation (Klock & Helvey, 1976; Yoshikawa et al., 2003). As the moisture that would have been transpired is retained in the soil, the high soil moisture can be maintained for two to ten years before it transitions into a drier state than adjacent unburned areas (Liang et al., 1991; Klock & Helvey, 1976; Yoshikawa et al., 2003). This is due to a deepening permafrost table (lowering of the aquiclude) and the regrowth of transpiring vegetation (Yoshikawa et al., 2003). If permafrost does thaw deeply in areas which were wet prior to fire, the loss of the frozen aquiclude provided by the permafrost table will enable soils above the water table to dry out (Swanson 1996).

Positive porewater pressures were recorded just above the thaw plane by Lewkowicz and Harris (2005a) at recent fire sites in the Mackenzie Valley. These positive pore pressures develop as a result of water being released by thawing ice-rich permafrost faster than it can drain away through the overlying unfrozen soil (Morgenstern & Nixon, 1971; McRoberts & Morgenstern, 1974a).

Radiation Budget

Fire causes surface albedo to fall by up to 50% and net radiation to increase by 10% due to surface darkening (Rouse, 1976; Rouse & Mills, 1977; Yoshikawa et al., 2003). The ground heat flux/net radiation ratio increases as more short wave radiation is absorbed by the darker surface, and more long wave radiation is emitted by the warmer soil. Increased sensible heat and ground heat fluxes are balanced by a decreased latent heat flux. An overall reduction of net radiation is accompanied by warmer ground temperatures and wetter soils (Yoshikawa et al., 2003). High soil temperatures may also be enhanced by dry surface soil conditions and low evaporation rates (Rouse, 1976). The net effect of these processes is to conduct more heat downwards into the ground.

Burned/Unburned Temperature Differences

Ground temperatures have been shown to rise in burned forest compared to adjacent unburned forest (Rouse, 1976; Burn, 1993; Yoshikawa, 1998; Hanna et al., 1998). The combined effects of a loss of shading by the tree canopy, loss of insulation from the organic mat, higher thermal con-

ductivity of moister soils, and decreased albedo, allow for more summer heat flow into soils and consequent warming throughout the soil profile, the impact of which will be attenuated with depth (Yoshikawa et al., 2003). In the short term, Rouse (1976) found that burned areas in Alaska had stronger diurnal temperature fluctuations than unburned areas. Soil temperatures were found to be higher in burned areas during the summer growing season only. In the winter there was no difference found between burned and unburned areas in central Alaska and the southern Yukon (Rouse, 1976, Burn, 1998). As revegetation takes place over burned areas, temperatures generally drop (Hanna et al., 1998).

Thaw Depth Differences

Seasonal thaw depths (active layer thickness) generally increase in the years following forest fire (Yoshikawa et al., 2003). Thaw depth increases are locally controlled and there may be regions where none occurs, such as in Inuvik, NWT (Mackay, 1995) and central Alaska (Lopspiech et al., 1973). In some cases in central Alaska there has been a decrease in active layer depth (Kryuchkov, 1968; Yoshikawa et al., 2003).

Active layer depth discrepancies between burned and unburned terrain may last for only two years in central Alaska (Johnson & Viereck, 1983), or for as long as forty years in the southern Yukon (Burn, 1998).

Thie (1974) found that natural fire had no long-term effects on permafrost thaw in northern Manitoba. Yoshikawa et al. (2003) found that soil temperatures can be warmer for many decades in burned areas in central Alaska. These variations could be due to differing terrain and the characteristics specific to each location, depending on where the permafrost is on the continuum from climate-driven to ecosystem-protected (see Shur & Jorgensen, 2007).

The aspect of a burned slope can affect the degree of disturbance due to fire. Thicker vegetation and organic material on north-facing slopes provide a greater degree of thermal insulation than the relatively thin organic layer on south facing-slopes. Therefore there will be a greater degree of thermal disturbance once they have been burned (Swanson, 1996; Lewkowicz & Harris, 2005b).

Revegetation and Permafrost Recovery

Vegetation recovery after forest fire and the regeneration of the organic mat has a major influence on the stabilization of the permafrost table. The warm ground surface and moisture availability of burned soils promote plant growth and forest succession. Growth is rapid in the first several years, but decreases with increased competition for moisture and shading of the ground surface (Johnson & Viereck, 1983). The complete recovery of the ecosystem to pre-burn condition can take up to 50 years in interior Alaska (Swanson, 1996).

As the permafrost table gradually rebounds upwards, seasonally frozen ice lenses are incorporated into the permafrost (Shur & Jorgensen, 2007). This ice is the result of downwards water

movement due to the thermal gradient into the permafrost and to gravity. Eventually the surface energy balance, vegetation and active layer thickness will all return to that of their pre-fire conditions, assuming climatic conditions have remained the same (Viereck, 1973; Rouse, 1976; Mackay, 1995; Burn, 1998). If revegetation is slow, the climate is warming, or the permafrost is ecosystem-protected and mean annual air temperatures are very close to 0ºC, lowering of the permafrost table may continue indefinitely (Burn, 1998; Shur & Jorgensen, 2007).

The temperature of the permafrost, the temperature of air and nature of the insulation between the two determine whether the permafrost table will continue to lower, will stabilize at a certain depth, or will begin to reverse direction and aggrade upwards. Mackay (1977, 1995) found that the permafrost table stabilized 5-20 years after fire in cold permafrost near Inuvik, whereas Burn (1998) found a descending permafrost table 40 years after fire near Whitehorse, Yukon. In interior Alaska, 25-50 years was estimated to be required for stabilization (Viereck, 1982; Van Cleve & Viereck, 1983). Recent climatic warming trends have been hypothesized to affect short-term permafrost recovery and stabilization (Yoshikawa et al., 2003; Shur & Jorgensen, 2007).

Permafrost Slope Instability

Slope instability (landsliding) in periglacial regions often occurs after a disturbance to the regional thermal equilibrium that maintains the permafrost (Yoshikawa et al., 2003; Shur & Jorgensen, 2007). This occurs through human engineering activities (Niu et al., 2005), forest fire (McRoberts & Morgenstern, 1974a, 1974b; Lewkowicz & Harris, 2005a, 2005b), or hydraulic erosion (McRoberts & Morgenstern, 1974b). Summers with unusually warm or wet weather

have also been found to induce thaw and trigger failure activity in high Arctic locations (Lewkowicz & Harris 2005a; Lewkowicz, 2007).

Slope instability in permafrost regions falls into two broad categories depending on the location of the failure plane. Back-rotational slumps and other deep-seated failures move over an arcuate shear plane that runs through the permafrost (McRoberts & Morgenstern, 1974). Active layer detachment failures (Lewkowicz & Harris 2005a, 2005b), skin flows (McRoberts & Morgenstern, 1974b) and debris flows (Lewkowicz & Hartshorn, 1998) involve movement in the active layer and do not intrude into the permafrost. The disturbance to the thermal regime by deep or shallow mass movements may initiate thaw of deeper permafrost and trigger further movements such as retrogressive thaw slumps (Burn, 2000). In this thesis, only shallow active layer failures are examined.

Shallow, slide dominated features have been called active layer detachment slides by Lewkowicz (1990) and active layer glides (Mackay & Matthews, 1973). Flow features have been called skinflows by McRoberts & Morgenstern (1974a). Detachment sliding in response to forest fire is shallow and each individual slide does not transport much material. However, if there has been a large fire over susceptible terrain, great numbers of these slides may appear causing widespread landscape modification. If the recurrence interval is governed by fire, this process can occur suddenly following every fire over a large portion of the landscape (Lewkowicz, 1988).

Permafrost Hydrology

As porewater pressure has a significant impact on slope stability, the flow of water above and through permafrost on an annual basis is important in determining the timing of landslides and the zones of potential shear weakness.

Completely dry frozen soil has much the same geotechnical properties as unfrozen soil. The presence of ice in a soil alters many of its most fundamental geotechnical and engineering properties. The transition between thawed and frozen states can occur due to a very small temperature change, but radically alters the soil properties, turning a massive, competent mineral into a viscous fluid (Morgenstern & Nixon, 1971). However, the phase change of water from solid to liquid can occur over a significant temperature range depending on factors such as salinity and pressure which depress the freezing point (French, 1996). An understanding of the movement of groundwater is important in the identification of areas of high porewater pressure and low shear strength.

The permafrost table forms an impermeable barrier to most water entering the ground from the surface, limiting its vertical travel to the depth of the active layer. There are several consequences of this process, of which the impacts on storage capacity and slope runoff are of particular interest, as the seasonally changing nature of the permafrost "aquiclude" produces unique conditions not found in non-permafrost regions (Woo & Steer, 1983). When active layer storage is exceeded, water is forced onto the surface with the rising water table and becomes visible as surface flow.

The transient layer is the region of soil just below the typical maximum depth of summer thaw. Thermal gradients and gravity draw water into the top of permafrost, where it freezes as interstitial or segregated ice (Mackay, 1983). This creates a thin, ice-rich zone that, in the absence of environmental change, thaws very infrequently. The transient layer's ice-rich nature serves as an important buffer for the permafrost from seasonal heat pulses through the latent heat of thawing, stabilizing deeper thermal regimes (Shur et al., 2005).

If water is released into the active layer from thawing permafrost or precipitation faster than it can drain away, it can lead to high porewater pressures within the soil. Rainstorms dumping large amounts of water in a short time may also overload the shallow active layer's low groundwater storage capacity, rapidly elevating porewater pressures (Woo & Steer, 1983). High porewater pressures can create artesian conditions on hill slopes, where the water re-emerges at the foot of the slope as a pressurized spring. Elevated porewater pressures decrease the soil shear strengths, causing slope instability (Morgenstern & Nixon, 1971).

Porewater exists in the voids between soil particles. As the ratio of water to soil increases, contact between soil particles decreases, reducing the bearing capacity and shear strength of the soil to the point where the soil particles cannot carry the load of the overlying soil. In this case the water must escape or bear some of the load. If the water has to carry part of the load the entire mass begins to act in a fluid manner (McRoberts & Morgenstern, 1974b).

Subsurface flow through the active layer is slow and fed by supra-permafrost groundwater. As the active layer deepens, flow patterns change due to the unevenness of the top of permafrost and produce emergence and subsidence zones of surface flow (Woo & Steer, 1983). Groundwater ponds may form which eventually breach their frozen sills and move downslope as groundwater pulses (Woo & Steer, 1983).

Active Layer Detachment Failures

Active layer detachment failures occur when all or a portion of the active layer separates from the permafrost beneath and moves as a semi-competent mass downhill over the lubricated slip surface of the thaw plane. Failures may involve flow or slide mechanisms, but are similar in that they occur within the active layer or the transient layer and are triggered by high porewater pressures over frozen ground. The depth of the initial failure plane is limited by the position of the permafrost table (Leibman, 1995; Harris & Lewkowicz, 2000). The potential shear plane changes location within the soil profile as the thaw plane progresses downwards throughout the summer. Subsequent movements may strip off newly thawed material that was previously part of permafrost (Lewkowicz, 2007).

Detachment failure types are named according to their mechanism of movement, which varies along a continuum from slide-type movement to flow-type movement (Table 2.1). All of the features named in Table 2.1 have the same basic morphology, differing in their relative proportions

of slide and flow movement. An attempt has been made to group the terms based on descriptions in the original papers.

Table 2.1: Shallow Periglacial Mass Movements.

Dominant Process	Feature Name	Reference
Flow	Tundra Mudflow; Mudflow	Sigafoos & Hopkins (1952) Anderson et al., (1969); Carter & Galloway, (1981)
	Skin Flow	McRoberts & Morgenstern, (1974b); Stangl et al. (1982)
Slide	Active Layer Detachment Glide	Mackay & Matthews (1973)
	Cryogenic Landslide	Leibman 1995; Leibman & Ergov, 1996; Leibman et al., 1993; 2003
	Active Layer Detachment Slide	Harris & Lewkowicz, 2000; Lewkowicz & Harris 2005ab

Skin flows and tundra mudflows have a high proportion of viscous flow and differ from active layer detachment slides or glides, which involve the sliding of a competent mass of displaced material (Lewkowicz, 1988). Flow-type features tend to move in long, thin ribbon-like stripes over a slope (Harris, 1981). Extremely shallow in comparison to their length, they may coalesce into broad sheets of instability (McRoberts & Morgenstern, 1974b). This was also true of some slides on Ellesmere Island (Lewkowicz & Harris 2005a).

Detachment failures of all types can be triggered by rapid thawing of ice-rich sediments near the base of the active layer or within the top of permafrost, thaw being due to high late summer air temperatures, extreme temperature or precipitation events or forest fires (Hardy & Morrison, 1972; Hughes et al., 1973; Mackay & Matthews, 1973; McRoberts & Morgenstern, 1974; Cogley & McCann, 1976; Hodgson, 1977; Carter & Galloway, 1981; Stangl et al., 1982; Mattheson

& Mayer-Cole, 1984; Harris & Lewkowicz, 2000; Lewkowicz & Harris, 2005a, 2005b). They can develop on steep and low-angled slopes, and may also be initiated by river undercutting of a slope (McRoberts & Morgenstern, 1974b). In the case of those caused by forest fire, movement may occur on slopes with gradients of only a few degrees (Hughes et al., 1973) between several months and up to four years after fire (Huscroft et al., 2004b; Lipovsky et al., 2006).

Detachment slides tend to be long, thin, shallow translational movements, although bell-shaped and complex forms exist (Lewkowicz & Harris, 2005b). Compact forms are generally wider than they are long, and are found near the base of slopes terminating in streams, while elongate forms often begin high on a slope, and extend in long, thin ribbons downhill. They often have defined lateral berms thrown up by the bulldozing of the moving mass, as well as folded and convoluted debris piles, while compact forms show less lateral deformation and less deformation of the displaced mass due to limited movement (Lewkowicz & Harris, 2005a; Lewkowicz, 2007). Through examination of the internal structure of displaced masses and scar floors, Harris and Lewkowicz (1993a, 1993b) concluded that for all the failures they examined, the sliding occurred across a basal shear plane or zone a few centimeters thick.

Active layer failures may occur at any point on a slope but there are certain zones of strain and moisture concentration that may reduce shear strength. Leibman (1995) found most failures to be confined to concave portions of slopes and runoff hollows, which were the dampest portions of the slope. Stangl et al. (1982) suggested that most failures were initiated along the upper and middle portions of a slope, with moisture content and inclination being the most important con-

tributors to slope instability. Lewkowicz and Harris (2005a, 2005b) found that active layer detachments occurred frequently in silty clays and could only take place when effective shear stress was extremely low, such as in thin (low weight) detached masses and low angled slopes.

Harris et al. (2008) found that in laboratory scale simulations of detachment failures similar to those observed in Steele Creek, shear stresses only exceeded shearing resistance once thaw had reached depths over 0.6 m. Pore pressures were observed to rise rapidly in concert with upward seepage, causing soil liquefaction. This process was proposed as a physical model for thaw related debris flow failures in the central Yukon (ie. Lyle, 2005; Lipovsky et al, 2006).

Flow-type active layer detachments may occur when a significant portion of the active layer becomes fluidized as the result of high porewater pressures. Flow-type failures move rapidly and are often found on steep, wet slopes such as in the Mackenzie Valley (Hanna et al., 1998; Dyke, 2004; Lewkowicz & Harris, 2005a, 2005b). Slide-type active layer detachments may occur when a shear zone just above the permafrost table achieves excess porewater pressures. The overlying material, which is not saturated, then slides on the lubricated slip plane (Lewkowicz & Harris, 2005b). Slide-type failures are slow-moving and found on gentle, drier slopes, such as Ellesmere Island (Lewkowicz & Harris, 2005a, 2005b; Lewkowicz, 2007). A range of intermediate types encompassing forms and processes common to both may exist in the same locations.

Long-term effects of active layer failures include subsequent retrogressive thaw slumps, as well as higher rates of runoff in slide scars, which create elevated higher rates of erosion and maintain

bare scar floors (Kokelj & Lewkowicz, 1998). In a thaw slump scar in the central Yukon, Burn (2000) found that depth to the top of permafrost could be increased by as much as 10 meters as compared with undisturbed forest. Re-vegetation of the scar floor was required before temperatures stabilized and a significant organic layer combined with cold climatic conditions would be required before permafrost could re-aggrade.

Previous Active Layer Detachment Failure Studies in the Yukon

There have been few studies of active layer detachments in the Yukon. An overview of landslide activity, which included study of some active layer detachments along the western Yukon section of the Alaska Highway corridor, was conducted by Huscroft et al. (2004a, 2004b). Lyle (2005) studied a number of slides including a large back-rotational slide, a skin flow and a retrogressive thaw slump near Little Salmon Lake in the central Yukon. Lipovsky et al. (2006) studied active layer detachments in the Dawson City region after the 2004 forest fires. The author contributed to this Yukon Geological Survey bulletin with data from Steele Creek.

Chapter Summary

A common natural cause of permafrost thaw is forest fire. In the boreal forest, fire is often followed by widespread active layer detachment sliding. Forest fire, with a typical recurrence interval of 50-200 years, kills adult trees, destroys much of the insulating mossy organic layer and blackens the ground surface. This blackened surface lowers the albedo, leading to a greater absorption of solar energy into the soil. The heat is conducted down into the permafrost by an active layer with a dramatically raised thermal conductivity due to higher moisture contents. When the heat reaches the permafrost, it may thaw the ice-rich transient layer, which lies just below the seasonal average maximum depth of thaw. Water released by this process may destabilize slopes sufficiently to cause active layer detachment sliding.

Active layer detachments are flow or slide-type mass movements which are limited in depth to the thickness of the active layer. They often occur after forest fire in the boreal forest and during unusually warm or wet weather in tundra regions. Detachment failures can be significant at both a local and landscape scale. The potential for climate-change induced thaw of permafrost, larger and hotter forest fires, as well as increased northern development raise the possibility of greater active layer detachment failure activity in the future.

Chapter 3: Study Area

Indian River Valley Overview

Fieldwork was carried out between September 20, 2004 and September 16, 2006 in areas affected by the Haystack Mountain fire of July 2004. The study area encompasses the southern portion of the Klondike goldfields between the Indian and Stewart Rivers. The two main study sites were located in the Steele Creek Valley and the Indian River Valley. The valley of Steele Creek is located 55 km south-southeast of Dawson City at approximately 63°35'N and 138°59'W and spans elevations of 580-920 m asl (Figure 3.1). The main watercourse is approximately 8 km long and drains north from the Black Hills into Montana Creek, which is a tributary of the Indian River. Study locations along the Indian River Valley were located in the Bishop Creek Valley (63˚ 41'N and 139˚ 00'W, elevation 539 m a.s.l.). The Bishop Creek Valley is a small tributary valley that contains an ephemeral stream that drains into the Indian River just upstream of the Indian River Farm.

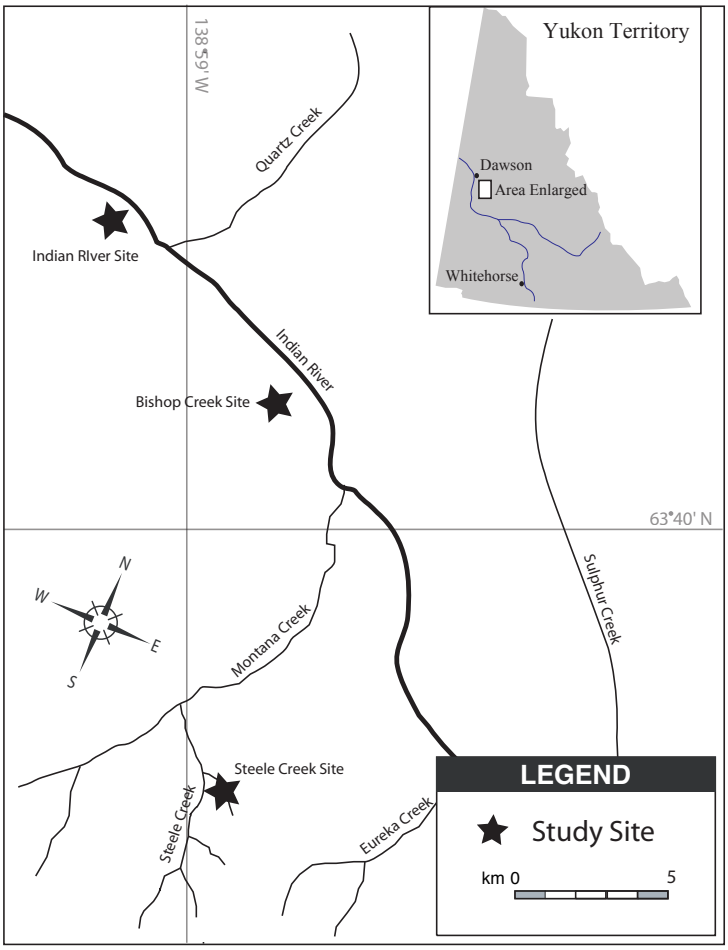

Figure 3.1 Study Area Map.

There are currently no placer mining operations on Steele Creek, but mineral prospecting and active claims exist. Evidence of historical placer works was found, and was likely associated with the abandoned and overgrown Dawson-to-Whitehorse winter stagecoach trail located along the length of the valley bottom. Extensive gravel road networks link the placer mining creeks of the Klondike and provided access to study areas.

Physiography

The area was not subject to glaciation during the Quaternary and is characterized by V-shaped valleys and rolling hills (Figure 3.2) with rounded summits (Bostock, 1948; Froese et al., 2000). Slopes are moderate, typically 10˚ to 30˚ and are blanketed with colluvium, terminating in small creeks. These creeks form a dendritic drainage network, eventually feeding into the larger tributaries such as the Indian and Klondike Rivers which discharge into the Yukon River. Bedrock outcrops are rare, although rocky tors are occasionally present along ridge tops. Valley bottoms are filled with glaciofluvial or alluvial gravels, the latter derived from local colluvium.

Figure 3.2: Unglaciated hills with dendritic drainage in Klondike Region north of Steele Creek.

Climate

The central Yukon plateau has a sub-arctic continental climate with an annual temperature range of up to 80ºC (Wahl et al., 1987). The Yukon Wildfire Management climatic data station at Henderson Dome near Steele Creek (Elevation 914 m.a.s.l.) recorded an annual average air temperature of -5.2°C and mean annual liquid precipitation total of 265 mm in 2004-2005 (Table

3.1). Prevailing winds at this site are from the west and blow with an average speed of 9 km/hr. Early summer temperatures were warmer and drier than normal in 2004, the year when the forest fire and majority of detachment failure activity took place (Figures 3.3 and 3.4)

Table 3.1: Henderson Dome (63°35'29.69 N, 138°56'56.24 W elev. 984 m) Climate Averages July 2004-2005 (Yukon Wildfire Management Monitoring Station) Dawson City Airport (64° 02'38.75 N, 139°07'29.65 W elev. 340 m) climatic averages 1970-2000 (Environment Canada, 2007).

	Henderson Dome	Dawson City Airport
Mean Annual Air Temp.	-5.2°C	-5.3°C
Max Temp	26°C	23°C
Min Temp	-38°C	-30.9°C
Annual Precipitation	265 mm	324 mm

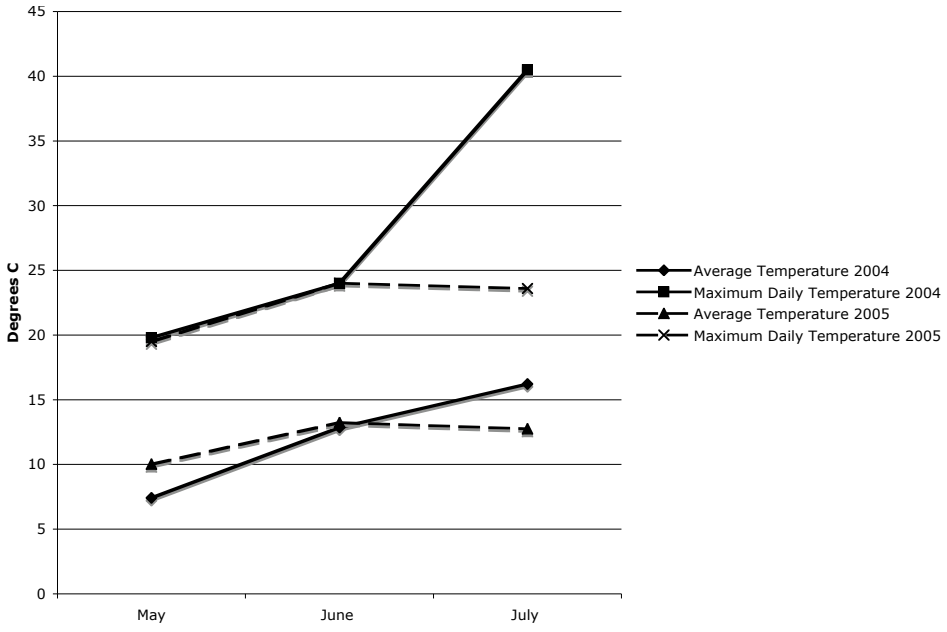

Figure 3.3: Henderson Dome Temperatures 2004-2005.

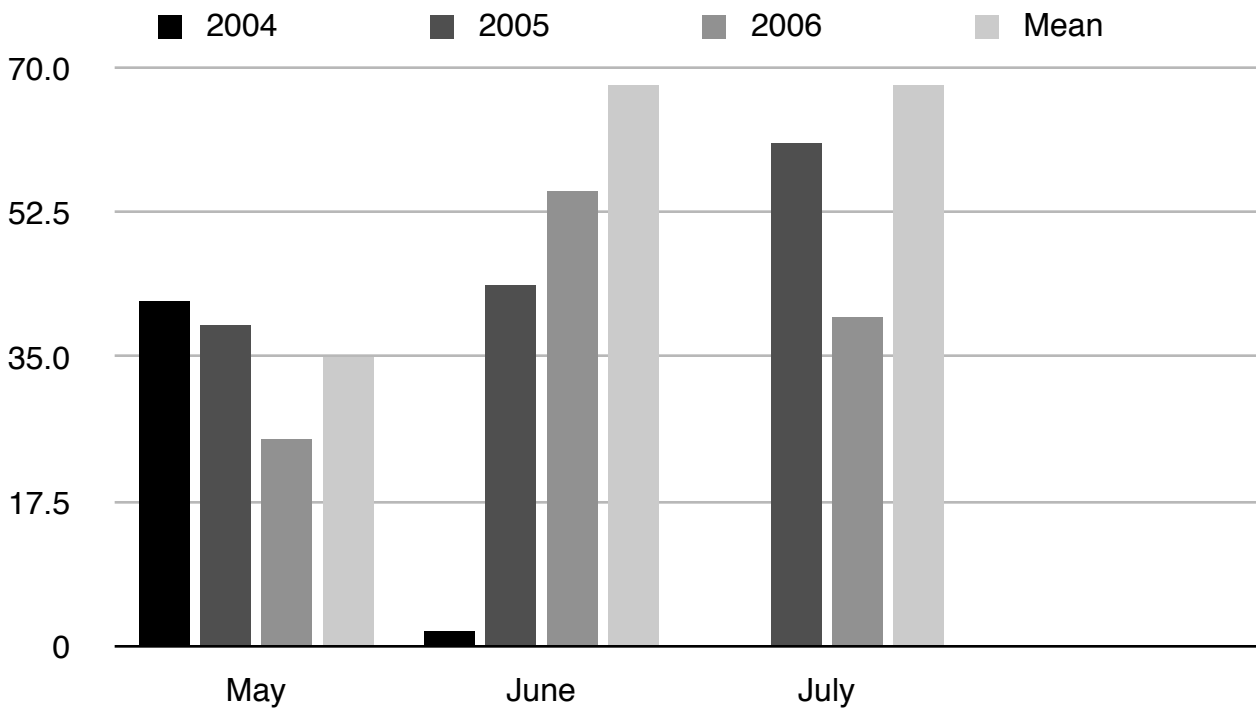

Figure 3.4: Henderson Dome Precipitation 2004-2005. Mean precipitation 1988-2005.

Permafrost Conditions

The study area is near the northern boundary of extensive discontinuous permafrost, as defined by Heginbottom et al. (1995) (Figure 3.5). Therefore, the majority of the terrain is expected to be underlain by permafrost of varying thicknesses. In the Klondike region, permafrost distribution is well understood due to extensive placer mining excavations (Yukon Ecoregions Working Group, 2004).

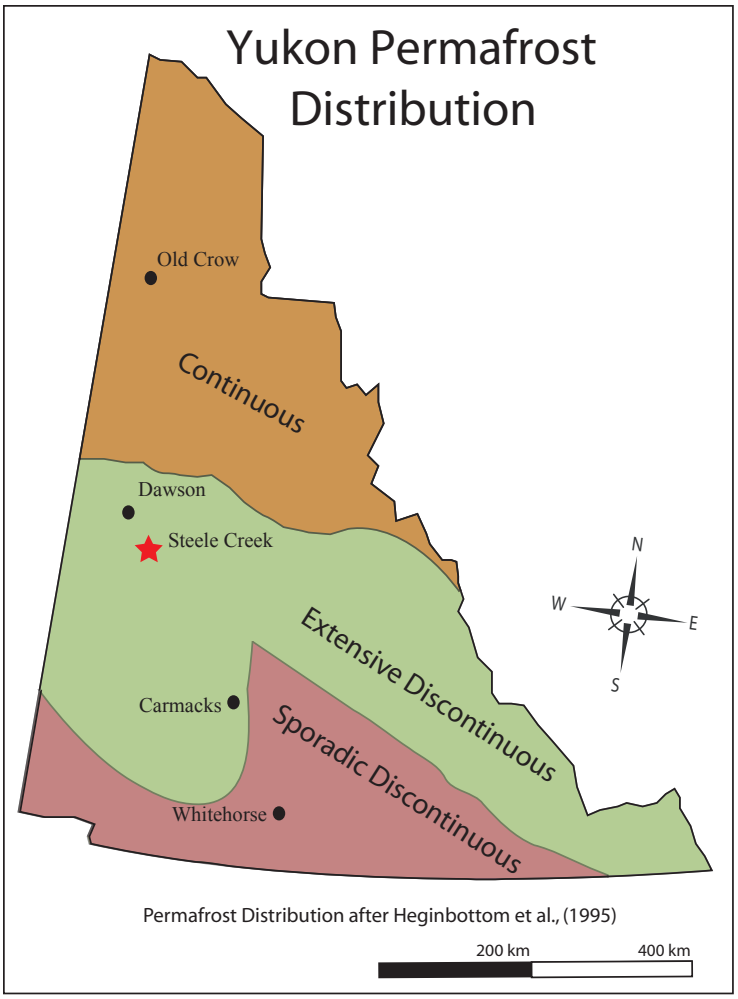

Figure 3.5: Yukon permafrost distribution. Star marks study site. (After Heginbottom et al., 1995)

North-facing slopes are generally forested with black or white spruce 3-5 m tall, with an understorey of shrubby Labrador tea. A mat of moss 30-60 cm deep covers the mineral soil. Under north-facing slopes, permafrost can be up to 60 m deep (Yukon Ecoregions Working Group, 2004). Active layers were observed to range from 20 to 150 cm in depth. Conversely, south-facing slopes are often permafrost-free, well-drained, and are covered with balsam poplar, willow, alder and birch forest (Yukon Ecoregions Working Group, 2004). They have an understorey of horsetail and alder, with scattered grasses and herbs growing on a thin (3-10 cm) organic layer

over the mineral soil. East-facing and west-facing slopes vary between the two extremes, depending on the subordinate aspect and vegetation. Slope gradient is also a factor, as steeper slopes experience a greater or lesser exposure to incident solar radiation. Therefore, steep south-facing slopes are less likely to have permafrost, while steep north-facing slopes are more likely to be perennially frozen (Naldrett, 1981).

Permafrost is not found beneath water bodies that are unfrozen year-round. This does not include the widespread swampy regions of muskeg, which freeze annually and owe their existence to the impermeable layer of permafrost beneath. Under smaller streams and rivers, an unfrozen talik may be present, depending on the size of the stream and temperature of the water. Permafrost is considered to have a warm thermal profile and to be sensitive to thermal disturbance (Naldrett, 1981).

Bedrock and Surficial Geology

Hillslopes are blanketed in colluvium derived from the underlying Nasina assemblage of graphitic quartzite and muscovite-quartz schist bedrock (Gordy & Makepeace, 2000). Colluvium was observed to be up to three meters deep in a road cut near the study area. In places, loess deposits and tephra bands were observed. Distinct units of weathered bedrock are gradually transported downslope as stacked layers of colluvium (Bond & Sanborn, 2006).

Forest Fire Activity

The Goldfields Complex of forest fires, which included the Indian River Fire (also known as the Haystack Mountain Fire), burned during the summer of 2004. MODIS satellite imagery recorded fires starting in the upper Steele Creek valley on July 1, which spread down its length to the confluence with Montana Creek by July 4 (Lipovsky et al., 2006). The 2004 Flat Creek Fire, which burned some 50 km to the east of the Indian River fire, destroyed forest which had been burned 50 years previously in 1953 (Figure 3.6).

Figure 3.6: Roadside sign near Flat Creek fire, Dawson City, Yukon.

When Steele Creek was visited in December 2004, brush piles in an old placer mining area were still actively burning, despite temperatures below -20°C and more than 20 cm of snow (Figure 3.7).

Figure 3.7: Smoldering brush piles. Steele Creek. December 2004.

Landslide Activity

Aerial photos taken by Jim Leary of the Yukon Department of Energy, Mines and Resources Client Services and Inspections Division on August 26th 2004 revealed a number of detachment failures on the slopes above Steele Creek some 53 days after the valley burned. The presence of burned trees buried in debris piles indicates that the failures occurred post-fire. Other fossil failures were found in the Steele Creek valley that pre-dated the 2004 fire.

Chapter 4: Methodology and Measurement Sites

Observations During 2004

Preliminary observations of active-layer detachments and ground thermal conditions were made during the fall of 2004 while the author was employed by the Yukon Geological Survey. The Steele Creek valley itself was visited only once in December 2004, which allowed for ground-level confirmation of the presence of detachment failures in December 2004 and observation of extensive groundwater icings.

From September to December of 2004 ground temperature monitoring work was conducted in the Indian River Valley. Forty-meter transects were laid out across the boundary between burned and unburned forest at six sites encompassing different aspects and terrain types. North-facing and hilltop sites were located on the south bank of the Indian River west of Quartz Creek, and east-facing, south-facing and valley bottom sites were located in Bishop Creek, some 20 km to the east (see Figure 3.1). Probing to the permafrost table was conducted at 1 m intervals along each transect, approximately every two weeks from mid-September to early December. Observations were also made of vegetation, degree of burn and snow depths at each site. Observations at the east-facing and valley bottom sites were repeated two years later in mid-September 2006.

Detachment Failure Aerial Photography and Mapping

All existing detachment failures in Steele Creek were photographed from the air on May 18, 2005. As this was immediately after snowmelt and thaw depths were less than 35 cm, this inventory represented failures that had occurred in the summer of 2004 in the months immediately following the fires.

The inventory revealed that 35 detachment failures had occurred in 2004 along a 3.7 km section of the main Steele Creek valley and on slopes within its tributaries. Five new failures developed by mid-August 2005 and two failures from 2004 reactivated. No more failures developed in the summer of 2006. Each of the failures was visited during 2005 and basic morphometric dimensions (length/width/depth/ aspect/scar length) were recorded, the failure was sketched and GPS coordinates were taken at the top of the headscarp. This point was marked with survey tape and photos were taken using the tape as a reference point for identifying further movement.

Detachment Failure Ground Mapping and Soil Sampling

Five representative detachment failures in Steele Creek from 2004 and 2005 were mapped in detail in the field using 50 m tape measures and an Abney hand level. At the time of mapping, probing to the permafrost table was conducted outside the failure perimeter and within the scar floor. Inspection pits were excavated in scar floors, tracks and displaced masses to examine soil stratigraphy. Soil samples were removed from each soil stratum for laboratory analyses. In the summer of 2006 the failure locations were checked on the ground at intervals of 2-3 weeks to

determine if there had been any additional activity. The last visit was during September 16-22, 2006.

Meteorological and Active Layer Observations

In May 2005, two-channel Onset Hobo Pro temperature loggers (accuracy ± 0.2°C) were placed on burned slopes within the Steele Creek valley that approximately faced the four cardinal directions (see below, Figure 4.2). These temperature loggers were used to measure 1.4 m screen height air temperatures (external thermistor) and surface ground temperatures (internal thermistor) at hourly intervals. The latter were placed approximately 2 cm beneath the surface to prevent direct irradiation. Two more loggers of the same type were installed on unburned north and south-facing slopes in mid-June. Four-channel Onset Hobo 8 temperature loggers were also installed at the same sites and their external thermistors (accuracy ± 0.5°C) were inserted in the ground at a variety of depths (Table 4.1). The thermistors at some sites were moved deeper into the ground during the summer in order to track the position of the permafrost table. Loggers were left in position at the end of summer 2005 and operated through to September 2006. Some gaps in the data exist due to battery or logger failure (Table 4.1). Logger coordinates are located in Appendix A.

Data was infilled into the ground temperature data gaps using the method of least squares to fit a straight line through the existing temperature data and predict the value of the missing data points at depth. In the case of the south-facing unburned site, air and surface temperatures were missing from May 29 to June 30, 2006. A different method was used, as ground temperatures at depth cannot be used to predict surface or air temperatures at the same site. These values were

filled in using a 4th order polynomial correlation between temperatures at the south-facing burned and unburned sites. Missing air and surface temperatures at the east-facing site were in-filled using the close correlation with those of the west-facing site.

Table 4.1: Thermal Monitoring Station Dates of Measurement and Data Gaps.

Site	Dates of Measurement						
	Air	**Surface**	**25 cm**	**50 cm**	**70 cm**	**100 cm**	**135 cm**
South-facing Burned	5/20/05 to 9/16/06	5/20/05 to 9/16/06	5/20/05 to 9/16/06	5/20/05 to 9/16/06	5/20/05 to 9/16/06	5/20/05 to 9/16/06	
South-facing Un-burned	6/12/05 to 5/27/06, 06/05/06 to 7/01/06	6/12/05 to 5/28/06, 06/05/06 to 6/28/06	06/22/05 to 07/02/06	06/22/05 to 09/16/06	06/22/05 to 09/09/06	07/11/05 to 08/29/06	
North-facing Burned	05/20/05 to 09/16/06	05/20/05 to 16/09/06	05/20/05 to 16/09/06	05/20/05 to 16/09/06	05/20/05 to 16/09/06	07/11/05 to 16/09/06	
North-facing Un-burned	06/13/05 to 09/16/06	06/13/05 to 09/16/06	06/21/06 to 9/16/06	06/21/06 to 9/16/06	06/21/06 to 9/16/06	07/11/05 to 9/16/06	
East-facing Burned	05/20/05 to 06/04/06	05/20/05 to 06/04/06	5/20/05 to 09/16/06	5/20/05 to 09/16/06	05/20/05 to 09/16/06	7/11/05 to 09/16/06	7/13/05 to 2/10/06, 06/04/06 to 07/11/06
West-facing Burned	05/20/05 to 09/16/06	05/20/05 to 09/16/06	05/20/05 to 09/16/06	05/20/05 to 09/16/06	05/20/05 to 09/16/06	07/11/05 to 09/16/06	

Steele Creek Valley was studied again six times during the summer and fall of 2006. In the summer of 2006 failure locations were checked on the ground at intervals of 2-3 weeks to determine if there had been any additional failure activity.

Active layer depth in Steele Creek was calculated by estimating the position of the 0°C isotherm. A linear interpolation was used between the two thermistors on either side of the freezing plane. The x-axis intercept of this line was then calculated. This method likely slightly overestimates the actual depth of thaw as the thermal profile often becomes curvilinear near the freezing point. 15-day averages were plotted in order to smooth the curves. Probing to determine the progression of the depth of the permafrost table was conducted during every visit to Steele Creek in 2006 at 20 points in a line up and downslope of each temperature measurement site. This was compared with the calculated values (Figure 4.1). Standard deviation of probed thaw depths was 6.6 cm, and the average difference between calculated and measured thaw depths (probing) was 6.8 cm. This indicates that the calculated values are close to actual conditions. However, significant differences could be due to a large frozen fringe, where the freezing point is depressed below 0˚C, the temperature measurement sites not being representative of the probe transects, stones interrupting probing or error associated with the ground temperature measurements ($\pm$0.5˚C).

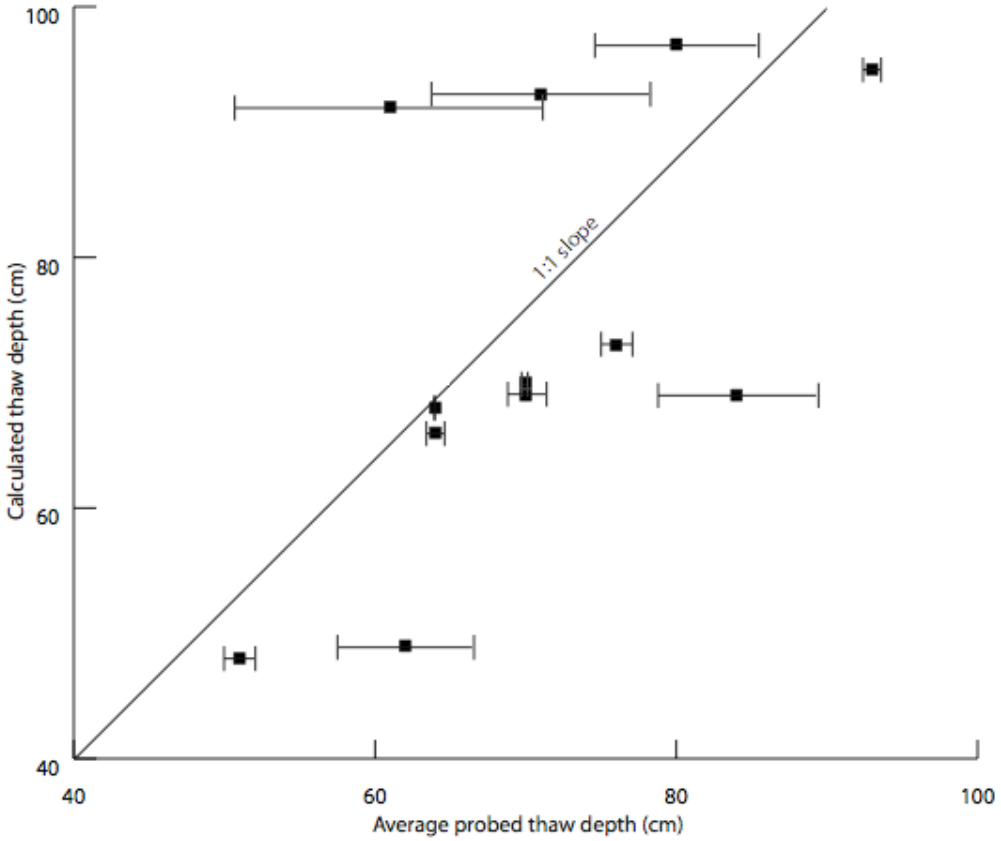

Figure 4.1: Relationship between average probed and thaw depths calculated from thermistor measurements. Average standard deviation over all points was 6.6 cm. Each point represents one site on one day.

Measurement Sites

As noted above, six ground temperature sites were set up in Steele Creek in 2005 (Figure 4.2).

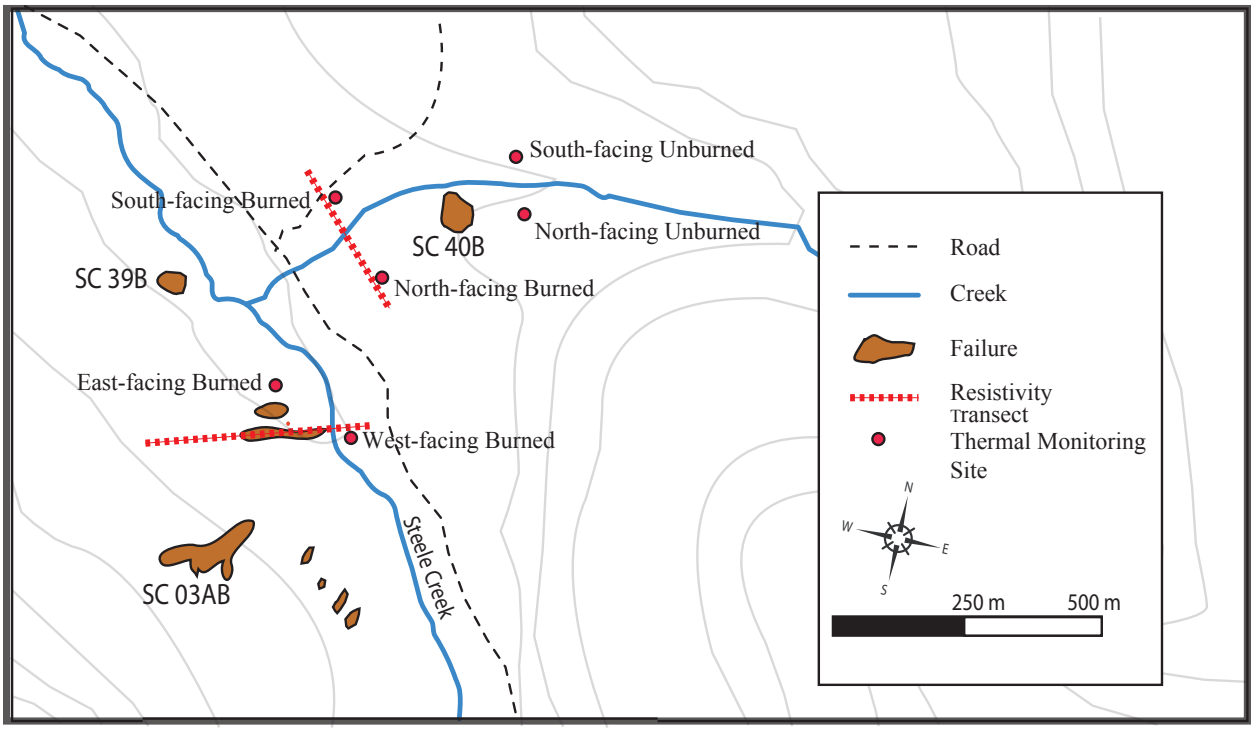

Figure 4.2: Steele Creek Thermal Monitoring Locations.

North-Facing Unburned Site

The north-facing unburned site was located on a tributary to Steele Creek, ¾ of the way up a 20 m high creek bank which sloped at 30˚. The aspect is approximately 10˚. The immediate area was unburned by the forest fire, but the fire came within 20 m of the site to the south. Vegetation consisted of 5-10 m mature black spruce, with an understory of willow and Labrador tea. The ground surface was covered with a 20-30 cm thick layer of moist sphagnum and feather moss interspersed with cranberry and mossberry plants. The creek below was subject to winter icings in excess of 1.5 m thick, which persist until late June.

On July 11, 2005, tension cracks were noticed downslope of the logger station. By August 16, 2005, these cracks had progressed into an active layer failure over the permafrost. On June 4, 2006, the failure retrogressed upslope to the point where the scar headscarp was 60 cm downslope of the lower guy wire for the air temperature logger pole (Figure 4.3).

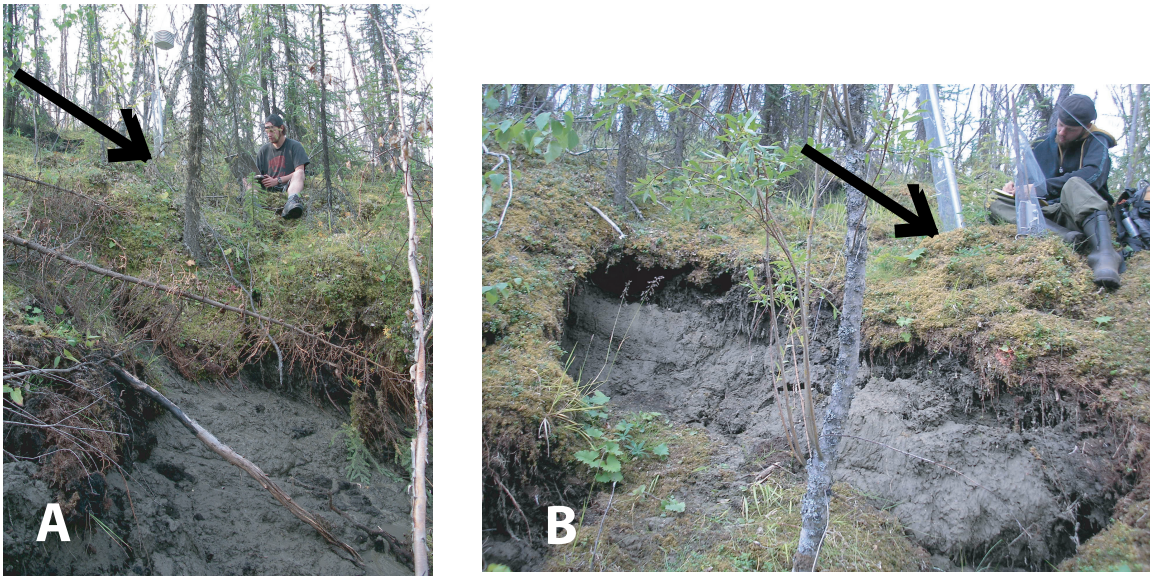

Figure 4.3: A: North-Facing Unburned Logger. July 20, 2005, B: July 22, 2006. Arrow indicates logger location.

By June 30, 2006, the failure had advanced upslope to within 30 cm of the logger post and had removed the lowermost guy wire, which was reset in another location. On August 17, 2006 the entire logger assembly was moved 5 m upslope to a location not affected by the slope failure.

North-Facing Burned Site

The north-facing burned site was located 100 m downstream of the unburned site on the same tributary of Steele Creek but closer to the confluence with Steele Creek and the old Dawson Coach Road. The monitoring equipment was installed 2/3 of the way up a 60 m long slope, which had an average incline of 15-20° (Figure 4.4). Aspect was approximately 355°. This slope was subject to a mass movement after the forest fire, which was not considered a detachment failure but more of a shallow thaw slump. The loggers were installed near the top of the disturbed area in severely burned terrain. Pre-fire vegetation at the time of installation was all dead, with burned 5-15 m black spruce, much of which had fallen over. There was some regrowth which is visible in Figure 4.4. The burn was severe enough to have completely consumed the organic layer, leaving bare, blackened mineral soil. Permafrost was present beneath this slope.

Figure 4.4: North-Facing Burned Site. May 20, 2005.

South-Facing Unburned Site

The south-facing unburned site was located directly across the tributary creek from the north-facing unburned site. The monitoring equipment was installed 20 m upslope of the creek on a 5° slope with an aspect of approximately 190° (Figure 4.5). Vegetation in the area consisted of 4-6 m high trembling aspen and spruce, with an understory of willow and the occasional birch. The ground surface had a thin (5 cm) organic layer consisting of fallen leaves and scattered herbs and grasses. The soil substrate was sandy gravel colluvium. There was no permafrost found on this slope

Figure 4.5: South-Facing Unburned Site. July 20, 2005.

South-Facing Burned Site

The south-facing burned site was located directly across the tributary creek from the north-facing burned site, and ten meters downslope from the Steele Creek Road. Monitoring equipment was installed near the slope crest 20 m upslope from the creek on a 10° slope with an aspect of approximately 180° (Figure 4.6). Vegetation consisted of dead, burned 2-5 m trembling aspen. This site was severely burned, with no organic layer and blackened exposed mineral soil. Soil substrate was gravelly colluvium with trace sand. No permafrost was found on this slope.

Figure 4.6: South-Facing Burned Site. July 22, 2005.

East-Facing Burned Site

The east-facing burned site was located on the west bank of Steele Creek 700 m upstream of its confluence with the tributary creek. The monitoring equipment was installed 75 m upslope from the creek on a 23° slope which continued uphill for almost a kilometer to the ridge crest (Figure 4.7). This slope was the site of several detachment failures, one of which was located twenty meters to the south. Aspect of the site was approximately 050°. Vegetation consisted of burned black spruce 5-10 m in height. This area had been severely burned, with exposed mineral soil in places. At the monitoring site a 10 cm burned organic layer remained. Surface and near-subsurface water flow was observed in this area, as well as tension gashes in the organic layer and artesian springs. Boulders were exposed in many places. The soil substrate consisted of sandy gravelly colluvium, with large, angular schist cobbles. This made installation of ground thermistors and probing difficult. Permafrost may be present, although the active layer was deeper than the 1.2 m probe or the thermistors.

Figure 4.7: East-Facing Burned Site. June 22, 2005.

West-Facing Burned Site

The west-facing burned site was located directly across Steele Creek from the east-facing site. Monitoring equipment was installed 20 m upslope from the creek on a 10° slope with an aspect of approximately 310° (Figure 4.8). Vegetation consisted of burned black spruce 5-10 m in height. The area had been severely burned, although there was 5-10 cm of burned organic material remaining on the surface. The remains were found downslope of a Klondike (circa 1898) dump consisting of corroded food and kerosene cans. The soil substrate consisted of sandy gravel. Permafrost was present at this site.

Figure 4.8: West-Facing Burned Site. June 3, 2006.

Permafrost DC Resistivity Survey

In early June 2006, two-dimensional electrical resistivity surveys were carried out collaboratively with Dr. Bernd Etzelmüller of the University of Oslo to examine the subsurface conditions and permafrost distribution across the north-south facing slopes between the north and south burned thermal stations, as well as up a failure scar across the valley from the west-facing thermal station (see Figure 4.2).

Resistivity geophysics is based on the principle that different soil materials have different electrical conductivities (Reynolds, 1997). Electrical conductivity varies according to the mineral material conductivity, chemical content of interstitial water, degree of saturation, and temperature of soil. Resistivity is the inverse of conductivity (Harada et al., 2000).

Resistivity imaging is useful in the detection of permafrost, given the large difference in resistivities between soil containing liquid water (~10 to 100 Ωm) and soils containing ice (~10^3 to 10^6 Ωm) (Hauck & Kneisel, 2006). Resistivity can detect permafrost in unconsolidated materials that contain ground ice (Etzelmüller et al., 2006). It cannot differentiate between frozen and thawed competent bedrock or frozen and thawed dry soil. A typical permafrost resistivity sounding curve shows abrupt changes in resistance at the base of the active layer and contact of overburden with bedrock.

The Steele Creek resistivity transects were conducted using an ABEM Lund (®ABEM Sweden) multi-electrode, high-resolution two-dimensional resistivity system. This system allows for a

maximum vertical penetration of 25 m. Fifty-meter electrode cables were used, with electrode spacing of 2 m in a Wenner array. After the system measures resistance and calculates the apparent resistivity, RES2DINV inversion software is used to conduct smoothness-constrained inversions using finite difference forward modeling (Loke & Barker, 1995). Specific resistivities for the model blocks in the two-dimensional grid shown are calculated by minimizing the difference between the observed and modeled apparent resistivity for each model block. Topographic surveying using Sokkia digital altimeter allowed for the inverted image to be topographically corrected before the inversion process. It is important to note that the interpretations of the resistivity images are in part subjective because no borehole information was available on these transects.

Shear Strength Analysis

In detachment failures selected for detailed mapping, pits were excavated down to the permafrost table after it had descended past the level of the failure plane. In-situ soil strength tests using a Geonor shear vane tester were conducted at intervals in the pit wall to determine the shear strength of each layer of soil strata. The vane was pushed horizontally into a cleaned trial pit face with five repetitions made at each depth to provide an average value (e.g. Lewkowicz & Harris, 2005a). Shear strengths measured in colluvial soils were not considered to be accurate. The blades of the shear vane almost invariably caught against rocks within the matrix, which increases apparent strengths. The only failure which provided consistent shear vane readings was SC 40B, which was seated in homogenous silt.

Laboratory Analysis of Soil Samples

Laboratory analyses consisted of the determination of soil grain-size distributions. Granulometry was measured by wet sieving to separate the sand from the silt/clay fraction. The sand fraction was then dried and sieved while the silt/clay fraction was determined using a hydrometer particle size analyzer as per ASTM standards (ASTM, 2007). The sand/silt split was located at the #200 sieve (0.1 mm), and silt/clay split was located at 0.002 mm.

Chapter 5: Steele Creek Detachment Failures

This chapter begins with a general description of all the detachment failures, followed by detailed examination of five that spanned the range of failure types in the Steele Creek basin. Morphological parameters of the failures are presented in the next section, where they are examined with respect to aspect and slope angle. The results are compared with those observed at other sites on Ellesmere Island and the Mackenzie Valley. Finally, similar post-fire failures that were observed in other parts of the Yukon are briefly discussed. Using all available data, a mechanism of failure is proposed.

Figure 5.1: Steele Creek Valley. Looking north showing failures SC 26A-SC 29A in the foreground. Photo taken May 24, 2005.

Most of the active layer detachment failures (36) occurred in 2004 after the July forest fire. A few occurred in 2005 (5) and none in 2006. The basic morphology of every failure in the Steele Creek valley was assessed (Appendix A) and the five presented here were selected as being representative.

Failures were present on both east and west-facing sides of the valley, as well as on a north-facing slope (Figure 5.2). The slope failures on the east and west-facing sides of the valley were seated in sandy gravelly colluvium, while the one on the north-facing slope was seated in silt. The failure seated in silt was different in form and mechanism from those in the coarser sediment. No failures were observed in motion, but several were examined within days of their occurrence.

Failures were found on all lower slope positions. Initiations were often near convex breaks of slope. Several of the failures reached Steele Creek, but the majority petered out higher upslope. In some cases sediment-laden water was discharged from the debris piles to flow downslope over the organic mat. Occasionally this reached Steele Creek.

There were no failures on permafrost-free slopes. Two failures (SC 36A, SC 37A) were found on slopes which had a southerly aspect, but these were underlain by permafrost and covered with sphagnum and black spruce, vegetation more typical of north-facing slopes.

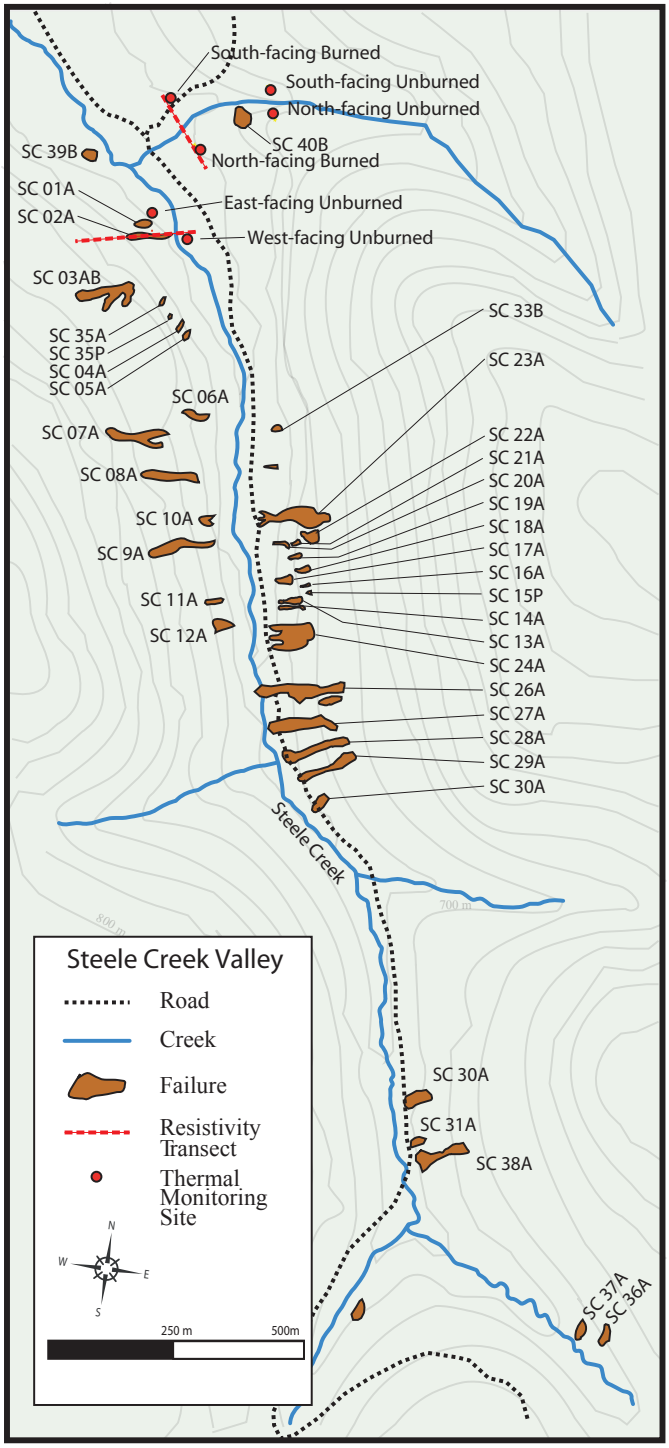

Figure 5.2: Map of Detachment Failures in Steele Creek. From Lipovsky et al., 2006. A-suffix denotes fires that occurred in 2004, B-suffix those that occurred in 2005, and P-suffix those that occurred previous to the fire.

Detailed Failure Site Plans

The methodology for surveying and mapping of failures was similar to that used by Lewkowicz and Harris (2005a). The goal was to describe the failures in sufficient detail that the failure mechanism could be inferred. The failures described are: SC 13A, chosen because it represents a 2004 west-facing failure; SC 03AB, chosen due to its reactivation in 2005 as well as representing a 2004 elongate failure; SC 33B, chosen because it represents a elongate 2005 failure; SC 39B, chosen because it represents a spatulate 2005 failure; SC 40B, because it represents a north-facing failure. The basic parameters of all the other failures are presented in Appendix A. Although most of the failures occurred in 2004 rather than in 2005, three 2005 failures were chosen for detailed study in order to observe the hydrological and permafrost conditions as soon as possible after the events.

SC 13A

SC 13A is an elongate failure that is visible on the May 2005 aerial photographs and therefore occurred in 2004 with no successive activations (Table 5.2). This failure is on the west-facing slope of Steele Creek in the midst of a concentration of failures (see Figure 5.2) and has a form typical of most of the 2004 detachment failures.

Table 5.1: SC 13A Morphological Parameters (N7052008, E600039).

Initiation	Slope°	Aspect°	Depth (cm)	Length (m)	Width (m)	Scar (m)
2004	24	275	35	24	8	21

The headscarp is located mid-way down a 50 m slope, on the crest of a slight ridge. The scarp is gentle, with organic material draped over the slumped mineral soil beneath. Vegetation around the failure consists of black spruce and birch forest with sphagnum moss. The area has been severely burned with mineral soil exposed near the headscarp.

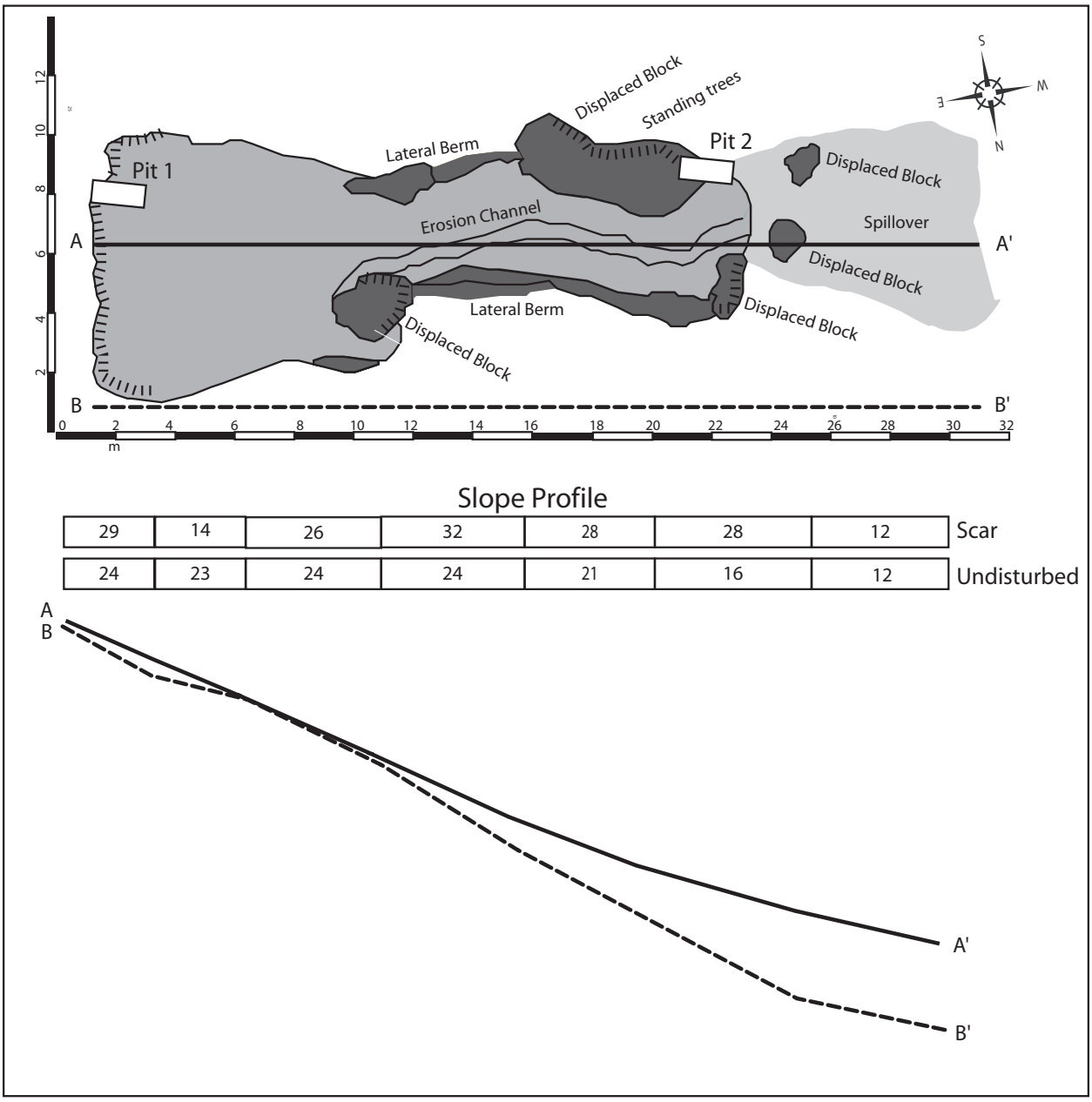

Figure 5.3: SC 13A Detailed Failure Plan. Gradients in slope profile are given in degrees.

The scar floor is cuspate, with depth of failure at the edges of approximately 35 cm, and in the centre of the scar approximately 80 cm. There is some channelization of the centre of the scar, possibly from post-failure erosion (Figure 5.4a).

The debris pile is folded with organic layers inverted and distorted. Trees in the displaced material are broken and twisted. There are a few trees left standing within the mass. The main block of displaced debris had come to rest where the slope decreases significantly in angle. In the secondary debris pile the organic layer remained intact and relatively undisturbed, but was rafted up and over the undisturbed organic mat (Figure 5.4b).

Outwash of sediment occurred over the organic mat downslope of the main displaced mass. Smaller displaced masses were rafted over the organic mat several meters downhill of the slide scar. As there was no mineral soil debris beneath these organic blocks, it appears that the blocks were rafted downslope on low-viscosity mud and debris which then percolated away through the organic mat.


A B

Figure 5.4: SC13A Photographs A: View upslope of the headscarp. Note the coarse material on the failure surface. B: Scar and debris pile. July 22, 2005.

This site was the subject of the most detailed grain-size investigation. Seven samples were taken from different strata in the headscarp excavation. Sandy gravels and gravelly sands with trace silt and clay were found in all strata, with no significant differences above or below the level of

the failure plane (Figure 5.5). Grain-size results are found in Appendix B.

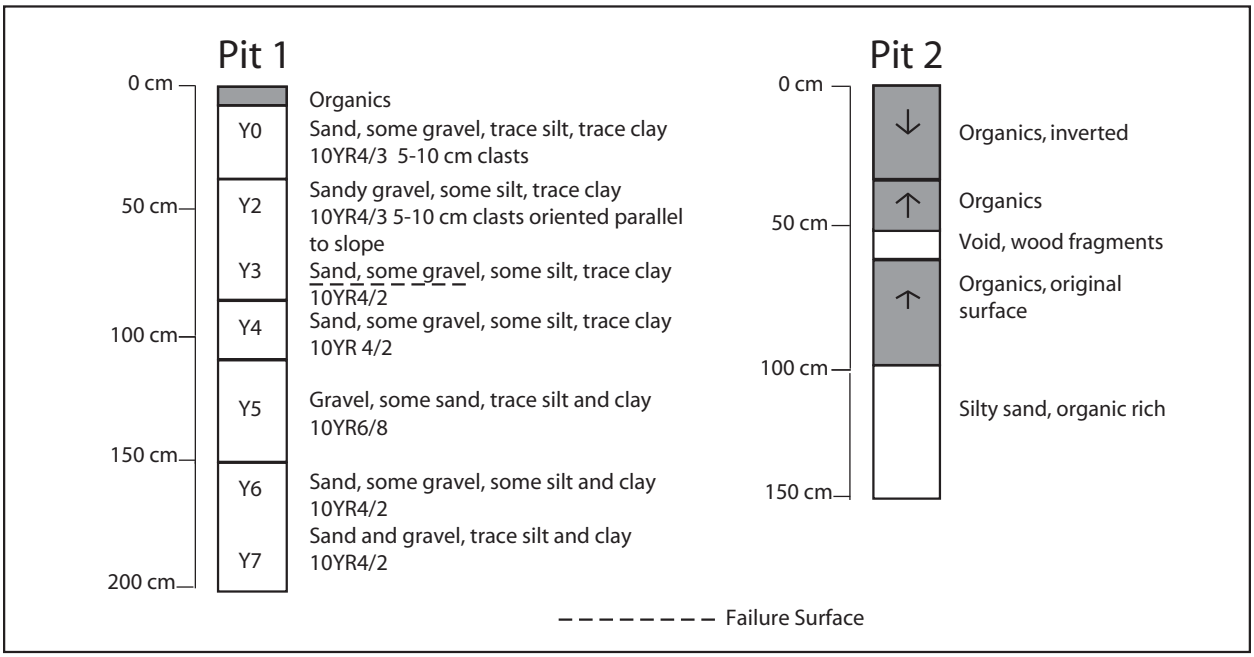

Figure 5.5: SC 13A Pit Diagrams. For locations, see Figure 5.3.

There were no reactivations in 2005 or 2006, although there was some erosion in the scar floor. The failure appears to have occurred in one rapid motion in which the organic layer was torn away and transported downhill over liquified mineral soil. It was then deposited when the slope gradient decreased. This failure shows more flow than slide component.

SC 03AB

This north-east facing failure consists of three 15 m to 40 m long, 10 m wide source zones, several large debris piles (See Figure 5.6) and a plume of sediment outwash flowing out of the debris pile and several hundred meters down over intact organics layer to Steele Creek (Figure 5.8). Failure SC03 AB was visible on the initial helicopter reconnaissance photos of the site taken in August 2004 and therefore developed within four weeks of the fire. It is located on an east-facing slope above the east-facing thermal monitoring station (see Figure 5.8). This failure had multiple distinct headscarps, each of which developed individually, a form that was unique in the Steele Creek Valley. The second and third activations occurred between site visits on July 2 and July 10, 2005 (Table 5.2).

Table 5.2: SC 03AB Morphological Parameters (Uppermost headscarp N 7052955, E 599702).

Initiation	Slope°	Aspect°	Depth (cm)	Length (m)	Width (m)	Scar (m)
Previous to 20/04/2005 Reactivations: 2/7, 10/7 2005	19	51	80	80	20	60

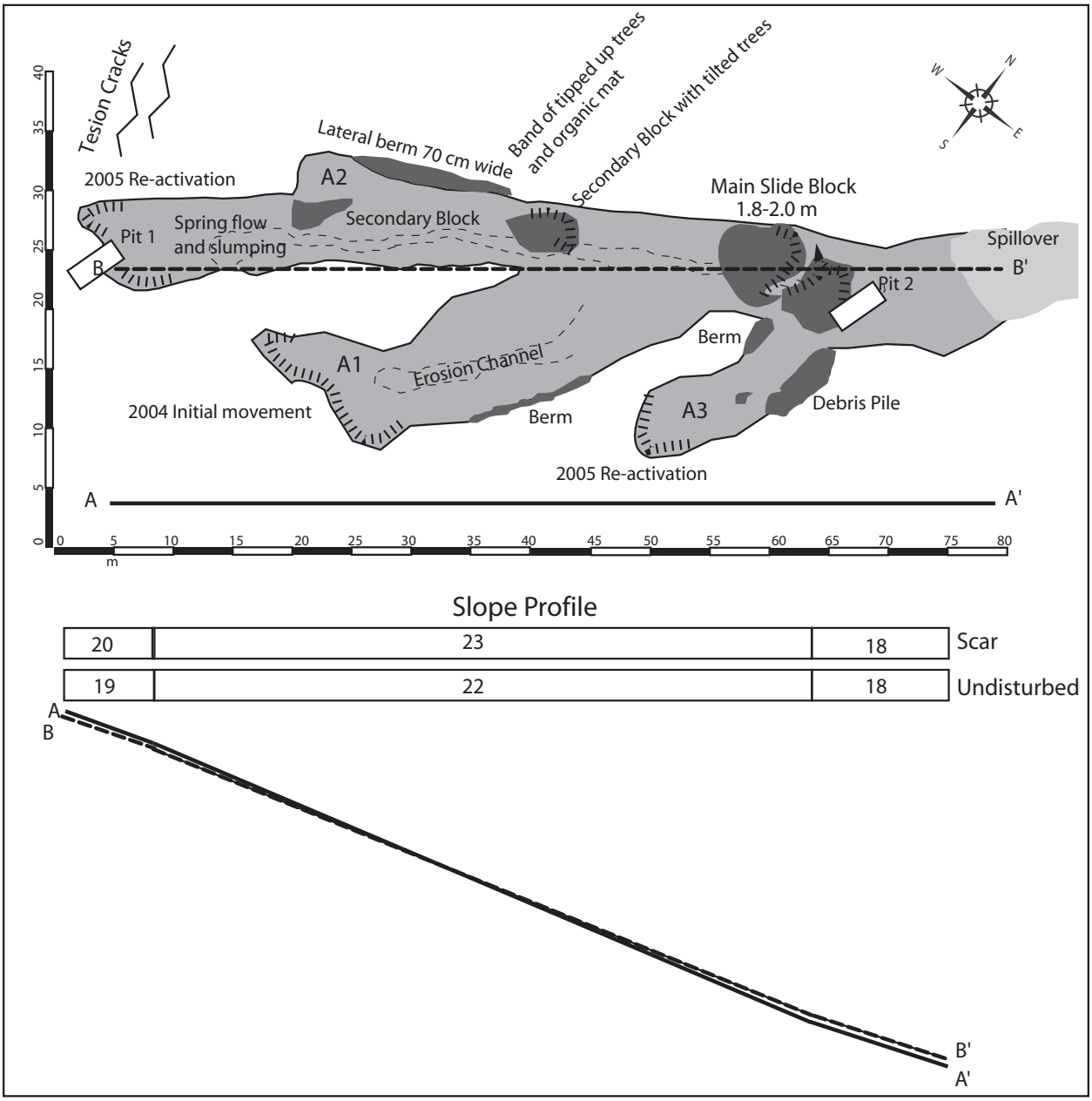

Figure 5.6: SC03AB Failure Plan. Note: A1 is original failure, A2 and A3 are subsequent re-activation paths. Gradients in slope profile are given in degrees.

Vegetation consists of severely burned black spruce and sphagnum moss. In many places the organic layer has been completely ashed, and mineral soil was exposed. Thaw in undisturbed terrain adjacent to SC 03AB as measured on July 2005 varied from 70-80 cm in depth. Thaw in the scar floor in July 2005 varied from 42-114 cm several weeks after the activation of the failure

path. Failure planes were approximately 80-90 cm in depth relative to the adjacent terrain in both 2004 and 2005 activations, even though, given the timing in the two different years permafrost tables were probably different. The failure is seated in sandy gravels (Figure 5.7). There are few to no fines present (Appendix B). At the base of the slope artesian springs were observed, and water was heard flowing beneath the organic mat over top of the mineral soil near the headscarp on August 16, 2005.

The headscarps of all three activations are just below a convex break of slope (Figure 5.8A). Tension gashes with tree roots stretched across them are visible on either side of the headscarp (Figure 5.8B). Upslope of the failure, a shallow trough-like depression indicates that drainage may have been concentrated in this area.

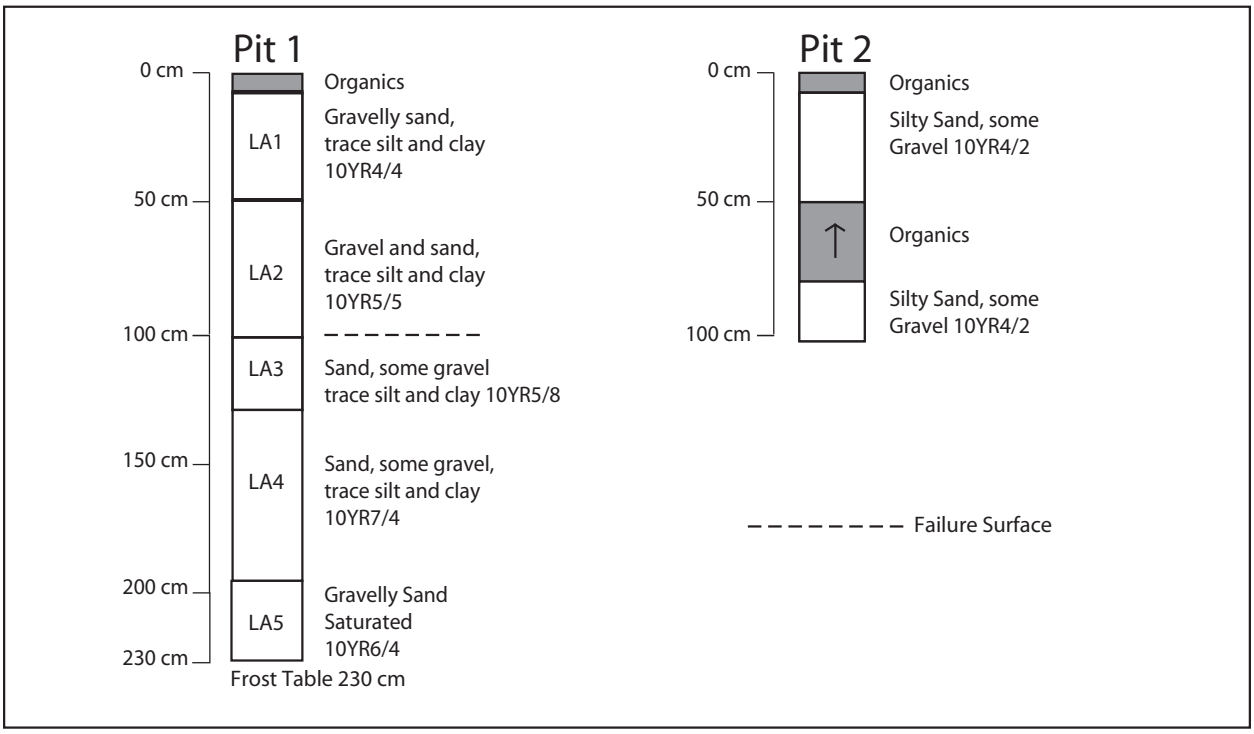

Figure 5.7: SC03AB Pit Diagrams. Frost table depths measured August 16, 2005.

The initial movement consisted of a block of the organic layer and upper mineral soil moving 50 m downslope. The organic material is piled and folded at the base of the scar, with the majority of displaced trees remaining standing in the debris pile (Figure 5.8C). Mineral soil is mixed, and no intact stratification was observed in Pit 2 (See figure 5.7) within the debris pile.

Figure 5.8: SC03 AB Photographs. A: View of failure from opposite slope showing extensive sediment plume development (July 2005). B: Tension gash near headscarp (August 16, 2005). C: Scar Floor looking downslope (July 20, 2006). D: Main displaced mass viewed from downslope (August 16, 2005).

Lateral compression ridges were formed on two of the failure paths but not on the third, where the organic layer was smoothly torn away with no material thrown up onto the sides. The scar floor in SC03AB is not flat, as would be expected with a failure which had occurred over the permafrost table. Instead it dips towards the centre, more like a flow channel. Some of this is probably due to post-failure erosion in the scar floor (Figure 5.8).

Near the headscarp on July 10, 2005, positive porewater pressures were observed. A secondary debris flow was triggered when a boulder was stepped on several meters below the headscarp. Within a few minutes a debris flow had started which flowed downslope to the main debris pile and out over the organic mat downslope. The debris flow was ~30 cm wide, 20 cm deep, lasted for 30 minutes, formed marginal berms and created an amphitheater-shaped source depression of approximately 4 cubic meters. This provides an indication of the instability of the local soils and the groundwater pressures within the active layer at most 8 days after the two 2005 reactivations had occurred.

The separate activations of failure SC 03AB were similar morphologically and it could be considered to be three separate failures with one conjoined toe and debris pile. The second and third ran out into the united scar, assisted by the lack of buttressing downslope. Clearly, this site was prone to instability but without appearing morphologically or geologically different from adjacent areas or the other slopes in the valley. As with other parts of the east-facing slope, no excess ice was observed in the bottom of soil pits excavated near the headscarp. However, porewater pressures were certainly very high in summer 2005. The source of this water is assumed to be

from downslope movement of precipitation-derived and thaw-derived groundwater over the permafrost table.

Near the headscarp of this failure and many other east and west-facing failures the burned organic mat was not in contact with the mineral soil substrate. The remains of the burned moss were suspended by tree roots, leaving a void between the dry organic mat and the moist or saturated soil below. The organic mat was dry while the soil below was saturated. There appeared to be very little root penetration below 15 cm into the mineral soil, although organics could occasionally be found deeper within the soil profile. The detached organic mat allows for groundwater flow over the surface without being obstructed. Near-surface saturation and free water flow may then occur without being readily observed at the surface. Where tension cracks were observed, the organic mat had pulled cleanly away from the mineral soil, with no evidence of root cohesion.

At SC 03AB, as well as at many of the other failures, a depression was present beneath the organic mat upslope of the failure headscarps extending as much as 4 m upslope. Thaw consolidation or erosion by flowing water beneath the organic mat were probably responsible.

SC 39 B

This elongate detachment failure (Figure 5.9) is northeast-facing and located almost directly across from the confluence of Steele Creek and its tributary creek and occurred between site visits on July 21 and August 15, 2005 (Table 5.3). Its headscarp is near a convex break of slope, although the latter is not as well defined as that near other failures. Depth of failure is approximately 80 cm.

Table 5.3: SC 39B Morphological Parameters. (Headscarp located N7053325, E599646).

Initiation	Slope°	Aspect°	Depth (cm)	Length (m)	Width (m)	Scar (m)
21/7-15/8/ 2005	25	55	80	34	14	25

Pre-fire vegetation at the site consisted of black spruce with scattered birch and moss organic layer. The area was severely burned, although there was little exposed mineral soil. Permafrost exposed in the bottom of Pit #1 had no visible ice content. Soils at the site consist of gravelly sand with traces of silt and clay (Figure 5.10).

The headscarp is broad and poorly-defined, with organic material draped over the mineral soil. The scar floor is flat, and exhibits a convex break of slope approximately 10 m from the headscarp. Angular, flat schist cobbles, 5-15 cm in diameter are scattered across the scar floor (Figure 5.11B). There is some channelization or other erosion over the convex break of slope roughly half way down the scar (Figure 5.9). Lateral berms up to 20 cm in height are present on both sides of the failure scar.

The three displaced masses of organic and colluvial material at the toe of the debris pile (see Figure 5.11C) show evidence of considerable deformation. Organic layers are folded and inverted (see Figure 5.10), trees are shattered and colluvial debris is piled up to 1 m thick on top of intact organic material. Considerable outwash of sediment occurred downslope of the failure over and around the displaced masses of material. The base of the failure terminates on the gentler foot-slope several meters from Steele Creek.

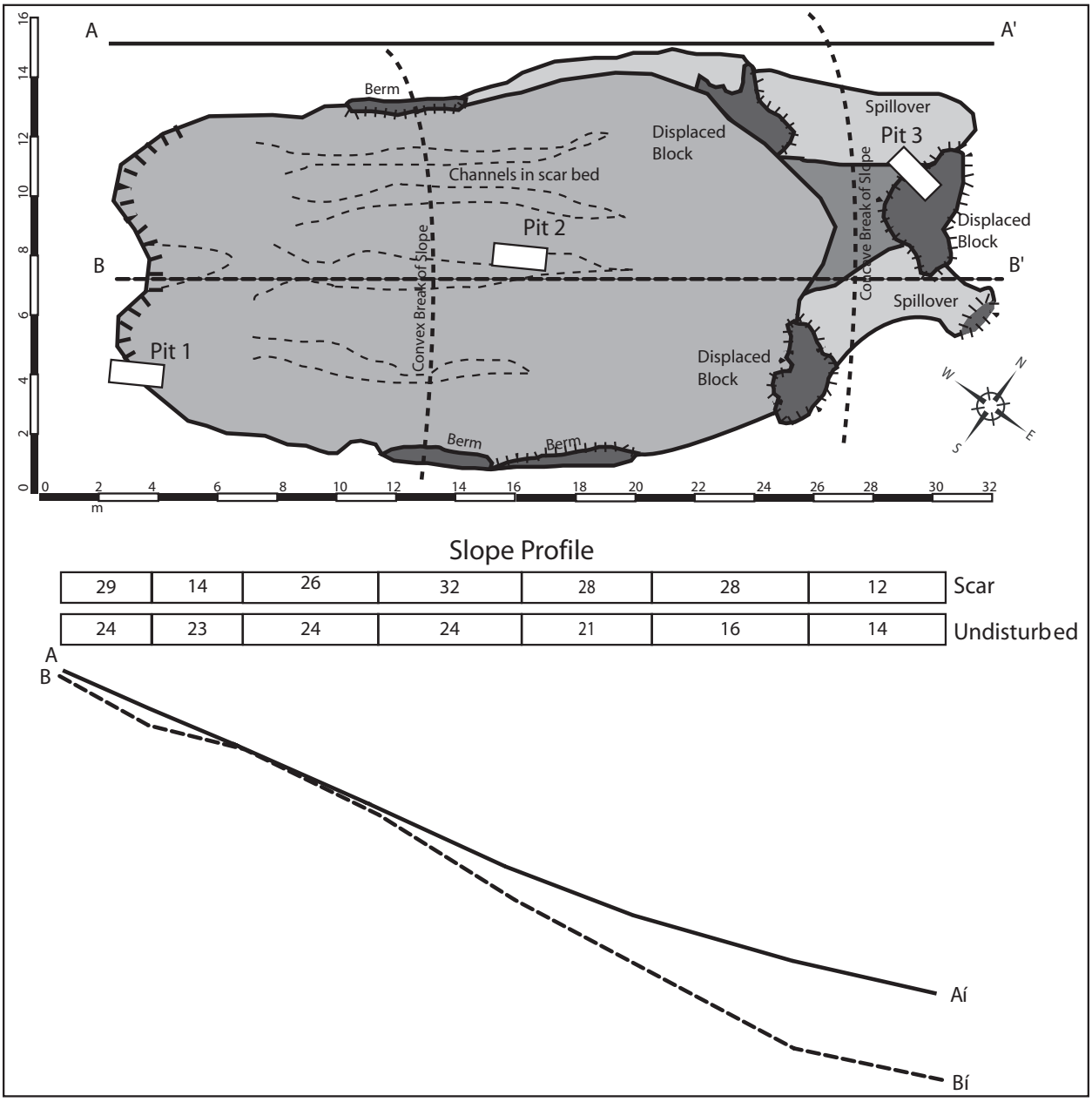

Figure 5.9: SC 39B Detailed Failure Plan.

Pit #1 was excavated into the headscarp. Materials which were encountered consisted of sandy gravel from the base of the organic layer to the permafrost table (Figure 5.10). The failure plane consisted of sandy gravel with a reddish colouration. This colouration was seen in many of the other failures at the failure plane. The colouration seems to be the only difference between this

and other strata. A convex break of slope is present in the scar floor but not in the surrounding undisturbed terrain. Pit #2 was excavated in the break of slope, but no stratigraphic differences were discovered which could explain the break of slope. Pit #3 was excavated near the toe of the debris pile, and shows the stacked, folded organic layers.

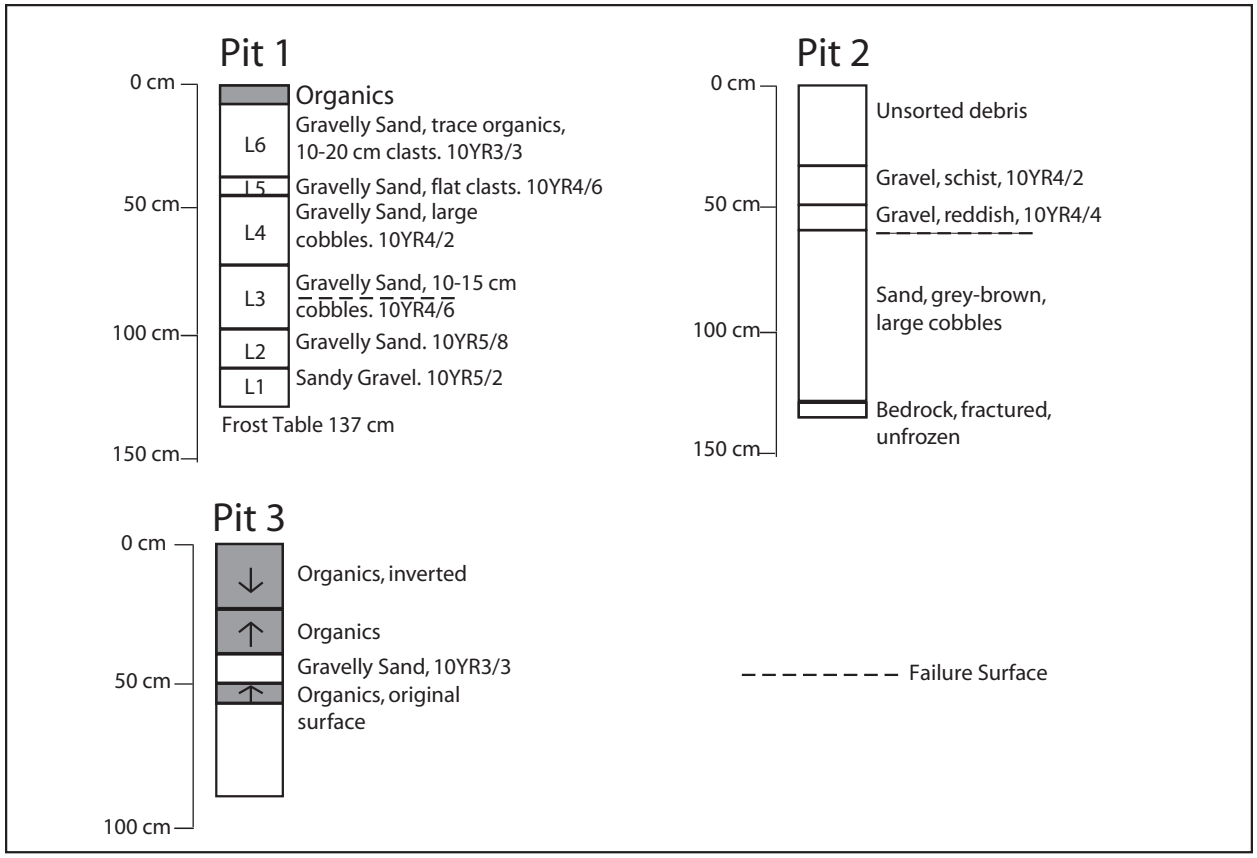

Figure 5.10: SC 39B Pit Diagrams. Frost table depths measured on August 17, 2005.

The condition of the displaced material indicates that movement occurred rapidly, possibly in a single motion, and with no subsequent reactivation. The depth of this failure (~80 cm) is close to the same depth as the nearby failure SC03 AB, which occurred in 2004, although the active layer depth was almost certainly deeper in late summer 2005 due to fire-induced thaw. Although the

failure took place above the permafrost table, there is no indication that it slid along the permafrost table.


A


B


C

Figure 5.11: SC 39B Photographs A: Failure surface showing convex slope. B: Headscarp showing uneven failure surface and exposed colluvium. C: Looking downhill showing standing trees in debris pile and uneven scar floor. All photos August 17, 2005.

SC 40B

The entire north-facing burned stream bank of the tributary valley was subject to numerous small movements, but this is the only failure large enough to be mapped as a discrete landslide (Table 5.4). It developed approximately half-way between the north-facing burned and unburned thermal monitoring sites. It was first noticed on July 10, 2005 but had not been observed during the previous visit on June 20, 2005. The failure headwall subsequently retrogressed by 2-3 m over three days. The failure eventually attained a length of 26 m and width of 22 m (Figure 5.12 and 5.13). The undisturbed slope varied between 23° and 45°. The final failure angle averaged 23° over the entire failure, with some steeper sections. The headscarp occurred at the break of slope where the upper bank transitioned into a nearly flat plateau. The failure plane was immediately above the permafrost table, 0.5 m below the surface on July 10, 2005 (Table 5.4).

Table 5.4: SC 40B Morphological Parameters. (Headscarp N7053483, E599870).

Initiation	Slope°	Aspect°	Depth (cm)	Length (m)	Width (m)	Scar (m)
20/6-10/7/ 2005	23	343	50	26	22	16

Vegetation consists of moderately to severely burned black spruce and moss, as well as dense thickets of willow and alder near the base of the slope. Five to 10 cm of organic material remained after the fire on the steeper slope segments, while the upper break of slope was burned down to mineral soil. At the base of the slope near the creek the organic mat was intact and only lightly scorched. Permafrost exposed in an excavation near the base of the slope had approxi-

mately 5% visible ice. Soils in test pit 1 were homogenous silt with trace sand and clay (Figure 5.15). No artesian springs or other signs of positive porewater pressures were observed.

Figure 5.12: View of SC 40B. From across the valley showing displaced masses with standing trees in centre of the slope (August 15, 2005).

The headscarp is sharp in some areas, with a clean face that extends from the torn organic mat to the frost plane. In other areas the organic mat is draped over the scar floor at the headscarp. Above the headscarp an area of collapsed organic material indicates thermokarst or erosional development beneath the organic mat. Tension cracks in the organic layer and 10-15 cm of underlying sandy silt are present in undisturbed terrain upslope of the retrogressing headwall.

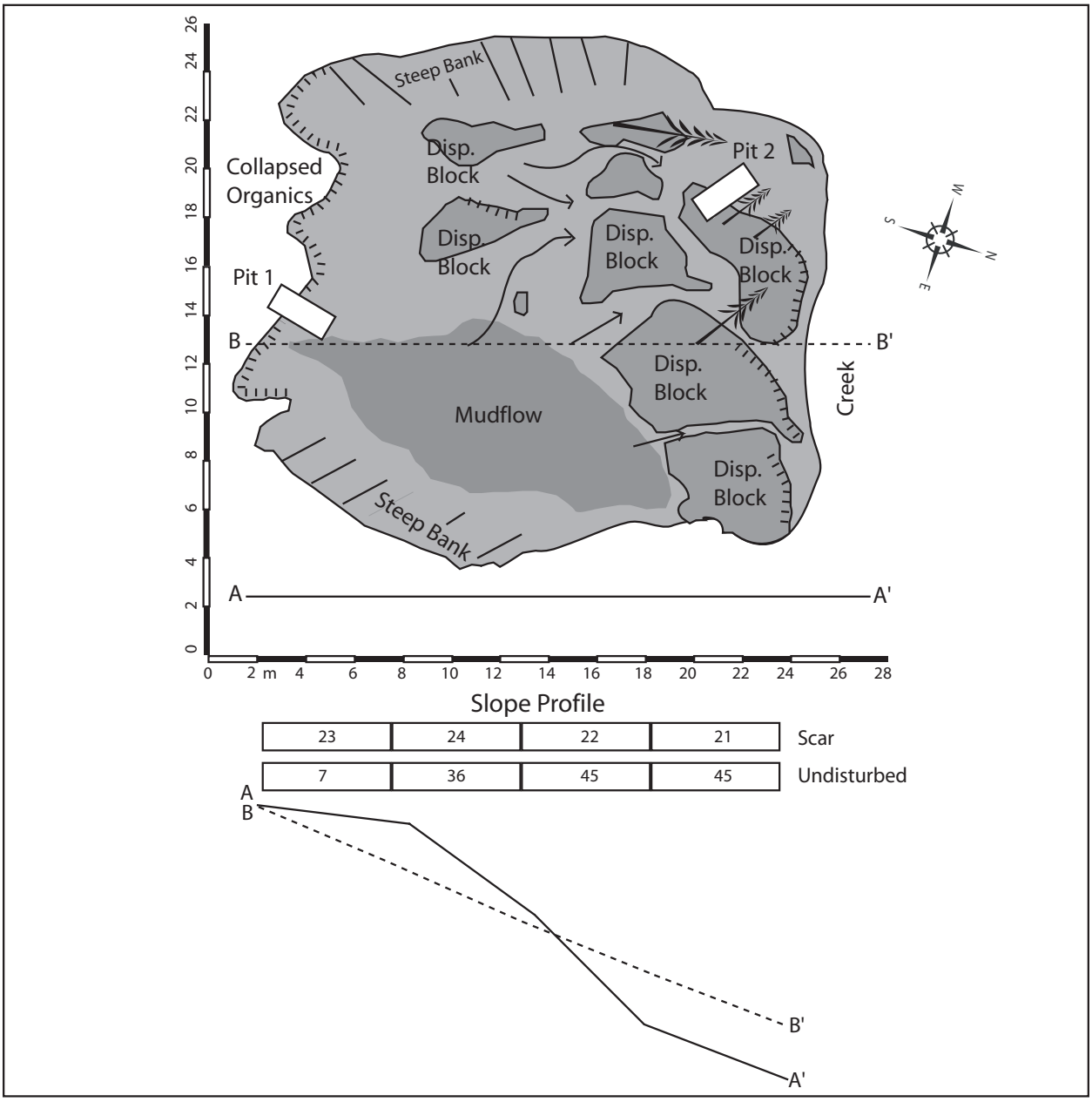

Figure 5.13: SC 40B Detailed Failure Plan. Gradients in slope profile are given in degrees.

The failure plane is smooth and clearly related to the thaw plane. After blocks moved downslope, further thaw occurred (Figure 5.14).

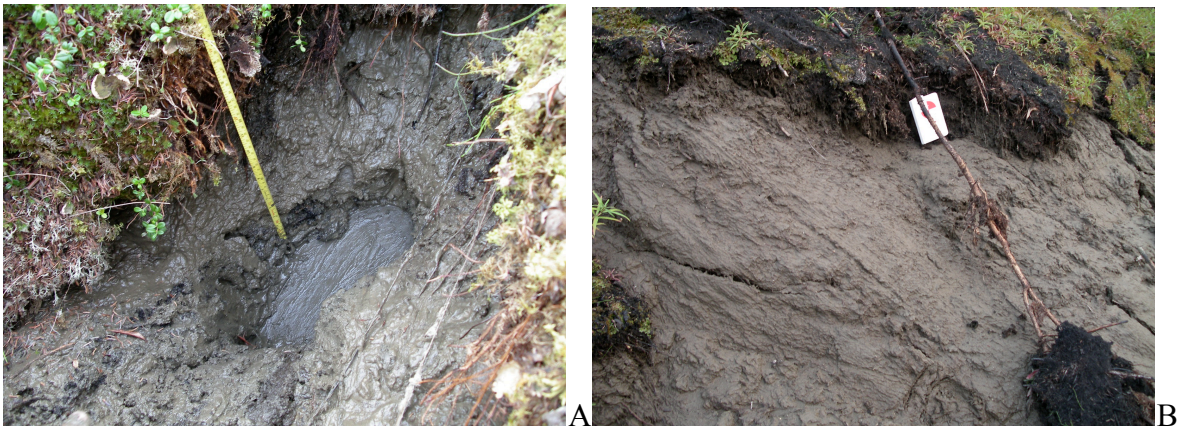

Figure 5.14: SC 40B Photographs. A: Exposure of permafrost in scar floor. Depth below failure surface represents several days of thaw (August 15, 2005). B: Stretched root between headscarp and displaced organic block during secondary movement.

Downslope of the upper steep headscarp the scar floor is a saturated mudflow up to 1 m deep. Arrows on Figure 5.13 indicate the observed direction of flow of mud. Displaced pieces of the organic mat were rafted on the mudflow. There is no lateral berm development.

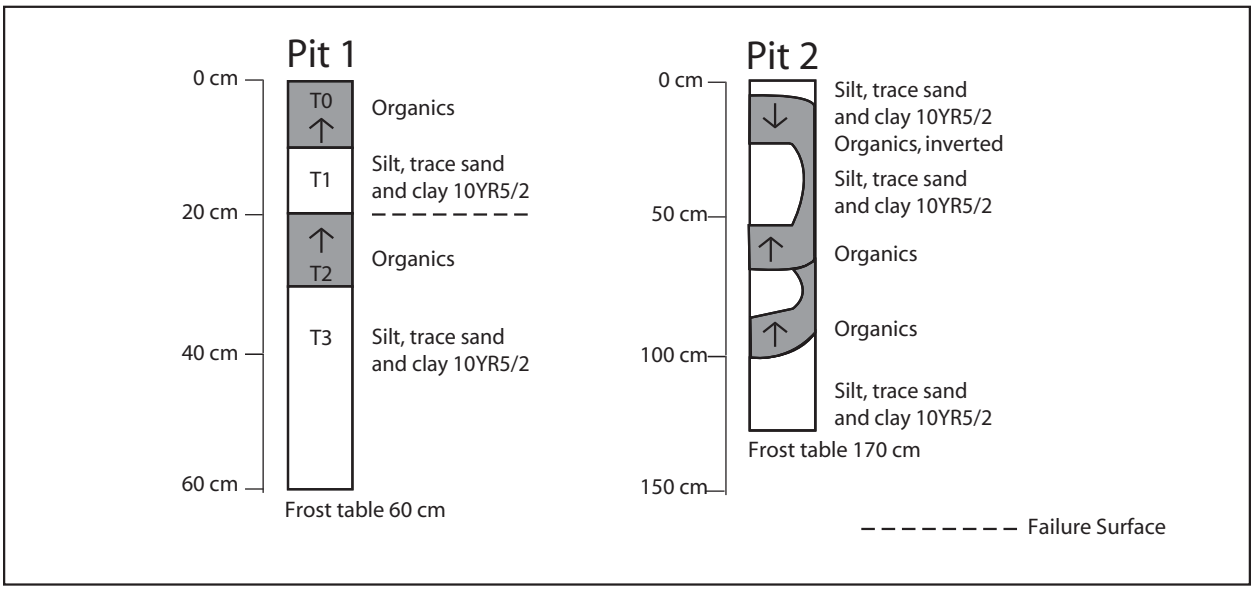

Figure 5.15: SC 40B Pit Diagrams. Frost table measured August 15, 2006.

The debris pile is much wider than it was long, stretching along the base of the scar. There is little deformation of the displaced material within the debris pile when compared with other failures in the valley, although organic material is folded and inverted in several places. Standing trees 10 m in height are present on displaced organic masses (Figure 5.12). The displaced material does not intrude into the tributary creek at the base of the slope, although sediment was observed flowing into the watercourse.

In Pit 1 a thin, burned organic layer was encountered. Below this was homogenous silt which extended to the permafrost table (Figure 5.15). Shear vane readings were taken in the cleaned wall of this pit on August 18, 2006. These indicated lower shear strengths immediately above the permafrost table (Table 5.5). In Pit 2, organic layers were neatly folded on top of one another, but were not torn or mixed with the mineral soil matrix (Figure 5.15).

Table 5.5: SC 40B Shear Strength Measurements (Permafrost table 185 cm).

Depth (cm)	Shear Strength (KPa)	Standard Deviation (KPa)
100	50	5
180	26	5

Note: Permafrost table was at 185 cm, standard deviation based on 5 repetitions.

There are several significant differences between this failure and all others mapped in detail in Steele Creek. The failure developed progressively over a period of weeks from late June 2005 to August 15, 2005 (Figure 5.16). It was on a north-facing slope, and was seated in fine-grained

sediment rather than coarse colluvium. This was the only failure mapped which was similar in morphology and soil characteristics to those observed in the Mackenzie Valley and on Ellesmere Island by Lewkowicz and Harris (2005a, 2005b), but the slow, progressive development was not similar.

In the fall of 2005 and spring of 2006, there was extensive slumping in the silty soil on the north-facing burned slope of the tributary creek. This extended the area of existing failures such as SC 40B. The sliding progressed slowly and episodically throughout the summer of 2006, with minimal distortion of the displaced material. It was not continuous enough to be labeled as an individual failure, but affected much of the burned terrain on the north-facing slope.


A

B


C

Figure 5.16: Successive Views of SC 40B. Progressive development: A July 2, 2005. B: July 22, 2005. C: August 15, 2005.

SC 33B

Failure SC 33B was not visible in aerial photos taken on May 24, 2005 (See Figure 5.2) but had occurred by July 10, 2005 (Figure 5.17). This is an elongate west-facing failure (Table 5.6). There is no convex break of slope proximal to the headscarp. The failure plane is approximately 70 cm below the surface, while the frost plane was also close to 70 cm deep in undisturbed adjacent areas on July 10, 2005.

Table 5.6: SC 33B Morphological Parameters. (Headscarp N 705258, E 600014).

Initiation	Slope°	Aspect°	Depth (cm)	Length (m)	Width (m)	Scar (m)
24/5-10/7/ 2005	23	323	72	25	9	16

The organic layer was severely burned, with 5-10 cm of blackened material remaining and bare mineral soil exposed in some places. Burned vegetation consists of black spruce and sphagnum moss. Soils are sandy gravel with some silt and trace clay. The gravel contains many large (>10 cm long axis) angular particles. On the date the failure was mapped, an artesian spring was discharging sediment near the headscarp.

The failure is hourglass-shaped, with a wide source area, slightly narrower scar floor and wide debris pile (Figure 5.17). The headscarp slopes gently from the organic mat into the mineral soil rather than being an abrupt scarp (Figure 5.18) and is similar to other Steele Creek colluvium failures but dissimilar to the steep headscarps seen on other detachment failures in the NWT and

Nunavut (Lewkowicz & Harris 2005a, 2005b). The headscarp soils were saturated and Pit #1 filled with water and collapsed soon after excavation.

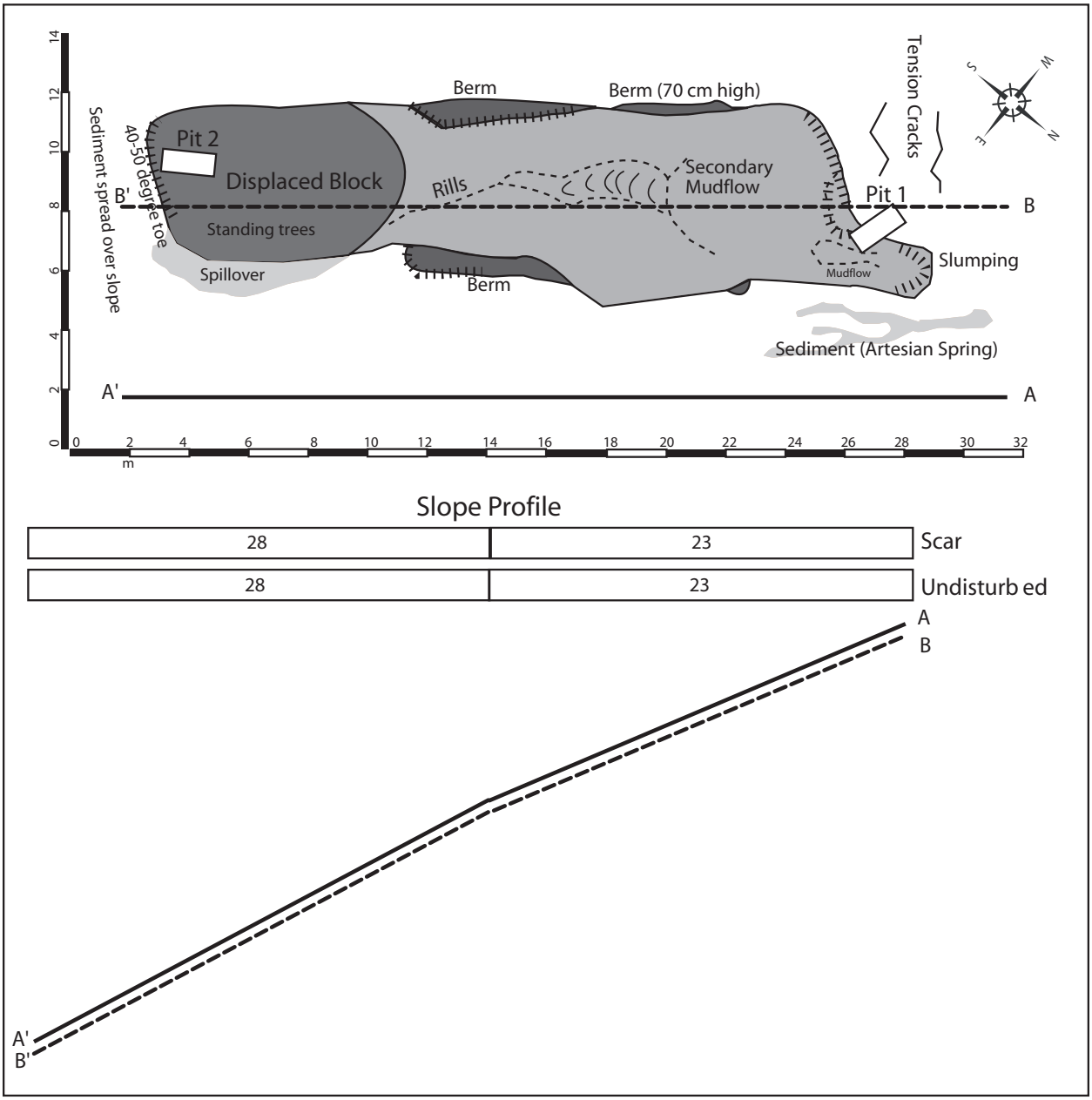

Figure 5.17: SC 33B Detailed Failure Plan. Gradients in slope profile are given in degrees.

Lateral berms had been thrown up over the organic mat on both sides of the failure (Figure 5.19). Channelization in the scar floor indicates that erosion of saturated sediments had occurred. The

scar floor is cuspate, although it is not clear if this is due to the original movement or subsequent erosion.

Figure 5.18: SC 33B. Gently sloping headscarp and excavation of Pit #1. August 16, 2006.

The displaced material is piled 30 cm high with a steep toe at the base of the scar. Several trees remain standing in the debris pile, while others were crushed within the folded organic material. There is little outwash of sediment over the organic layer downslope.

Figure 5.19: SC 33B Scar. Lateral berms, scar floor and displaced material. Looking downhill from mid-scar. July 6, 2005.

Pit #1, excavated in the headscarp (Figure 5.20) revealed several layers of sandy gravel or gravelly sand with trace silt. The layers differ only slightly in colour, and none differed significantly in composition above or below the failure plane. Exposed permafrost at the bottom of Pit #1 had no visible ice content. Pit # 2, excavated in the debris pile, revealed several folded and inverted organic layers with intervening layers of saturated and well-mixed sandy gravel.

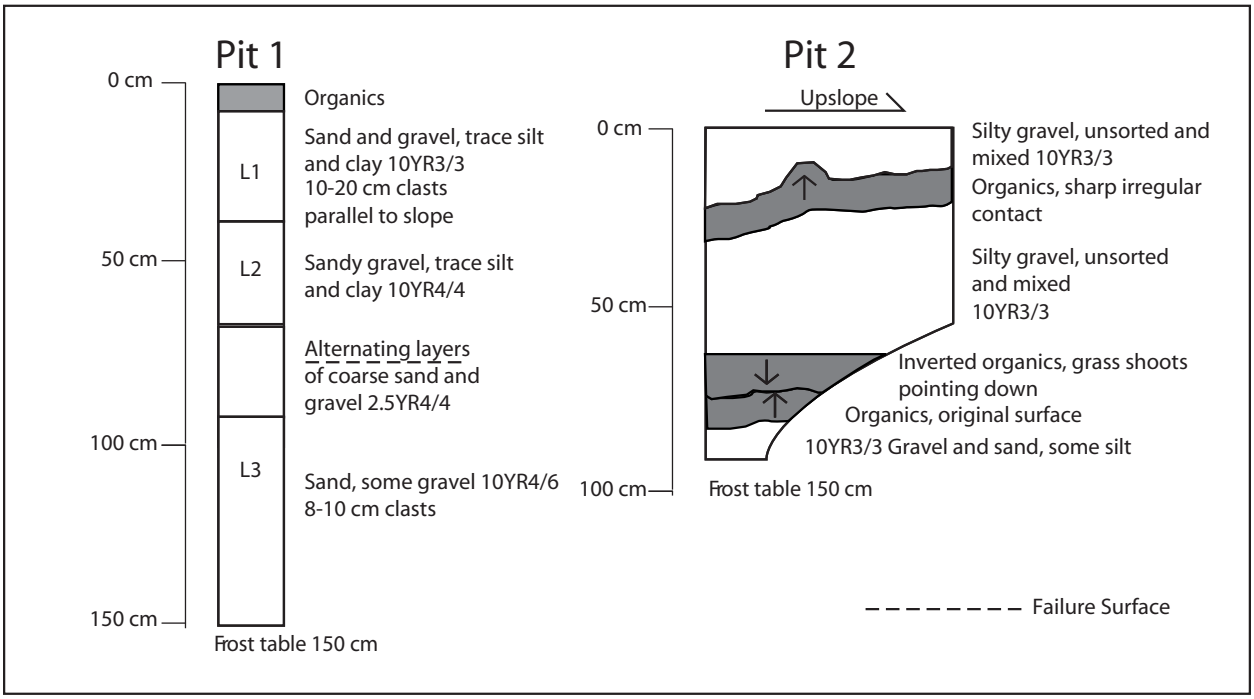

Figure 5.20: SC 33B Pit diagrams. Frost table measured July 6, 2005.

Artesian springs and groundwater encountered in excavations indicate that the phreatic surface reached or exceeded the soil surface and that positive porewater pressures were present. The single debris pile and lateral berms indicate that movement occurred as a single motion, and there were no indications of secondary remobilization except for small mudflows in the exposed scar floor. The folding and distortion of the organic material and mixing of mineral soil suggest flow rather than sliding as a competent block. The lack of sediment outwash over the slope below could be due to the low slope angle, which would favor percolation into the organic mat rather than rapid flow over top.

This failure is interpreted as a flow slide that occurred suddenly and rapidly, and rafted a section of organic material on top of the flowing material. The organic layer is folded and distorted in a

manner that suggests considerable speed. This is supported by the presence of lateral berms consisting of organic material with mineral soil splashed on top. The failure occurred within material above the permafrost table, but did not use the top of permafrost as a lubricated slip plane (e.g. Lewkowicz & Harris 2005a).

.

Discussion of Failure Types

In the Steele Creek Valley, only elongate detachment failures were observed (e.g. Lewkowicz & Harris, 2005a). The majority of these failures and all of those on east- and west-facing slopes took place in coarse-grained soils with high porewater pressures at the time of failure. Head-scarps were coincident or proximal to convex breaks of slope.

Failure surfaces were generally higher than the inferred frost plane and dipped towards the centre of the failure scar. It is possible that some of the cross-slope concavity was due to pre-existing cross-slope depressions, however, at least one failure developed on a cross-slope ridge. Once the moving mass had accumulated sufficient mass and speed, it may have scoured all the way down to the permafrost table. This may explain why in many failures the headscarp and upper scar displayed no depth control by the permafrost table, while further downslope there was a flat base to the scar. In this case, the permafrost table provided both an aquiclude and a basal limit to sliding, but did not act as a plane of weakness.

Displaced soil and organic material in most debris piles was highly disturbed. Trees were left standing in debris piles indicating that the organic layer moved without overturning until it lost momentum or reached material that would not detach. It then piled up with liquefied mineral soil sandwiched between folded layers of the original surface organics. the densely packed trees probably helped support each other so that many remained standing despite the flow-type failure.

The Steele Creek failures are similar to those described elsewhere in the unglaciated Yukon (e.g. Lipovsky et al., 2006), but not to those in the larger body of literature (e.g. Lewkowicz & Harris, 2005a, 2005b; McRoberts & Morgenstern, 1974b; Leibman et al, 1993). Different soil and permafrost conditions, morphology and location of the failure plane point to failures which have a greater flow than slide component. In other regions, the failure plane was directly above the permafrost table and the entire active layer detached as a unit, then slid down over the lubricated slip plane of the permafrost surface. This type of failure was found in fine-grained, ice-rich soils (e.g. Lewkowicz & Harris, 2005a, 2005b; McRoberts & Morgenstern, 1974b; Leibman et al., 1993).

The only failure with a sliding mechanism similar to those observed in other areas was SC 40B, which was located on a north-facing slope in fine-grained soil. Movement in this failure involved the detachment of the entire active layer from the permafrost beneath. Sliding then took place over the smooth permafrost table. However the progressive movement over several weeks was at least an order of magnitude slower than the other reports (e.g. Lewkowicz, 2007).

Failure Morphometric Analyses

The number of failures examined allows statistical description of their morphometry. These parameters can then be compared with results from the Mackenzie Valley and Ellesmere Island (Lewkowicz & Harris 2005a, 2005b).

Aspect

The failure distribution for the Steele Creek Valley reflects the north-south valley trend (Figure 5.21). The majority of failures were found in roughly equal numbers on the east and west-facing slopes. There were few south and north-facing slopes in the study area, and consequently fewer failures on these slopes.

No truly south-facing slopes which were underlain by permafrost were affected by the failures and only 5% of slopes had any component of southern exposure (Figure 5.21). Slopes lacking permafrost have no aquiclude along the top of the permafrost table and can not generate water from thawing of the transient layer ice. South-facing slopes in this area were observed to be composed of coarse, well-drained material that would have prevented the saturation needed for high porewater pressures. The resistivity data presented in Chapter 7 suggests possible south-facing permafrost only in the valley bottom where there is shading from the opposite slope.

The small numbers of north and south-facing failures are not sufficient to determine the role of differential insolation, although there were more failures on the north-facing aspect. It was not possible to describe the role of insolation in failure frequency, given the different soil materials,

topographies and areas of the respective slopes. The presence of a convex break of slope may be more important than aspect in predisposing a section of slope to failure.

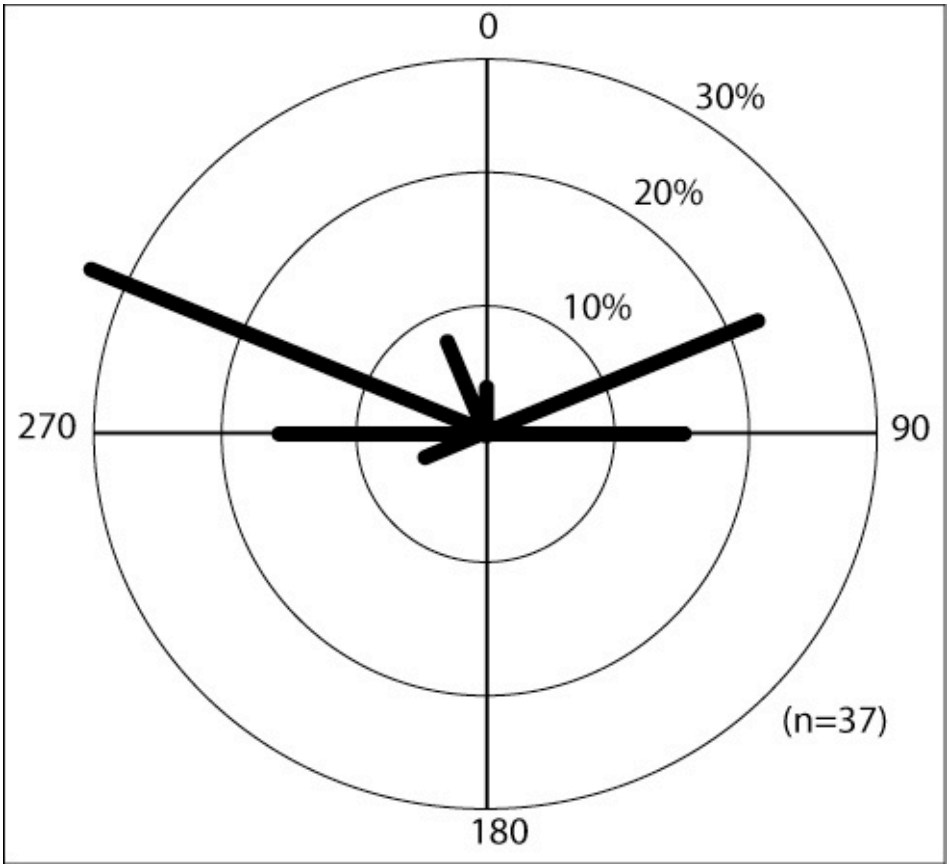

Figure 5.21: Failure Aspect Frequency Distribution. (n=37). Data not available for SC13A, SC 34P, SC32A.

Vegetation type in Steele Creek was closely related to slope aspect. The majority of failures on east and west-facing slopes took place in burned black spruce and moss-dominated forest, which provides a thick, strong, highly insulating organic mat. When this is destroyed completely during an intense forest fire, a greater thermal and mechanical disturbance is applied to the underlying strata than on other slopes due to the loss of the thermal protection of the moss insulation and mechanical stabilization of the interwoven root mat (Lewkowicz & Harris, 2005a, Yoshikawa et

al., 2003). The few failures that occurred on slopes with greater southern exposure were in birch forest, which also had a thick organic layer, and often grew in conjunction with black spruce on northwest- or east- facing slopes. There were no failures on south-facing slopes that were covered in aspen forest. The aspen forest had a minimal organic mat, and was often present on well-drained coarse-grained soils.

Failure Angle

Slope angles in failure scars varied between 12º and 32º (Figure 5.22). The slopes in the Steele Creek valley are generally within this range with the steepest slopes observed in the area having inclinations of less than 35º degrees. Initiation points were often just above or below a convex break of slope. The distribution of failure angles was approximately normal with a mean of 22.7º and a median of 22.5. Mean and minimum failure angles were similar to a mean of 19˚ and minimum of 12˚ observed at KP182 in the Mackenzie Valley (Lewkowicz & Harris, 2005a).

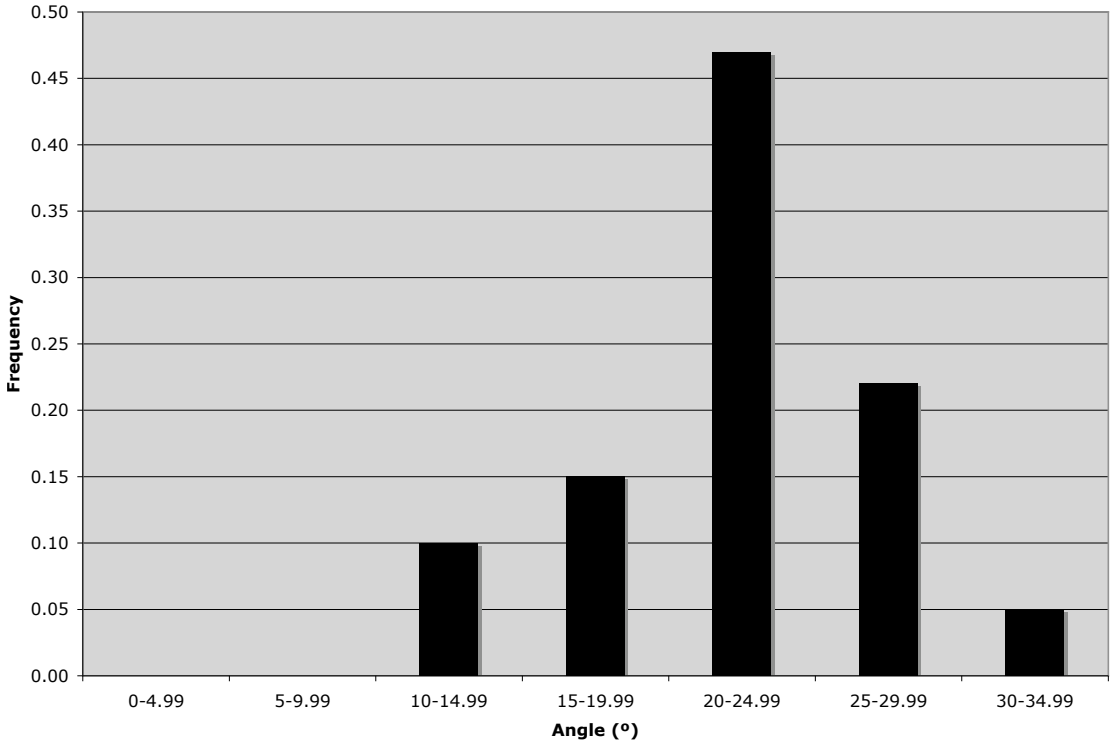

Figure 5.22. Failure Angle Frequency Distribution (n=40).

Failure Length, Width and Depth

Failure length and failure frequency were inversely related (Figure 5.23). There were more short failures and fewer long failures, with the greatest proportion (24%) in the <10 m category. Failure distribution declined steadily to 50 m in length, then remained constant at 2.5%, or roughly one failure per 10 m category. Median length was 22 m, and the longest failure was 105.5 m (Table 5.7). The failure lengths in almost all cases were much shorter than the available slope. Displaced material often came to a rest when slope gradients decreased slightly, although sediment spillover commonly traveled over the intact organic mat for some distance further downslope. In contrast, failures observed at KP182 by Lewkowicz and Harris (2005b) had a median length of 35 m and maximum length of 120 m, often terminating at the base of the slope.

KP182 failures utilized the entire distance between the crest and foot of the slope, whereas none of the Steele Creek failures did this. The differences in failure length between the two locations may be due to the soil conditions such as soil materials, permafrost distribution and ice content.

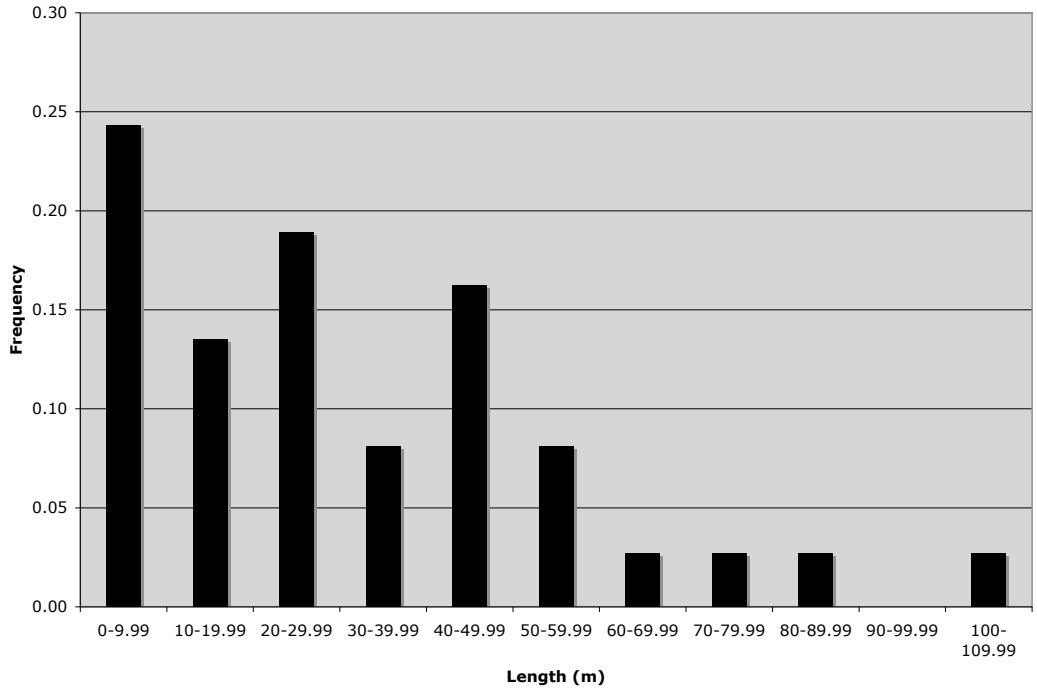

Figure 5.23: Failure Length Frequency Distribution (n=37). Data not available for SC13A, SC 34P, SC32A.

Table 5.7: Dimensions of Detachment Failures (m)

	Mean	Std. Deviation	Max	Min	Med	Mode
Failure Angle	23	4.8	32.0	12.0	22	19
Length (m)	32	25.3	105.5	5.0	25	5
Width (m)	7	5.5	23.0	1.6	6	2
Depth (cm)	48	29.1	160.0	17.0	35	80
Scar (m)	23	19.8	88.5	2.0	18	8
Length/Width ratio	4	1.9	10.6	1.2	4	2.5

Failure width-frequency distribution is similar to length distribution, but not as clearly defined, with higher numbers of narrower failures (Figure 5.24). The mean width is 7 m, median is 6 m and mode 2 m. The maximum failure width was 23 m. The lack of compact failures in Steele Creek means that there should be fewer wide failures. Widths were generally proportional to length, with wider failures also being longer. This is in contrast to the failures at KP 182, where the presence of compact failures produced a mean width of 14 m and maximum width of 78 m (Lewkowicz & Harris, 2005b).

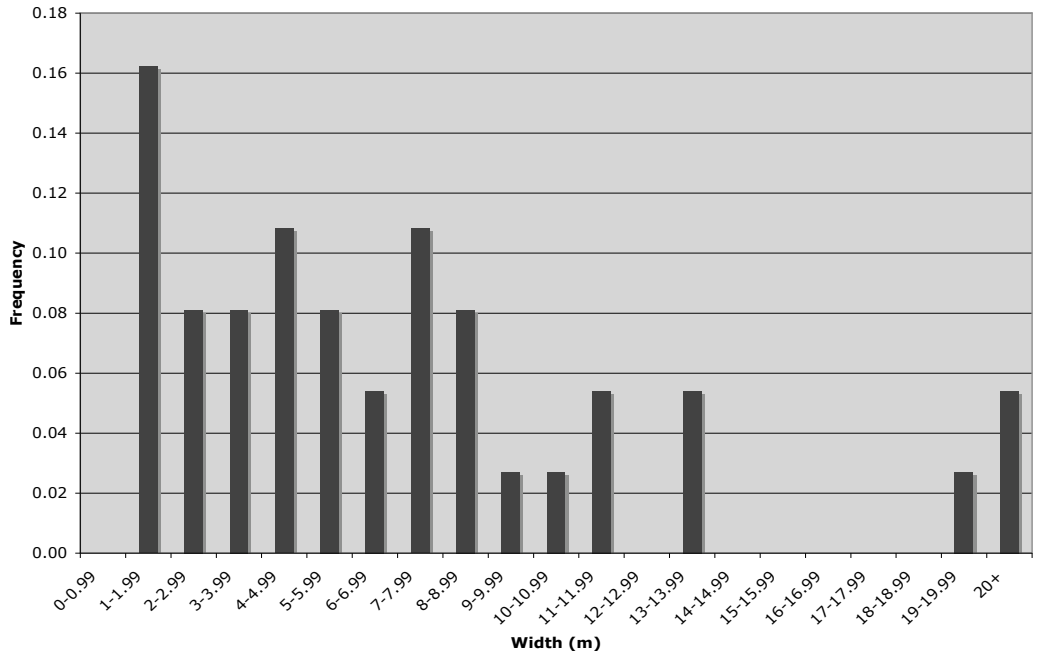

Figure 5.24: Failure Width Frequency Distribution (n=37). Data not available for SC13A, SC 34P, SC32A.

Table 5.8: Comparison of Steele Creek and Mackenzie Valley Detachment Failures.

	# of Failures	Med. Width (m)	Max. Width (m)	Med. Length (m)	Max Length (m)	Med. Failure Angle	Min. Failure Angle	Med. Scar Length (% total length)	Med. Length :Width Ratio
Steele Creek	40	6	23	25	105	22	12	72	4
KP 182*	45	14	78	34	120	20	13	50	2.5

*Lewkowicz and Harris (2005b)

The depth frequency distribution (Figure 5.25) shows a bi-modal distribution to the left, with a peak in to 20-29.99 cm category and a secondary peak at 70-19.9 cm. The mean and median depths are 47 and 35 cm, respectively. The smaller failures that make up the bulk of the Steele Creek population tended to have shallower failure depths. A number of the larger failures had depths close to 80 cm, which probably accounts for the spike in the 70-79.99 cm category. As mentioned earlier, these larger failures may have had enough mass for the flow of debris to scour down to the permafrost table. In this case the 80 cm depth may not represent the true initial failure depth, but rather the permafrost table depth. There were no smaller failures with deep (>80 cm) failure depths. There is a wide range of failure depths (160 cm to 17 cm) as compared to values of 70-80 cm measured by Lewkowicz and Harris (2005a, 2005b) at KP 182, probably because the thaw plane is not relevant as a control on depth in most of the failures.

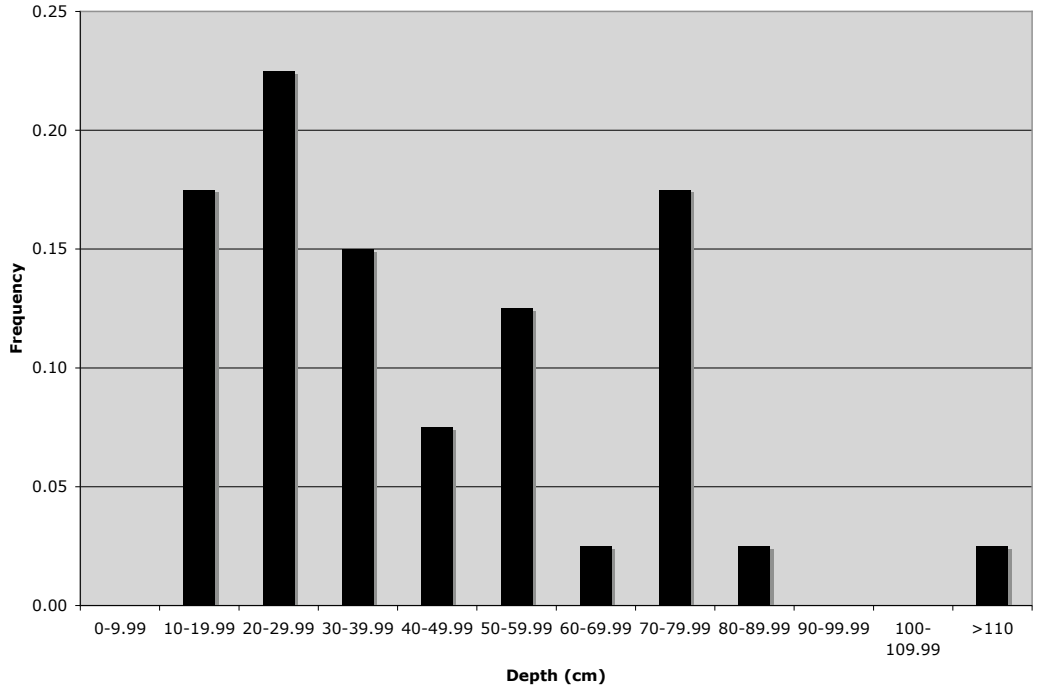

Figure 5.25: Failure Depth Frequency Distribution (n=40).

At KP182 and Ellesmere Island the failure plane was found to be immediately above the permafrost table. This was only observed in Steele Creek in the north-facing failure that developed in silt. At all the others, the failure plane was found to be 20-30 cm higher than the inferred location of the permafrost table at the time of failure. The permafrost table in Steele Creek would still have functioned as an aquiclude, providing an elevated water table and the high porewater pressures required to initiate instability.

Length-to-width ratios had a near-normal distribution, with median and mean values of 4 and modal range of 3-3.99 (Figure 5.26). The peak values indicated that more than 80% of failures were twice to six times as long as they were wide. The median length-to-width ratios were 4.4 on slopes with coarse colluvial soils as compared to 1.2 on the one failure developed in silty soil.

There were no failures wider than they were long. The position of the mode is probably related to the large number of smaller failures, which often had a less elongate morphology than the larger failures. At KP 182 Lewkowicz and Harris (2005a, 2005b) found a median length-to-width ratio of 2.5, with 18% of failures having a ratio less than 1. This is due to the presence of compact failures, which were absent from Steele Creek.

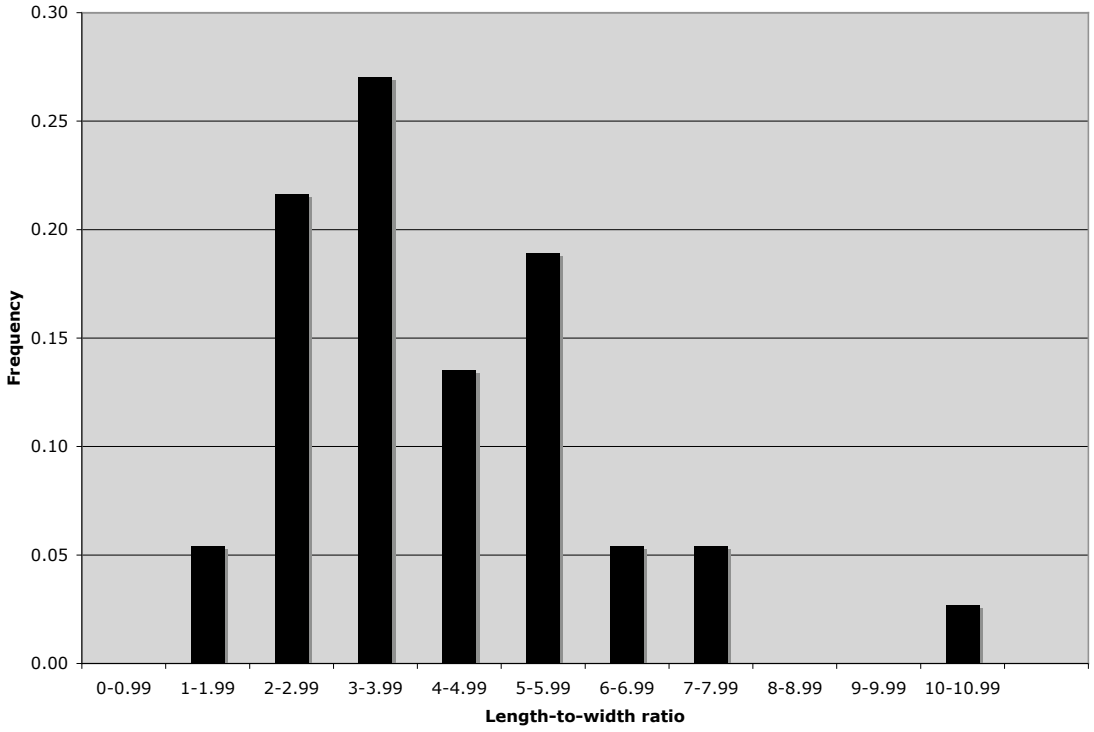

Figure 5.26: Failure Length-to-Width Ratio Frequency Distribution (n=37). Data not available for SC13A, SC 34P, SC32A.

The mean depth-to-length ratio was 2.3 %. At KP182 values were close to 2%, and on Ellesmere Island values were 1.5-2% in failures experiencing mainly sliding motion. These low values would indicate flow-type failures in non-permafrost regions (Lewkowicz & Harris, 2005a; Crozier, 1973).

Comparisons between morphological parameters on east- and west-facing slopes revealed no significant differences, although there were approximately 30% more failures on the west-facing slopes. Median failure width was 6.3 m on east-facing slopes and 7.2 m on west-facing ones. Median lengths were similar, around 32 m. The longest failure was 105 m and was on the west-facing slope. The median failure angles ranged from 22° on the west-facing slopes to 24° on the east-facing slopes. The median scar length as a percentage of the median failure length was around 70 % on both slopes. The median failure depth was about 40 cm on east-facing slopes, and 52 cm on east-facing slopes. The absence of difference is probably because insolation, granulometry, burn severity, slope morphology and pre-fire vegetation were similar on the two aspects.

The geology of the Steele Creek failures was significantly different from that found in the Mackenzie Valley and Ellesmere Island failures. While the single identified failure on the north-facing slope developed in silt with traces of clay and sand, all of the east and west-facing failures occurred in gravelly sand or sandy gravel with almost no fines and large cobbles and boulders. This material was not ice-rich, as opposed to thick ice lenses exposed on a failure plane at the KP182 site in the Mackenzie Valley (Lewkowicz & Harris, 2005b) and on Ellesmere Island (Lewkowicz, 2007).

Failure Volume

Total volumes of sediment moved were 2473 m^3 in 2004 and 552 m^3 in 2005. No new failures occurred in 2006, so more than 80% of the failure activity occurred in the first two months after the fire. Failure volume assumes that pre-failure ground surfaces were planar and did not have a pre-existing cross-slope depression.

Topography

Failure headscarps generally occurred immediately proximal to a convex break of slope below a long, unbroken slope. This is shown in Figure 5.27, where all of the failures in the photo have headscarps that coincide with a convex break of slope (dashed line). The long slope above could provide a catchment for groundwater collection and flow. The break of slope could also represent the upward progression of the historical failure scarp.

Figure 5.27: Failures SC26A, SC27A, SC28A and SC29A showing break of slope headscarp location (Dashed line indicates break of slope).

Fossil failures and debris piles were observed below this break of slope, but none above. Resistivity imaging (Chapter 7) indicates that there might be groundwater flow through intrapermafrost taliks that emerge near the headscarp. This water may be forced to the surface by a raised permafrost table or bedrock near the break of slope. Breaks of slope are also zones of increased shear stress as the slope steepens, and were often the location of shear gashes in organic materials. Lipovsky et al. (2006) also noted that failure headscarps were often located near a break of slope in Mickey Creek.

Summary of Failure Characteristics

With the exception of the north-facing failure, where movement was over the permafrost table, Steele Creek failures differed from those described by Lewkowicz and Harris (2005a, 2005b) from the Mackenzie valley in the following respects:

a) They were exclusively elongate.

b) The permafrost table was not the failure surface.

c) Soil materials were non-cohesive and mainly coarse (which precludes sliding).

d) Permafrost may not have been present beneath all of them.

e) High porewater pressures seemed to relate to water fed from upslope, not locally generated at the base of the thawing layer where the failure occurred.

f) Failure motion involved more flow-type deformation with rafting of the organic mat, not cohesive blocks of sediment in motion. The loss of strength of the organic mat due to fire may play a very important role in allowing failure to occur.

g) Ground ice contents were not very high as indicated by resistivity readings on the east-facing slope (Chapter 7).

h) Pre-existing taliks may be key to some failure locations (Chapter 7)

i) The failures occurred only in the lower parts of slopes and did not generally extend from crest to foot. The Steele Creek failures were similar to those at KP 182 in the Mackenzie Valley in the following aspects:

    a) The high porewater pressures were generated by deep thaw following fire.

    b) Failures occurred in the year of the fire (majority) and the following year (minority).

c) The gradient ranges of the slope subject to detachment failure were similar.

d) Depth-to-length ratios were very low at both sites.

Stabilization of Slopes

Those failure scars that had drained and revegetated by the fall of 2006 appeared to have stabilized. Some of the failures, particularly the one directly downslope of the north-facing burned thermal logger, were nearly completely revegetated by August 2006 to the degree that they were nearly indistinguishable from the surrounding intact but burned terrain.

Failure initiation decreased from 2004, when the majority of failures occurred, to 2006, when there were none. The increasing stability of slopes is likely due to the decreased availability of water. Water availability is critical to raising the porewater pressure to the point where the slope experiences instability. Abundant water produced during thaw of the transient layer immediately after the fire becomes depleted with time. The field observations suggest that this occurs after the fire year plus one additional year. After this, the scar areas become dry and no more failures occur. For example, SC 22B was completely dry when visited on July 22, 2006 while its scar was saturated on July 12, 2005. In 2005 water would have come from the thaw of ice-rich transient layer permafrost, as well as precipitation. In 2006 groundwater flow would have resulted from precipitation or thaw of ice-poor deeper permafrost. However, there was 25% less precipitation in the summer of 2006 than 2005 (Figure 3.3) so this would have influenced the degree of saturation. There may also have been greater evapotranspiration in 2006 compared to 2005 as vegetation became more established. All these factors probably contributed to reduce the moisture content at the failure sites.

The permafrost table may re-establish at a new equilibrium depth below the scar or, in the case of ecosystem-protected permafrost, continue to lower indefinitely (Burn, 2000; Shur & Jorgensen, 2007).

Thick (1-2 m) icings were observed in the tributary creek, as well as at the base of slopes in Steele Creek itself. The icing in the tributary creek appeared to be smaller in early June 2006 than it was in 2005. The icing had almost completely melted by June 30, with small pockets in shaded areas and under overhanging banks. The observations suggest that late-summer groundwater drainage was greater following the fire in 2004 than in 2005, leading to thicker icings in 2005 than 2006 (Figure 5.28).

Figure 5.28: Groundwater Icings. Emerging at base of east-facing Steele Creek slope downstream of SC 39B. December 2004.

Revegetation

By mid-summer 2006, there was much revegetation of all the burned areas of Steele Creek, mostly by horsetail, fireweed and grasses, as well as mosses and some willows. Horsetail and mosses were beginning to recolonize almost all of the failure scars. Displaced blocks of organic materials had especially luxuriant growth and appeared to serve as nuclei for revegetation (Figure 5.29). By August 17, 2006, failures were difficult to see from the road as vegetation had equally colonized the scars and the surrounding burned terrain.

The growth of vegetation was likely accelerated by the availability of water emanating from the thaw of ice-rich permafrost as well as the availability of unoccupied soil surfaces. It is this vegetation which shades and insulates the ground, allowing for permafrost table to stabilize (Mackay, 1995).

Figure 5.29: Revegetation of Scar Floor. At base of SC 21A August 2006. Note transported sections of the organic mat acting as nuclei for revegetation.

Preservation of Detachment Failures in the Sedimentological Record

Since detachment failures occur as a result of forest fire over permafrost, and fires are wide-spread in the Yukon, detachment failures are likely to have been occurring in unglaciated areas through much of the Quaternary. Consequently, evidence of these slope failures should be preserved in slope deposits. Investigation of these features took place at three Yukon sites (Figure 5.30).

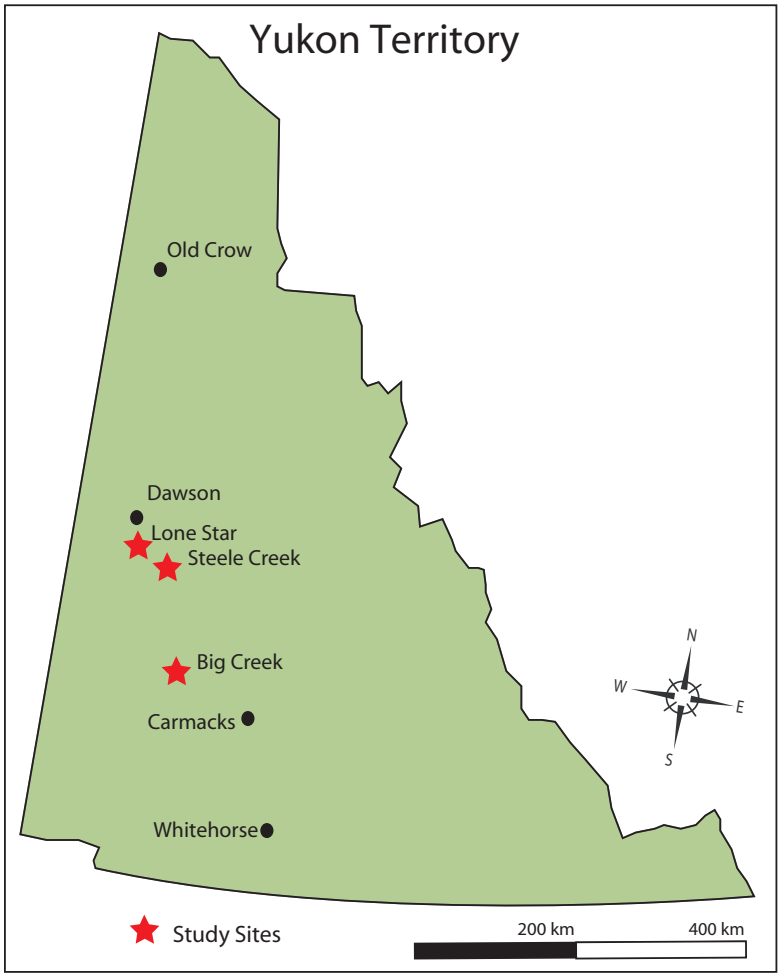

Figure 5.30: Fossil failure study sites.

In Steele Creek, a fossil failure was initially recognized by the outline of its debris pile and the depression of the revegetated scar. The entire site was covered by mature burned trees, and the

scar appeared to have been completely revegetated prior to the 2004 fire. Buried organics overlain by disturbed, unstratified colluvium and shattered woody debris were found beneath a mound interpreted as a debris pile from the toe of the fossil failure (Figure 5.31). A buried organic layer at a depth of 50 cm appeared to have been inverted and folded. This implies that detachment failure has occurred previously in the Steele Creek valley.

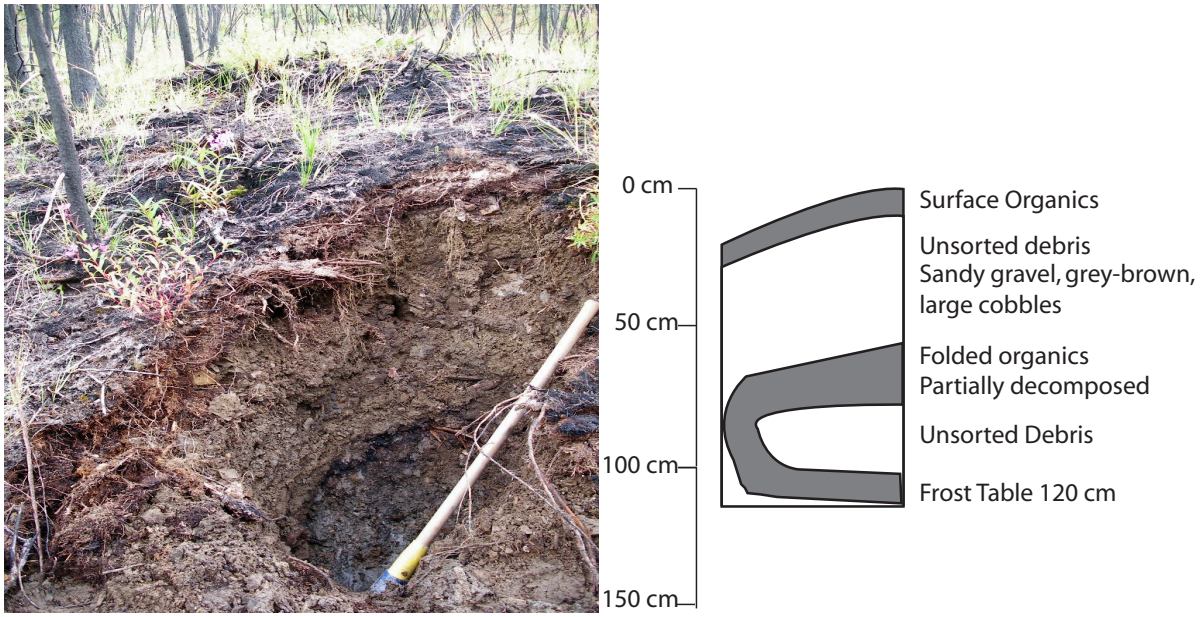

Figure 5.31. Excavation of Fossil Failure in Steele Creek. Mattock handle 1.2 m long. Dark organic material visible approximately 50 cm from the surface. June 20, 2006.

At the Lone Star Mine in upper Bonanza Creek (63º54'01 N, 139º15'18 W) some 50 km north of Steele Creek three pits were excavated in a road cut across the upper portion of a north-facing slope in association with soil sampling by Jeff Bond of the Yukon Geological Survey (Figure 5.32).

Figure 5.32. Lone Star Road Cut. Excavation approximately 5 m past people.

Evidence of failure activity was present in two of the three pits. This included buried birch branches frozen within permafrost, contorted and folded organic layers, and folded organic layers covered by colluvium containing coarse clasts (Figure 5.33). Lenses of sorted fine sands were visible in cross-section. These lenses could have been deposited by water flowing down a failure scar, and could not have been deposited by water flowing through the thick organic mat.

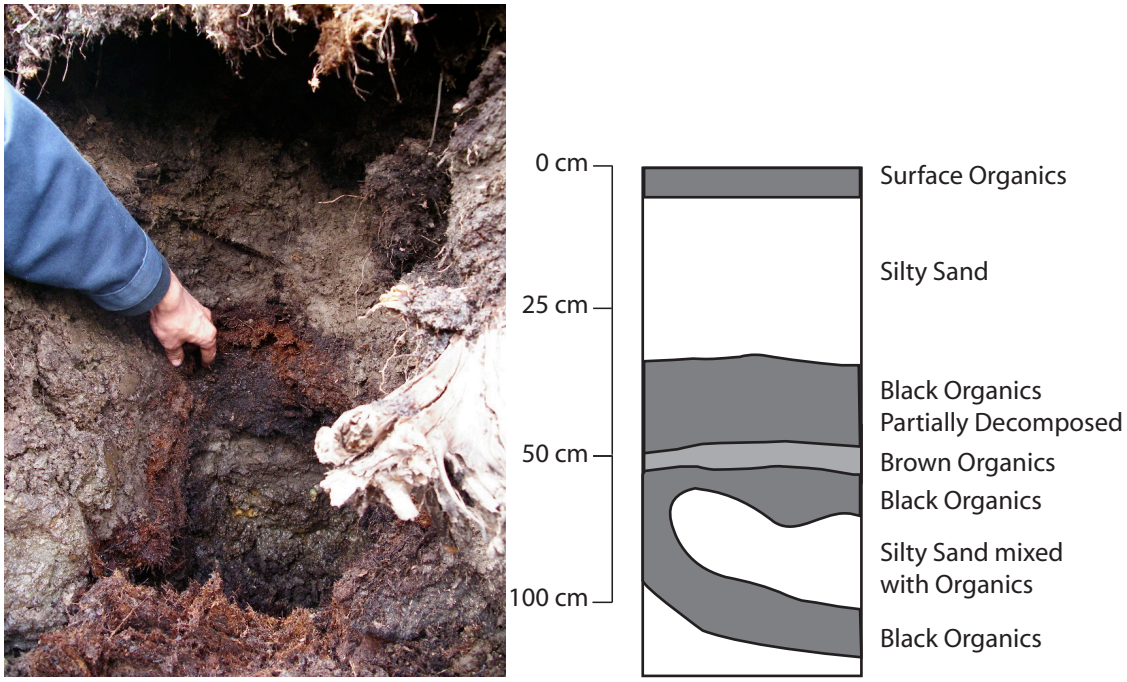

Figure 5.33: Buried Contorted Organic Material Overlain by Failure Debris. Lone Star Mine cut excavation. Entire section below organics frozen.

These observations and other reconnaissance-level observations made in the Big Creek area (62º30'26 N, 137º00'03 W), 250 km south of Steele Creek, all show that (a) detachment failure can occur repetitively in the same area, and (b) that the toe deposits from failure can be preserved in the stratigraphic record. In unglaciated areas of the Yukon, slopes may have been affected by forest fire hundreds to thousands of times during the Quaternary, raising the possibility that many slopes could exhibit stratigraphy affected by detachment failure.

Detachment Failures in the Literature

The Steele Creek detachment failures, which were flow-dominated in coarse, ice-poor soils, were not similar in this respect to others described in the literature. The skin flows described by Hardy and Morrison (1972) and McRoberts and Morgenstern (1974a, 1974b) in the Mackenzie Valley were often found on low-angled slopes and seated in fine-grained clayey material. All of the Steele Creek failures were on slopes greater than 19º and all but one occurred in coarse-gained colluvium. Dyke (2004) found that detachment failures near Thunder River, NWT, occurred on slopes with an average inclination of 13º. Leibman (1995) found that large detachment failures in Siberia occurred in sandy soils, as the sands were permeable enough to allow surface water to percolate down to the permafrost table and contribute to the loss of basal shear strength. In an infinite slope analysis by Dyke (2004), failures in saturated, purely frictional material were found to be possible at inclinations greater than 13º. In these cases loss of cohesion due to rapid rates of thaw in ice-rich ground was considered to be the cause of failure initiation.

Leibman (1995) found the majority of active layer failures observed occurred in concave slope sections, which were considered to be areas of concentration of strain. Stang et al. (1982) suggested that most failures were initiated along the upper and middle portions of a slope, with moisture content and inclination being the most important contributors to slope instability. The Steele Creek failures often occurred in the concave portions of slopes below a convex break of slope.

Tundra mudflows documented in Alaska by Sigafoos and Hopkins (1952) occurred when the surface vegetation mat could no longer hold back the viscous mass of super-saturated soil and colluvium. Weight and lubrication provided by interstitial water then destabilized the slope and allowed rapid downhill motion that may have had both sliding and flow components. However, these failures were seated in fine-grained materials.

Harris et al. (2008) found in centrifuge simulations of detachment failures that shear stresses only exceeded shearing resistance when thaw reached depths exceeding 0.6 m. Thaw depths at Steele Creek thermal stations had all exceeded this depth by mid July of 2006, regardless of their burn status, although burned locations thawed to this depth up to a month earlier than unburned locations. However, the mean failure depth was only 47 cm, with a bi-modal distribution showing a peak in failure frequency between 20 and 30 cm, as well as between 70 and 80 cm. The majority of the failures occurred at depths shallower than 60 cm, and all these occurred when the theoretical depth of thaw should have exceeded 60 cm. The liquefaction of soil as porewater pressures rose rapidly and upward seepage occurred after rapid thaw observed by Harris et al. (2008) appears to be a similar process to the high porewater pressures and liquefaction of soil observed in the Steele Creek failures.

Failure Mechanism

The detachment failures in Steele Creek occurred when the sub-surface mineral soil consisted of completely saturated coarse-grained material with low cohesion, the organic mat was weak on the break of slope but strong below and there was significant downslope stress. The saturated soil mass liquefied, as observed after the boulder in SC 03AB was agitated, and began to flow below the organic mat, which was elevated above, and detached from, the mineral soil. The largely intact organic layer was rafted overtop of the flowing, severely deformed soil beneath. When this movement generated enough shear stress on the organic material above, it sheared at the zone of stress concentration (break of slope) and produced the distinctive rectangular head-scarps. The detachment failures involve a combination of sliding and flowing beneath the surface organic mat.

These landslides appeared to have behaved as flows within unfrozen soils. The permafrost affected the failures by providing an aquiclude, which raised porewater pressures, and by supplying water released from the transient layer due to thermal disequilibrium caused by the forest fire. Supra-permafrost taliks elevated porewater pressures by concentrating groundwater flow. However, the permafrost table did not act as a failure plane.

In many locations, the organic mat was observed to have separated from the underlying mineral substrate. In these areas there was a 5-15 cm gap between the organic and mineral soil. Tree roots which were still anchored in the mineral soil supported the suspended organic mat. Near the headscarps of nearly all the failures tension cracks were observed with roots stretched across

them. These tension cracks were more common on convex breaks of slope. The breaks of slope are concentrations of strain. Near many of the failures, the organic mat was thinner near the headscarp but thicker downslope as a result of burning or pre-fire vegetation conditions.

The moving mass stopped when the slope gradient decreased, the water drained from the saturated mineral soil or more competent organic material was encountered. The maximum depth of the failure plane was also the maximum depth of saturated mineral soil. The drainage of the water from the soil as the mass slowed down produced the extensive outwash plumes that were visible downslope of the displaced masses.

Failures were similar in terms of length, width and width-to-length ratios when compared with other detachment failures reported from the Mackenzie Valley and Ellesmere Island. However, slope angle, depth of failure relative to the permafrost table and sediment properties were different. Fossil failures in the Steele Creek Valley and elsewhere in the Yukon point to detachment failure as an episodic process controlled by the incidence of forest fire.

Chapter 6: Forest Fire Thermal Impacts upon Permafrost

This chapter examines the impacts of forest fire on the active layer and upper permafrost. The Steele Creek sites provided complete thermal profiles from the air to 100 cm below surface (Table 6.1). Analysis of these profiles provided annual temperatures, temperature profiles, ground temperature envelopes, freezing and thawing degree days, n-factors and the thaw depth progression in 2005 and 2006. The Bishop Creek sites provided data on active layer depth changes from the fire season to two years later.

Steele Creek Thermal Results

Thermistors were placed in solar shields at 1.4 m above ground, buried 2 cm below the soil surface and at 25, 50, 75 and 100 cm depths. The following thermal profiles illustrate the differences between different aspects and burned/unburned terrain. Temperature envelopes and annual average temperatures spanned the time period from June 30, 2005-July 1, 2006 (see Chapter 3).

Ground Temperature Envelopes

Ground temperature envelopes are an indication of heat transfer into and out of the ground. For example, sites with high ground surface temperatures likely have less remaining insulation from the organic mat, and those with high or low temperatures at depth likely have soils with higher thermal conductivities. Ground temperature envelopes were determined by the coldest and warmest temperatures recorded at each thermistor from the time period spanning June 29, 2005- July 1, 2006 (Figure 6.1). At the north-facing burned site, the minimum temperatures were consistently 10˚C-15˚C warmer than the unburned north-facing site throughout the profile. Maximum temperatures at the north-facing burned site were greater at the surface, slightly less at 25 cm, and similar until the 100 cm depth, where both sites were identical.

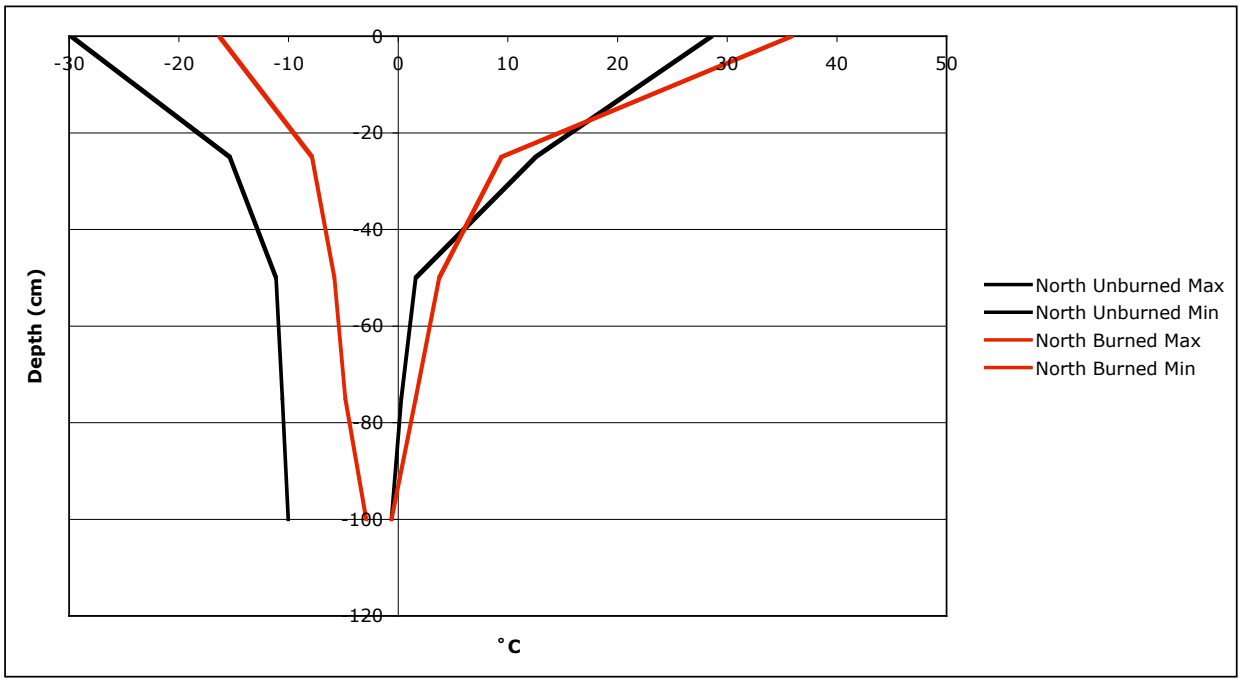

Figure 6.1: North ground temperature envelopes. June 29, 2005- July 1, 2006

At the south-facing burned site, minimum temperatures were roughly 10˚C higher at the surface than the unburned site, but then became approximately 5˚C cooler at depth (Figure 6.2). Maxi-

mum temperatures were consistently close to 10˚C warmer at the burned site throughout the profile.

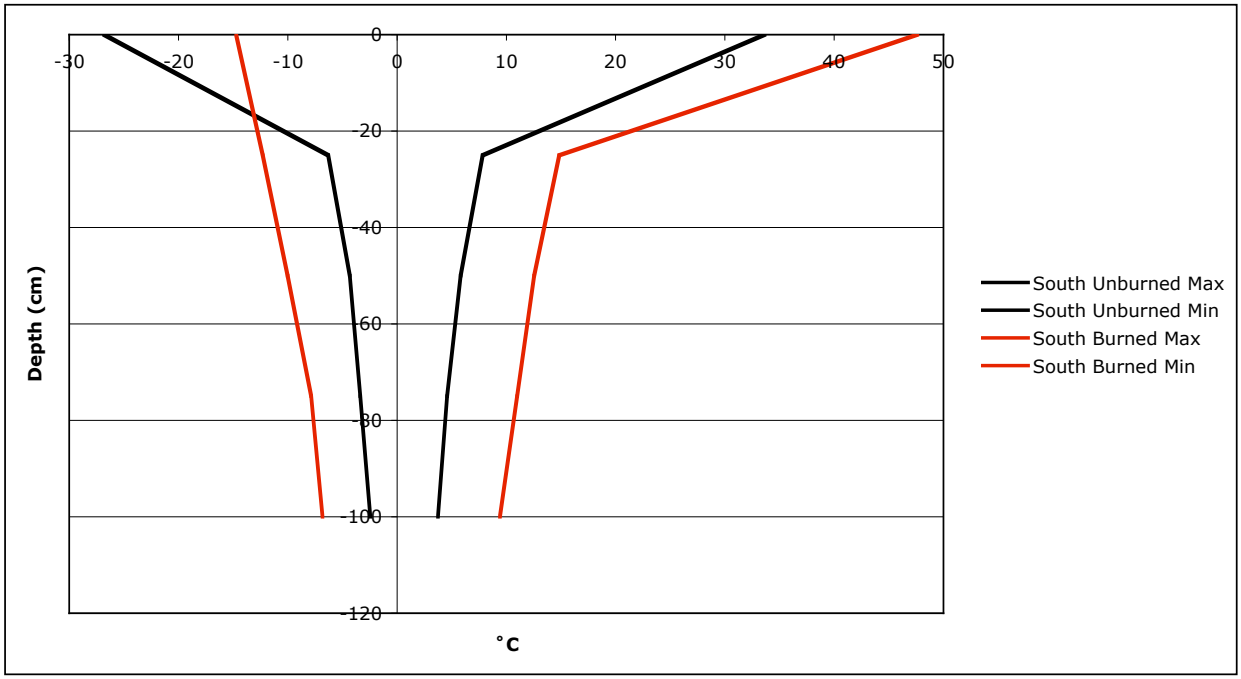

Figure 6.2: South ground temperature envelopes. June 29, 2005- July 1, 2006

The east and west facing sites had nearly identical minimum temperatures at the surface, but then diverged at depth, with the east-facing site achieving slightly lower temperatures at 100 cm (Figure 6.3). Maximum temperatures were over 10˚C higher at the west-facing site at the surface and identical at 25 cm depth, however, the east-facing site was over 5˚C at 100 cm depth. This may have been due to greater groundwater flow on the east-facing site which could have raised soil temperatures.

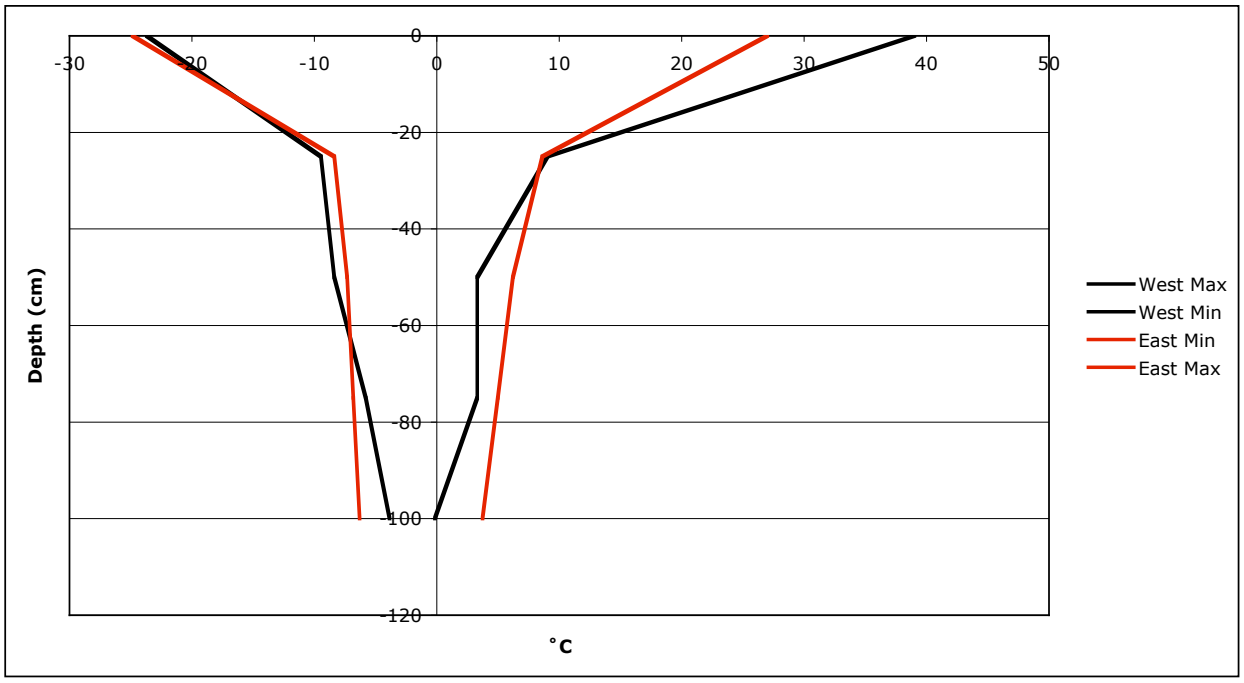

Figure 6.3: East and west ground temperature envelopes. June 29, 2005- July 1, 2006

Mean Annual Temperatures

Annual average air temperatures varied by up to 0.9˚C between sites with the lowest being -3.8˚C at the west-facing unburned site and highest being -2.9˚C at the south-facing burned site (Table 6.1). Mean surface temperatures were always higher than air temperatures and varied by up to 3.5˚C between 1.7˚C at the south-facing burned site and -1.9˚C at the north-facing unburned site. Four of the sites had permafrost, of which the north-facing unburned site was significantly colder throughout the thermal profile.

Table 6.1: Average Annual Temperatures (˚C) June 29, 2005- July 1, 2006

	Air	Surface	-25 cm	-50 cm	-75 cm	-100 cm	Perma-frost
South Burned	-2.9	1.7	1.1	1.1	1.2	1.0	No
South Unburned	-3.1	-0.3	0.5	0.5	0.4	0.4	No
North Burned	-3.1	1.2	0.2	-0.2	-0.6	-0.9	Yes
North Unburned	-3.4	-1.9	-2.6	-2.8	-2.9	-3.1	Yes
West Burned	-3.8	0.8	-0.2	-0.8	-0.9	-1.1	Yes
East Burned	-3.7	-0.3	0.0	0.0	-0.4	-0.6	Yes

The coldest site throughout the ground profile was the north-facing unburned site (Figure 6.4). The warmest site was the south-facing burned site. Below the surface the south-facing unburned site was the next warmest. East, north and west-facing burned sites had mean annual temperatures at or below 0˚C. At these sites permafrost was present beneath burned surface material.

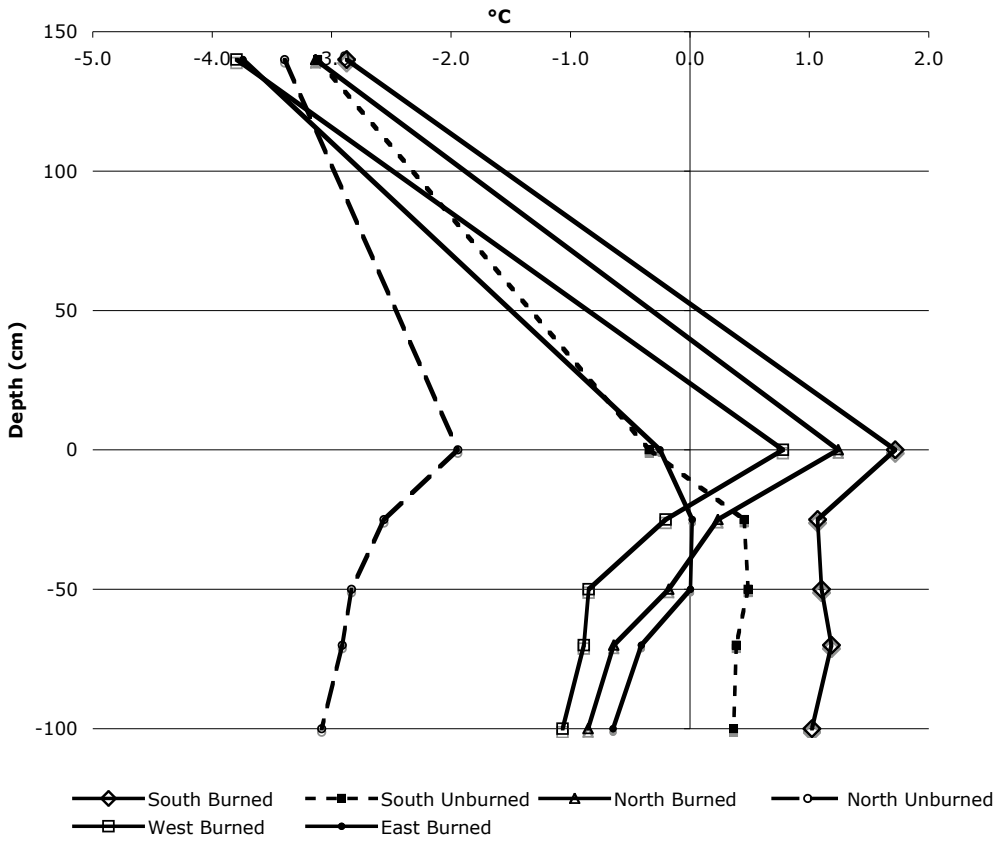

Figure 6.4: Mean Annual Thermal Profile. Mean annual values July 1, 2005- June 30, 2006. Note: Orientations shown are the directions that the slopes face. Interpolations were required for 10 of the 30 sensors for periods of up to 20 days (See Table 4.1). Straight lines between air and ground surface temperatures are to visually link air and ground temperatures for each site and do not imply linear trends.

At the south-facing sites the burned ground temperatures were an average of 0.8˚C warmer than unburned temperatures (Figure 6.5). There was an insignificant difference in air temperatures between the two sites, but the burned site was 2.1˚C warmer at the ground surface. This is attributed to the solar heating of the blackened mineral soil surface and lack of shading by vegetation. From the surface to 100 cm depth, the difference was constant at approximately 0.6˚C, indicating heat flow into deeper soil layers (Table 6.1). Neither of these sites had permafrost.

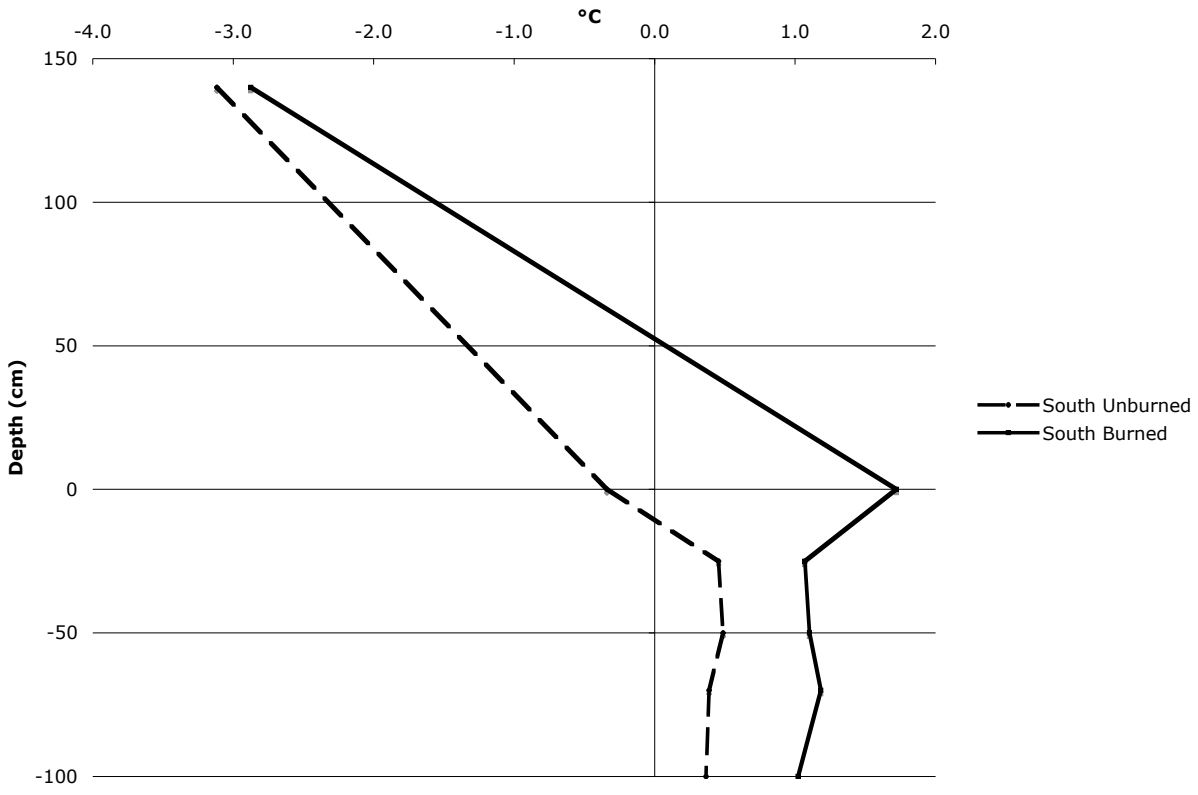

Figure 6.5: South-Facing Burned/Unburned Thermal Profile. Mean annual values July 1, 2005-June 30, 2006. Note: Averages include interpolated air and ground surface temperatures for the south-facing unburned site for May 28-June 5, 2006, and for July 1-11, 2005 for the 100 cm sensor at the same site. Straight lines between air and ground surface temperatures are to visually link air and ground temperatures for each site and do not imply linear trends.

At the north-facing sites the burned ground temperatures were an average of 2.2˚C warmer than unburned temperatures (Figure 6.6). Again, the air temperature differences were negligible (0.3˚C), but the difference at the surface was much greater (3.2˚C) than at the south-facing sites. The large temperature differences continue through the active layer and into the top of permafrost, where there was an average 2.6˚C difference between the burned and unburned sites (Table 6.1). The destruction of the thick organic mat at the north-facing burned site is likely responsible

for the large degree of thermal disturbance (2.2˚C) as compared with the south-facing sites (0.8˚C). The slight elevation in air temperatures at both north and south burned sites may have been due to sensible heat transfer from the warm, burned surface to near-surface air.

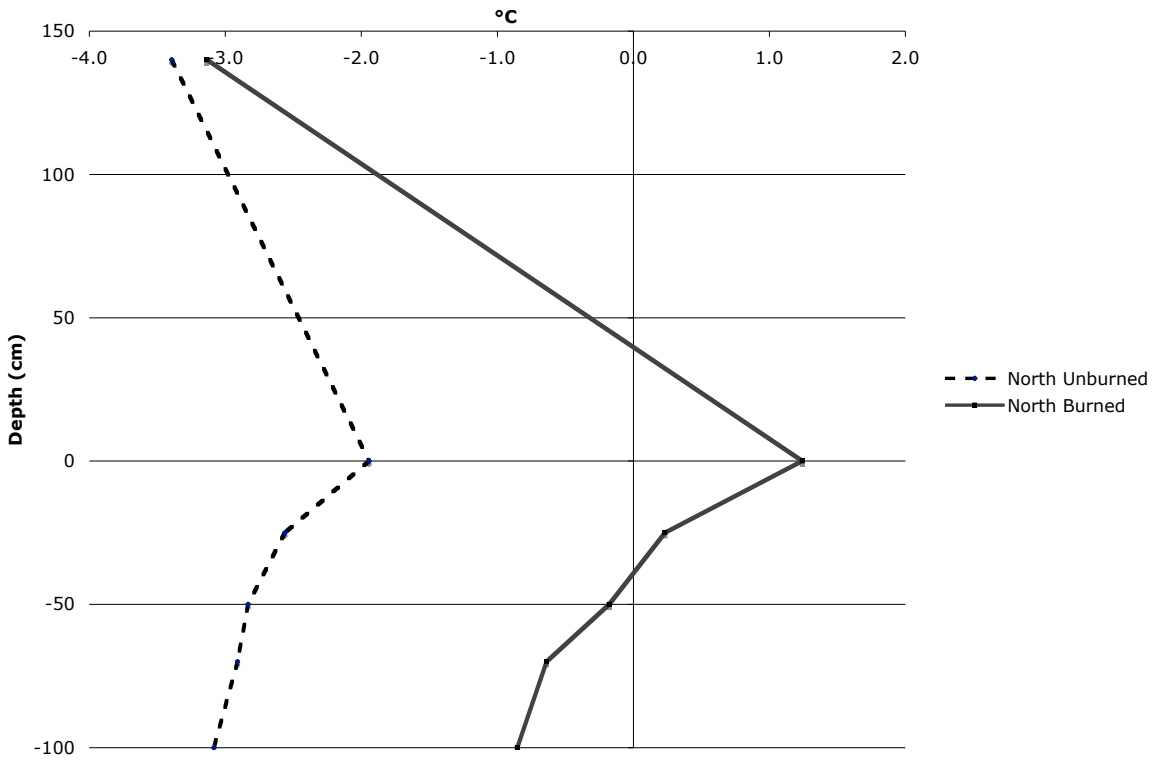

Figure 6.6: North-Facing Burned/Unburned Thermal Profile. July 1, 2005- June 30, 2006. Note: averages include interpolated temperatures for July 1-11, 2005 for the 100 cm sensor at both sites. Straight lines between air and ground surface temperatures are to visually link air and ground temperatures for each site and do not imply linear trends.

Thermal and Surface Offset

Thermal offset is the difference between mean annual surface temperature and temperature at top of permafrost (TTOP) and is representative of the impact of different frozen and thawed ground thermal conductivities (Romanovsky & Osterkamp, 1995; Riseborough, 2002; Karunaratne & Burn, 2003). In the case of seasonally frozen ground, the thermal offset was taken to be the dif-

ference between the temperature at the ground surface and 100 cm depth. Thermal offset (Figure 6.7) varied by 2.8˚C between sites, with the highest at the north-facing burned site (2.1˚C) and lowest at the south-facing unburned site (-0.7˚C). Burned sites had higher thermal offsets than their unburned counterparts and therefore had much warmer surface than TTOP temperatures. Thermal offset was highest at the north-facing burned site due to the presence of permafrost.

The thaw of transient layer permafrost may have served as a thermal buffer maintaining temperatures at the top of the permafrost table while solar energy absorbed at the soil surface raised active layer temperatures. The north-facing burned site soils were moist silts with no remaining organic material and a blackened surface. The moist active layer had a high specific heat capacity which modulated surface temperatures before they could reach the permafrost table. The south-facing sites and east-facing sites which had the lowest thermal offset had coarse-grained soils and little organic material remaining on the surface. These sites also had no permafrost or a deep permafrost table that allowed for rapid heat transfer into and out of the soil and a lower thermal offset as deeper soil layers adjusted quickly to surface temperatures. The south-facing unburned site was the only one with a negative thermal offset as its surface was cooler than deeper soil layers.

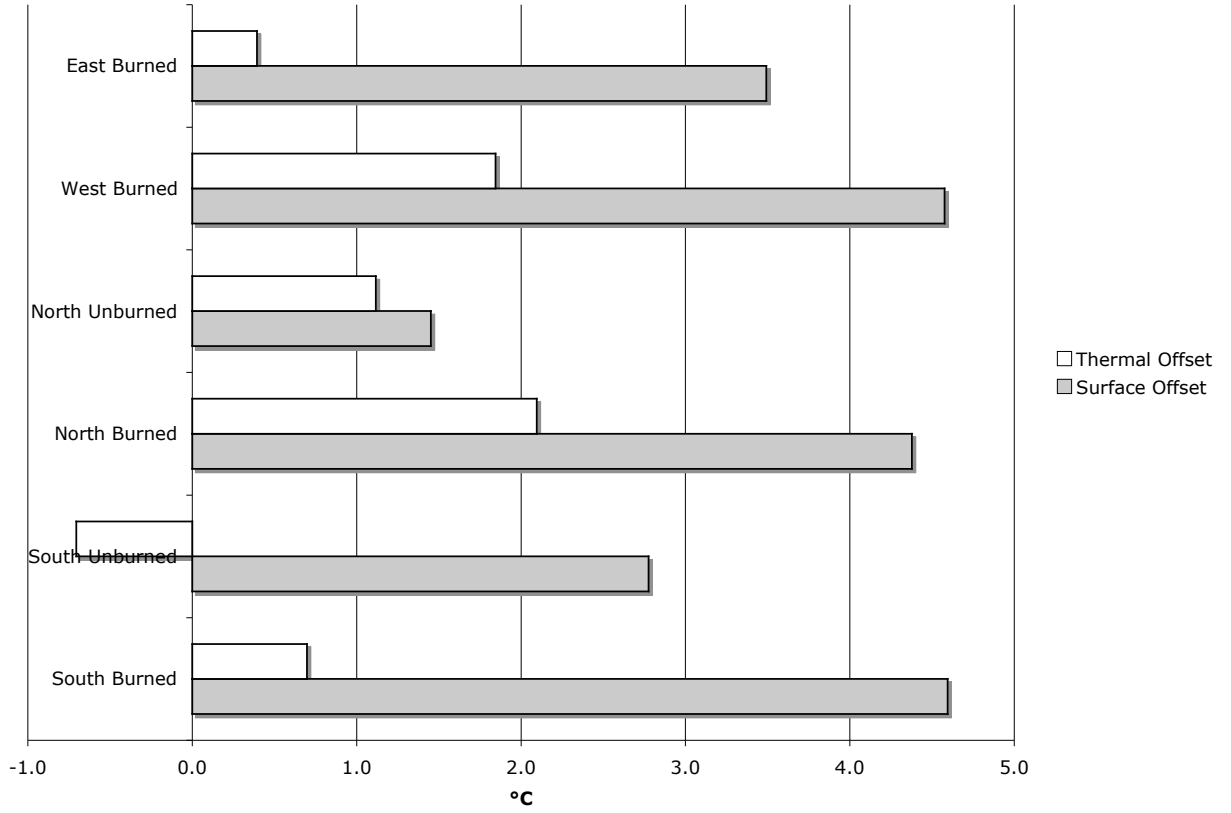

Figure 6.7: Thermal and Surface Offsets. July 1, 2005- June 30, 2006. Note: Thermal offset calculated to a fixed depth of 100 cm. Interpolations were required for the south-facing unburned air and surface sensors (28 May-June 5, 2006), the east-facing site and ground surface sensors (June 5-30, 2006) and the 100 cm deep sensors for all but the south-facing burned site (July 1-11, 2005) (see table 4.1)

Surface offset is the gap between mean annual surface and air temperatures and is controlled by surface characteristics such as vegetation, snow cover and moisture availability (Oke, 1978; Eaton et al., 2001; Beltrami & Kellman, 2003; Karunaratne & Burn, 2003). Surface offset (Figure 6.8) varied by 3.1˚C between sites, with the highest at the south and west-facing burned sites (4.6˚C) and lowest at the north-facing unburned site (1.5˚C). Burned sites had a significantly higher surface offset than corresponding unburned sites. The north and south-facing unburned sites, which were the only sites with intact vegetation canopies, had the lowest values. North,

south and west-facing burned sites had similar values, close to 4.6˚C, with the east-facing site slightly lower, at 3.5˚C. At these burned sites, the surface temperatures were much higher than the air temperatures due to solar heating of the surface in comparison to the relatively stable air temperature. Burned sites had higher surface offsets due to solar heating of the ground surface and lack of insulating vegetation. Differences between values for burned sites are due to variability in snow depths and between unburned sites to the insulating value of different vegetation types.

Degree Days

Thawing degree days (TDD) were calculated by taking the average daily temperature of every day when the average temperature was above 0°C, then adding together all such days over a one year period. Freezing degree days (FDD) used the same process for days when the average temperature was lower than 0°C. All of the sites had similar air TDD, between 1550 to 1700. The south-facing sites had the greatest number of TDD and the north-facing sites had the fewest. There was no significant difference between burned and unburned north-facing sites, and the south-facing burned site had slightly higher values than the corresponding unburned site.

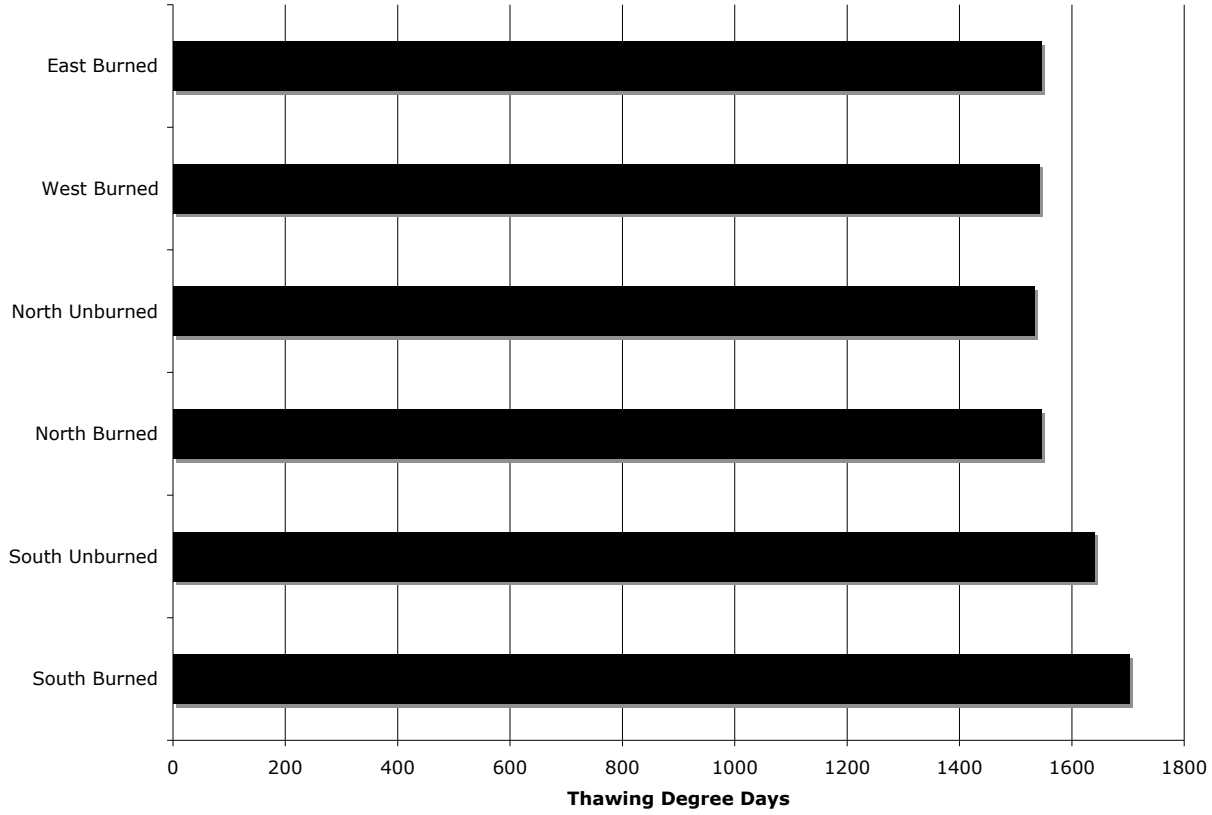

Figure 6.8: Air Thawing Degree Days. July 1, 2005- June 30, 2006. Interpolations were required for the south-facing unburned site (28 May - June 5, 2006) and the east-facing site (June 5-30, 2006) (see Table 4.1).

Ground TDD were greater at the burned sites when compared with corresponding unburned sites (Figure 6.9). The greatest number of ground TDD was at the south-facing burned site. The south-facing unburned site and north-facing burned site had nearly identical ground TDD. The west-facing and east-facing burned sites were similar, with the west-facing burned site 100 TDD higher. The lowest ground TDD was at the north-facing unburned site. The high values at the south-facing site are likely due to the greater insolation received upon the blackened mineral soil. Low values at the north-facing unburned site are due to shading by the coniferous vegetation canopy, northerly aspect and thick, insulating organic mat. High ground TDD may lead to to slightly higher air TDD due to sensible heat transfer from the soil into the air.

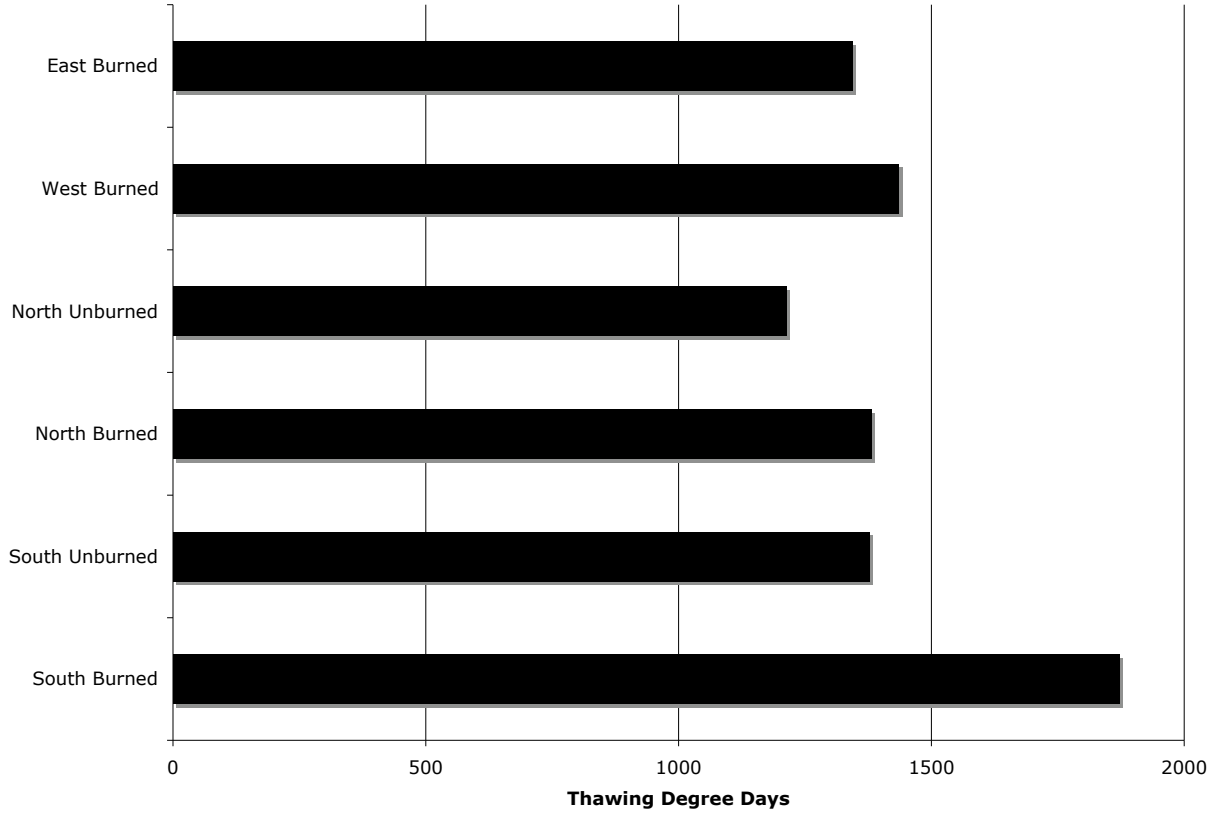

Figure 6.9: Ground Thawing Degree Days. July 1, 2005-June 30, 2006. Interpolations were required for the south-facing unburned site (28 May -June 5, 2006), and the east-facing burned site (June 5-30, 2006) (see Table 4.1).

Air freezing degree days were similar at the north- and south-facing sites (Figure 6.10) but the east- and west-facing sites which had nearly identical air FDD were higher than all of the others. This may have been due to cold air drainage in the main Steele Creek valley. The unburned sites had slightly, but not significantly, more air FDD than corresponding burned sites or greater long-wave radiation loss in the wider valley. The slightly lower FDD values at the burned sites are due to freeze-up occurring roughly a week later at these sites when compared to corresponding unburned sites.

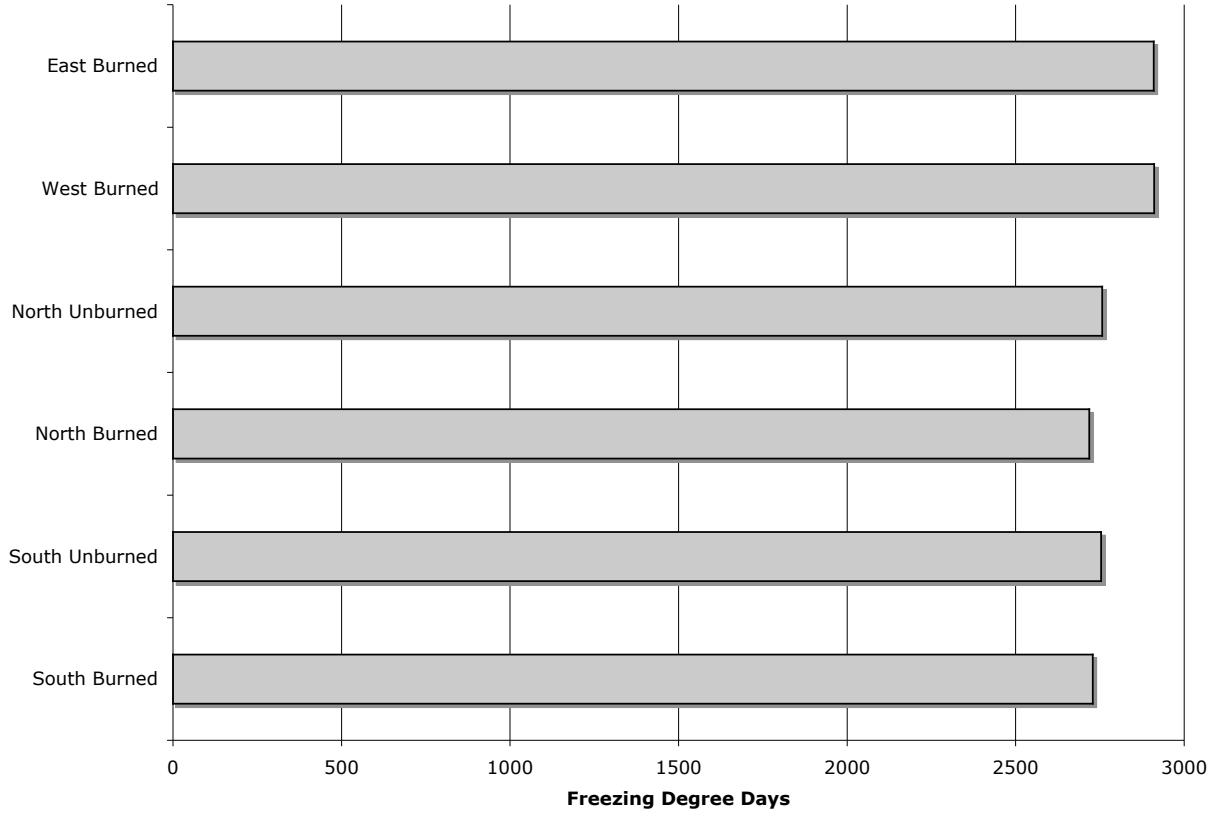

Figure 6.10: Air Freezing Degree Days. July 1, 2005- June 30, 2006.

The variability of ground FDD was higher (~480 FDD) than any of the other thawing or freezing indices (Figure 6.11). Ground FDD were greatest at the north-facing unburned site and were higher at unburned sites than burned sites. The difference between the east and west-facing sites may have been due to snowcover variability, as the west-facing site was in a lee slope in the valley bottom where snow could accumulate, lowering the ground FDD, while the east-facing site was exposed and higher up a slope where wind scour could reduce the snowpack and increase FDD. The north-facing burned site had the lowest number of freezing degree days and was also in a lee slope near the valley bottom, where it may have been subject to deep snow accumulation.

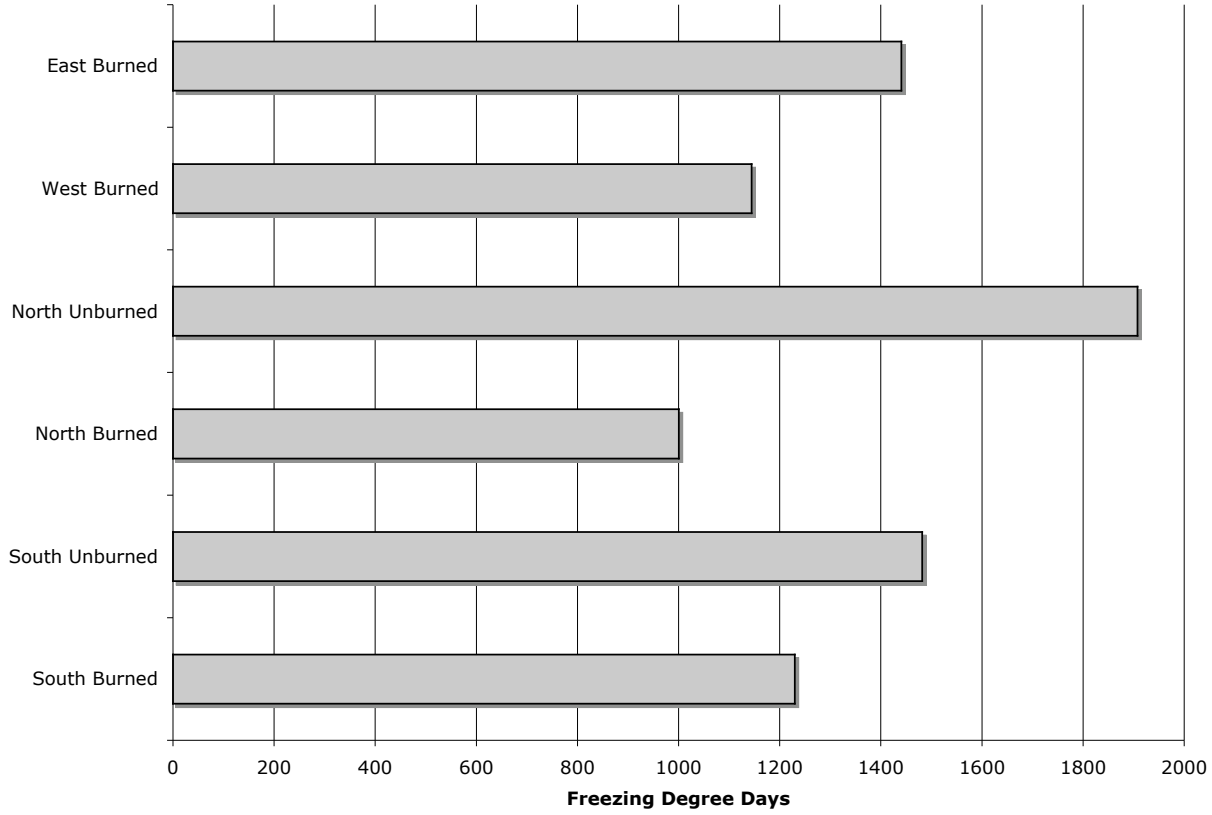

Figure 6.11: Ground Freezing Degree Days. July 1, 2005- June 30, 2006.

N-Thawing Factor

The n-factor summarizes the surface energy balance by comparing the ratio of ground freezing or thawing indices to air freezing or thawing indices (Karunaratne & Burn, 2003). It is calculated by dividing the ground surface thawing or freezing degree days by the air thawing or freezing degree days. N-thawing (nt) is controlled by near-surface thermal duffusivity which is influenced by vegetation shading and insulating organic layers. All of the burned sites had higher nt values than the unburned sites (Figure 6.12). The unburned north and south-facing sites had nt values lower than the corresponding burned sites. The highest nt values of 1.1 were found at the south facing burned site, which had little remaining vegetation and blackened mineral soil sur-

face. The north facing burned site had the lowest nt values (0.8) due to its intact, mossy organic mat and unburned coniferous tree canopy. The west-facing burned site had slightly higher values than the east-facing site, although both were similar to the north-facing burned site (0.9). All of the burned sites had higher nt values than the two unburned sites. Burned sites with permafrost had similar values regardless of orientation. Shading by vegetation reduced surface temperatures, lowering nt values while bare ground and especially dark surfaces have the highest nt values (Klene et al., 2001). Sites in the Mackenzie Valley and Alaska with thick organic layers have shown lower nT values than those with thin organic layers (Taylor, 1995; Klene et al., 2001).

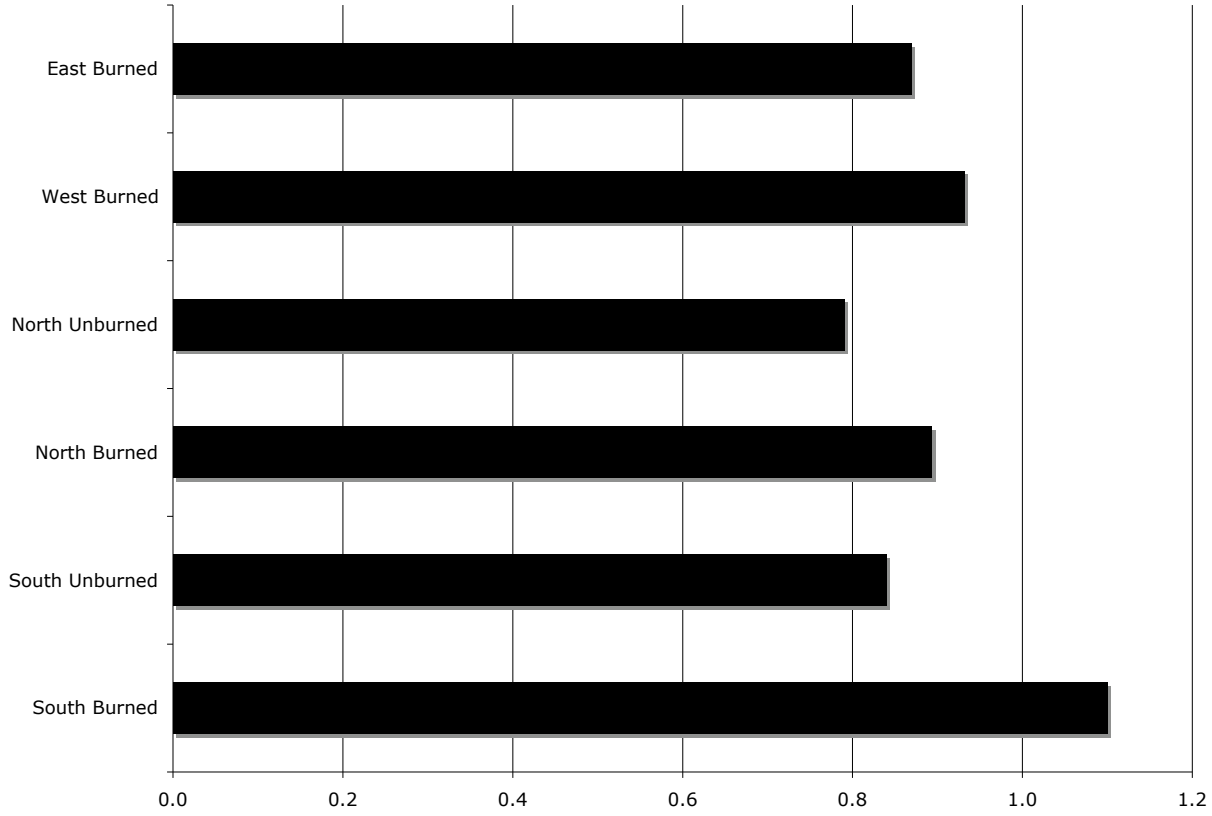

Figure 6.12: N-Thawing Factor. July 1, 2005- June 30, 2006. Interpolations were required for the south-facing unburned air and surface sensors (28 May -June 5, 2006), the east-facing air and ground surface sensors (June 5- 30, 2006) (see Table 4.1).

N-Freezing Factor

N-freezing (nf) describes the energy balance during the freezing season, and is most affected by snow depth. Where there is similar snow cover at different sites, the presence or absence of permafrost determines nf values through the release of latent heat as the active layer freezes (Karunaratne & Burn, 2003). In Steele Creek there was no snow cover data, and results may have been dependent upon variable distribution and thickness of snowcover. Both unburned sites had much higher nf values than their burned counterparts (Figure 6.13). This difference was most striking at the north-facing sites where the unburned site had nearly double the nf value of the burned site. As both sites had permafrost, similar active layer depths and similar soils, latent heat release during freeze-up was probably not responsible for the low north-facing burned values. Due to the lack of snow depth data for the sites, it is impossible to determine if the low north-facing burned values are due to deeper snow cover or other factors. Sites with permafrost did not necessarily have higher nf values than those without permafrost.

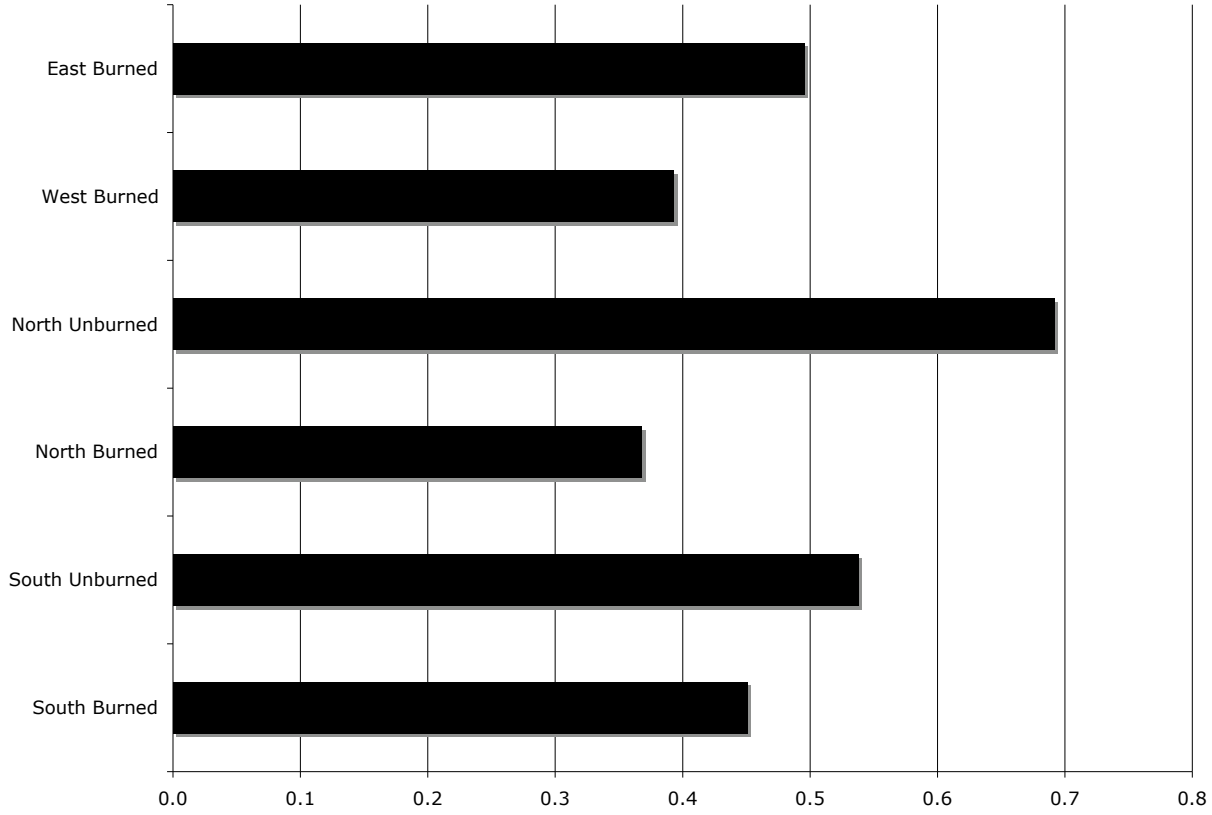

Figure 6.13: N-Freezing Factor. July 1, 2005- June 30, 2006.

Active Layer Thaw and Freeze-Back

The following figures show the impact of fire on freezing and thawing of the active layer in permafrost and non-permafrost terrain as well as freezing and thawing patterns relative to orientation. The 0°C isotherm was used to show freezing, although the actual phase change in the coarse soils of Steele Creek may have been -0.1°C colder. The 5, -2 and -4°C isotherms show the relative soil thawing and freezing at each site.

North-Facing Sites

At the north-facing sites permafrost was present, and the active layer froze completely (Figures 6.14; 6.15). In 2005 the active layer reached a maximum depth of 92 cm at the burned site, but only 80 cm at the unburned site. In 2006 thaw reached 100 cm at both sites. Winter cooling was deeper at the unburned site, with the entire active layer below -4°C from January to March. At the burned site the entire active layer was never below -4°C during the winter of 2006.

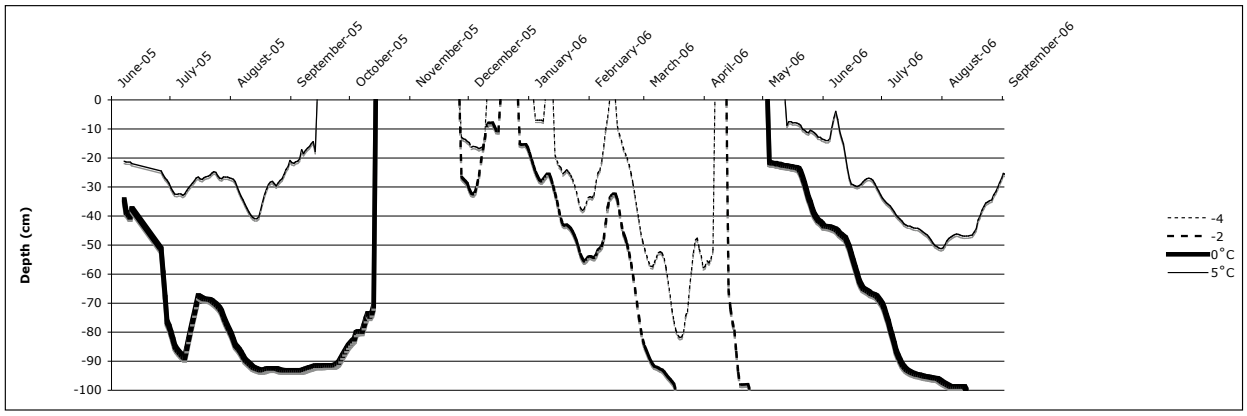

Figure 6.14: North-Facing Burned Site Isotherms. Isotherms were interpolated between measurement depths of 2 cm, 25 cm, 50 cm, 75 cm, 100 cm.

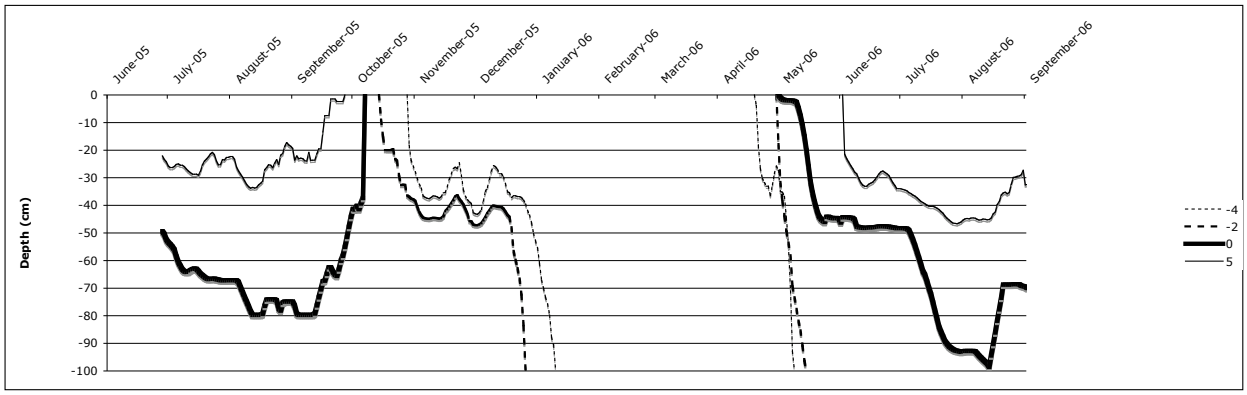

Figure 6.15: North-Facing Unburned Site Isotherms. Isotherms were interpolated between measurement depths of 2 cm, 25 cm, 50 cm, 75 cm, 100 cm.

South-Facing Sites

The south-facing burned site was warmer than the south-facing unburned site during the summer and cooler during the winter (Figure 6.16; 6.17). The entire soil layer to 100 cm was above 5°C at the burned site during both summer seasons. At the unburned site the entire soil layer to 100 cm never warmed above 5°C. During the winter the entire soil layer to 100 cm at the burned site was below -4°C from February until April, but at the unburned site the -4°C isotherm did not penetrate below 60 cm. Thaw and freeze-up patterns of the 0°C isotherm are similar at both sites, but the burned site began thawing slightly earlier and began freezing later than the un-burned site. The deeper freezing of the burned site was due to the lack of vegetation and hence, insulation. The exposed location of the site may also have made it prone to wind scour, which would have reduced snow pack thickness and aided cooling.

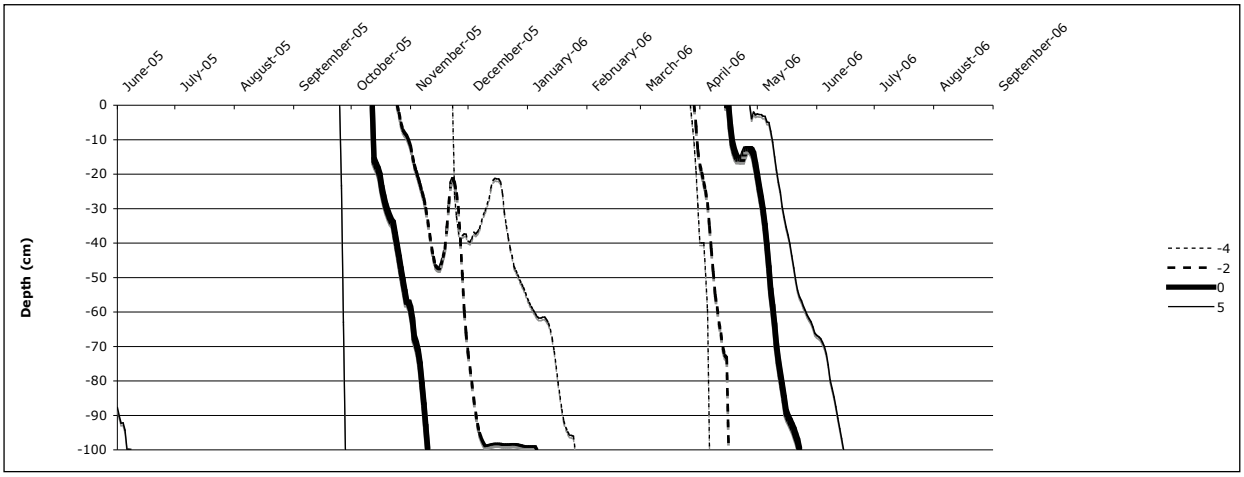

Figure 6.16: South-Facing Burned Site Isotherms. Isotherms were interpolated between measurement depths of 2 cm, 25 cm, 50 cm, 75 cm, 100 cm.

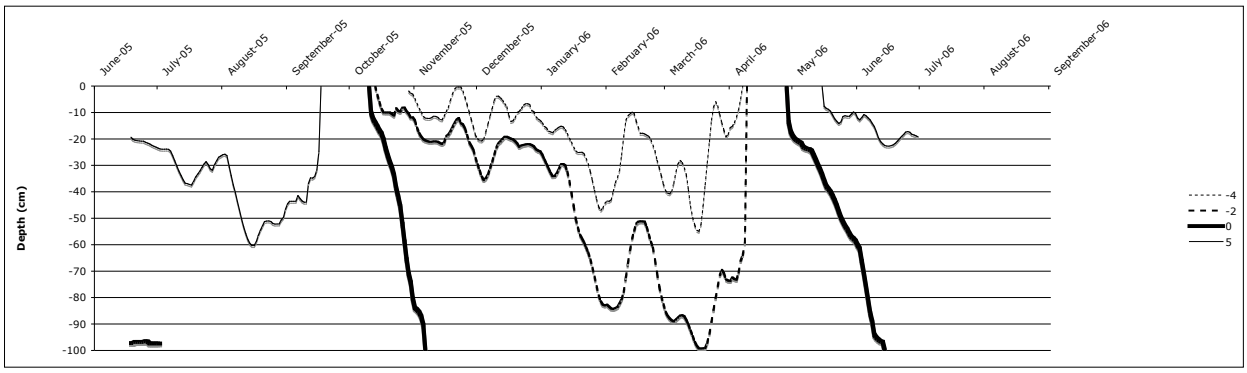

Figure 6.17: South-Facing Unburned Site Isotherms. Data not available after July 1, 2006. Isotherms were interpolated between measurement depths of 2 cm, 25 cm, 50 cm, 75 cm, 100 cm.

Comparison of Burned Sites

The west-facing site (Figure 6.18) thawed 20 cm deeper in 2006 than 2005, and had a considerably warmer active layer during the winter than the east-facing site (Figure 6.19). The east-facing site thawed to below the 100 cm depth of the lowest sensor. The active layer at the east-facing site was warmer in the summer but similar in the winter to the west-facing site. This may have been due to snow accumulation at the west-facing site. Groundwater which was observed moving through the active layer at the east-facing site may have been responsible for the elevated

summer temperatures. The south-facing burned site (Figure 6.20) was warmer during the summer but colder during the winter than the north-facing site (Figure 6.21). This may be due to snow accumulation at the north-facing site and deeper thaw. Thaw at the north-facing burned site was deeper in 2006 than 2005.

Prevailing winds in the Steele Creek region are from the west, but the valley channels air flow down from the south. The north-facing burned site and west-facing site were located in lee slopes where deeper snow accumulation due to drifting may have occurred. This may explain the low ground freezing values relative to air freezing values at these sites.

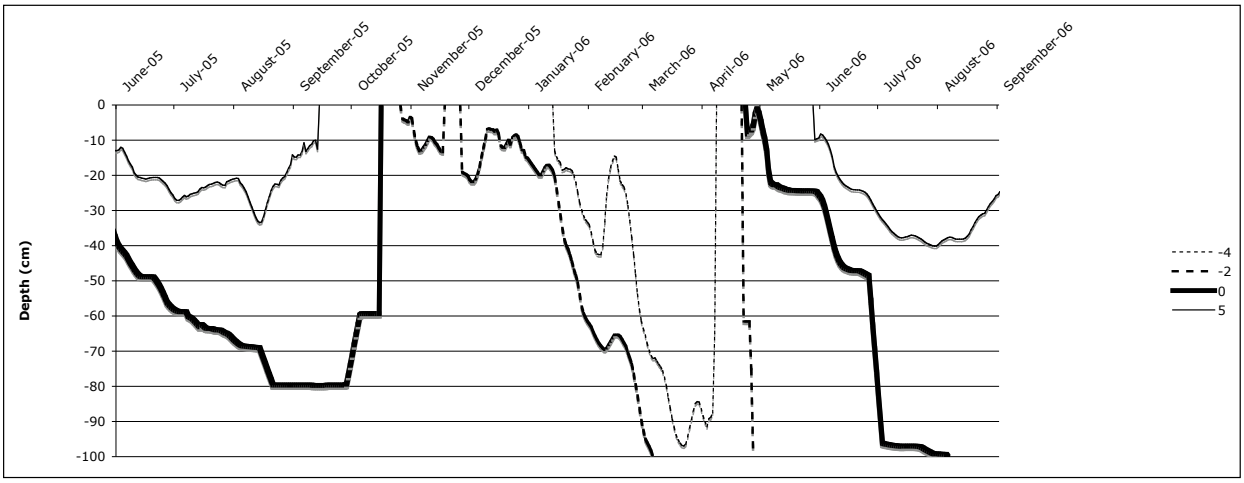

Figure 6.18. West-Facing Burned Site Isotherms. Isotherms were interpolated between measurement depths of 2 cm, 25 cm, 50 cm, 75 cm, 100 cm.

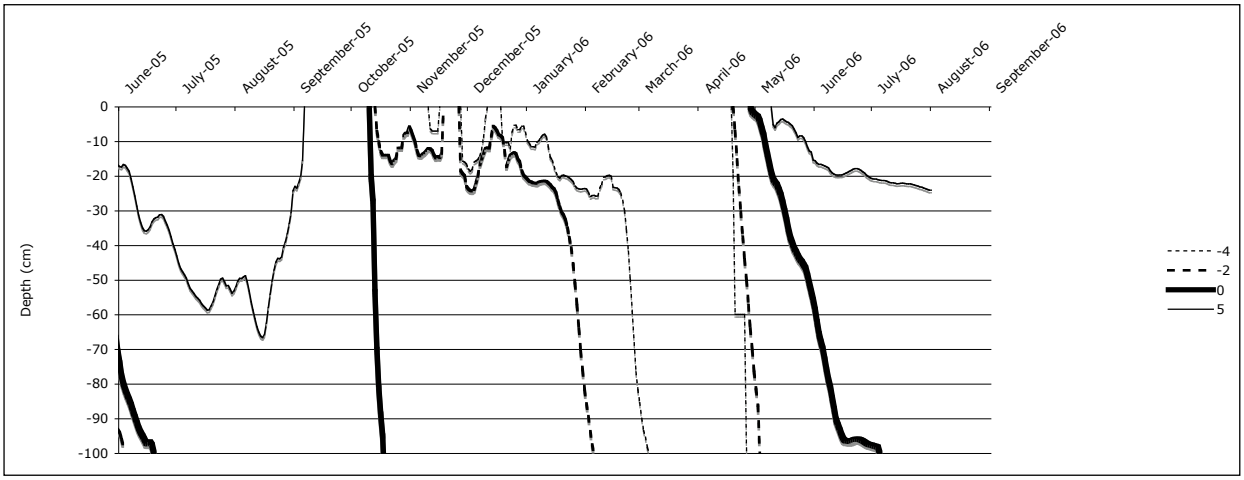

Figure 6.19: East-Facing Burned Site Isotherms. Isotherms were interpolated between measurement depths of 2 cm, 25 cm, 50 cm, 75 cm, 100 cm.

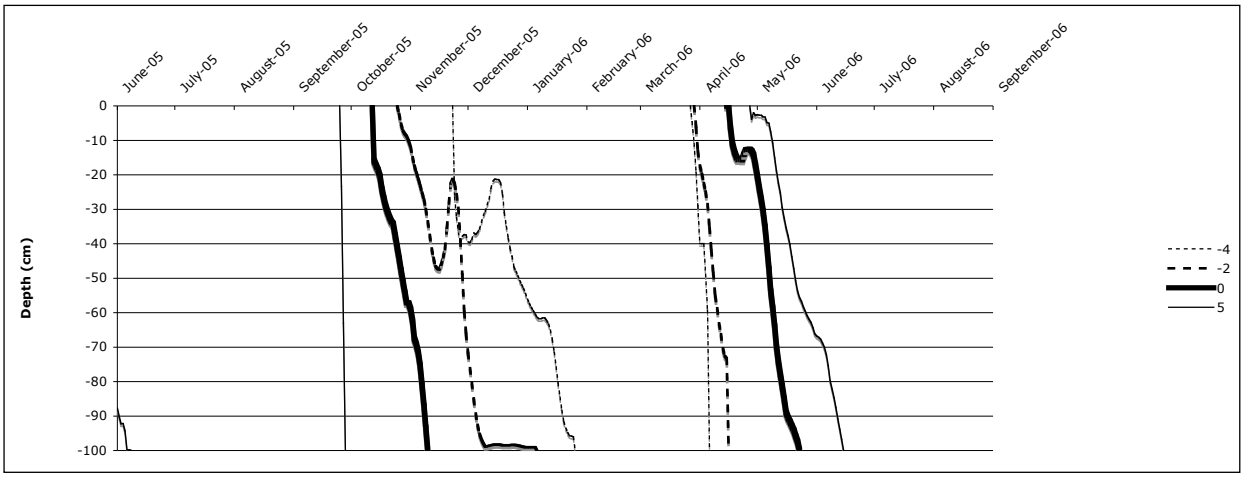

Figure 6.20: South-Facing Burned Site Isotherms. Isotherms were interpolated between measurement depths of 2 cm, 25 cm, 50 cm, 75 cm, 100 cm.

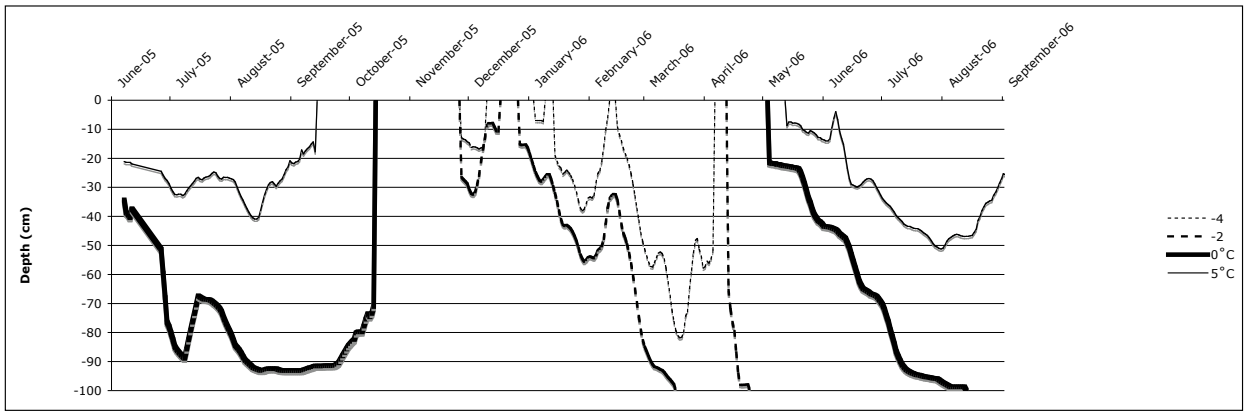

Figure 6.21: North-Facing Burned Site Isotherms. Isotherms were interpolated between measurement depths of 2 cm, 25 cm, 50 cm, 75 cm, 100 cm.

Surface thawing at the sites in 2006 began first at the south-facing burned and unburned sites in late April, followed by the west-, north- and east-facing burned sites in early May, and the north-facing unburned site in mid-May (Table 6.2). The active layer at the permafrost sites was thickest on the east-facing slope (~170 cm in 2005 and >200 cm in 2006) and thinnest on the north-facing unburned slope (~80 cm in 2005 and ~100 cm in 2006 - possibly influenced by local retrogression of a slope failure downslope (see pp. 44)).

Table 6.2: Dates and Types of Active Layer Freezing Processes.

	Start Thaw (2006)	Start Freeze-up (2005)	Cryotic Active Layer	Type of Freezing	Active Layer Depth (2005-2006)*
North Burned	May 4	October 6	October 15	Bi-directional	92 cm; 105 cm
North Unburned	May 13	September 15	October 15	Bi-directional	83 cm; 98 cm
South Burned	April 21	October 14	November 8 (to 100cm)	Unidirectional	Seasonal Frost >100 cm
South Unburned	April 22	October 14	November 3 (to 100 cm)	Unidirectional	Seasonal Frost >100 cm
West	May 2	October 1	October 15	Bi-directional	85 cm; 107 cm
East	May 6	October 14	November 21	Unidirectional	168 cm; >200 cm

* calculated from ground temperatures

Changes in Thaw Depths

At Bishop Creek, the depth of the permafrost table lowered on average by 18 cm from September of 2004 to September of 2006 in the burned valley bottom site (Table 6.3). In the adjacent unburned half of the transect there was a decrease of 1 cm. Similar results were obtained for an east-facing slope but the calculated thaw depth increase of 20 cm between 2004 and 2006 is a minimum because almost all of the readings taken in the latter year were deeper than the 115 cm length of the probe rod. A depth of 115 cm was substituted in calculations where the rod did not reach the permafrost table. The adjacent unburned region had increased by 1 cm. The east-facing site had a much deeper active layer than the valley bottom, both in burned and unburned sections.

Table 6.3: Permafrost Table Depths, Bishop Creek.

Site	September 2004			September 2006			Average Change 2004-2006 (cm)
	n	Avg. (cm)	S.D (cm)	n	Avg. (cm)	S.D. (cm)	
Unburned Valley Bottom	17	49	13	17	50	8	+1
Burned Valley Bottom	19	50	10	19	68	9	+18
Unburned East-facing Slope	16	85	8	16	84	13	-1
Burned East-facing Slope	15	94	10	15	114 [a]	N/A	+20 [a]

[a] Minimum value assuming all >115 cm depths are equal to 115 cm

A difference of means test was undertaken for the valley bottom site where both data sets were complete. This showed that thaw depths were not statistically different between burned and unburned sites in the valley bottom in 2004 but had become statistically different by 2006. Unburned thaw depths were not statistically different between 2004 and 2006. The burned sites were statistically different between 2004 and 2006. It is worth noting that thaw depths in 2004 would have already been affected by the fire some two months earlier which suggests that the control section (unburned) was naturally warmer than the burned part of the transect. However, this difference was slight enough not to be statistically significant. At the east-facing site burned thaw depths were already statistically different from unburned in 2004, and the difference increased to at least 30 cm by 2006. Unburned thaw depths were not statistically different in 2004 and 2006.

Discussion

Freezing Season

At the Steele Creek north and south-facing sites, there was significant difference between burned and unburned midwinter temperatures at 50 cm depth at both the north and south-facing sites. However, these differences were not consistent. The north-facing burned site was warmer than its corresponding unburned site, while the south-facing burned site was colder than its corresponding unburned site. Since only one site was monitored on each aspect and condition, it is not know to what degree these observations are site-specific. Burn (1998) found very little difference between burned and unburned areas near Whitehorse, Yukon at a 50 cm depth in midwinter when both areas were covered by a similar snowpack while Yoshikawa et al. (2003) found a ground surface temperature difference between burned and unburned areas that persisted until the active layer was completely frozen in central Alaska. The north-facing sites had permafrost while the south-facing sites did not, which may have affected the active layer temperatures. With no snow depth data it is impossible to determine the impact of fire on the different sites during the winter. However, air freezing degree days were nearly identical for all sites. Differences in ground freezing degree days and nf values were due to variability in snow depths, latent heat released during the freezing of the active layer and timing of thaw and freeze-up (Taylor, 1995; Burn, 1998; Riseborough & Smith 1998; Karunaratne & Burn, 2003). Air freezing degree days in Steele Creek did not vary greatly in comparison with thawing degree days. This is opposite to Yoshikawa et al., (1998, 2003) who found that the number of thawing degree days did not vary greatly in comparison with freezing degree days in similar burned terrain in central Alaska. In Steele Creek bi-directional freezing was observed at sites where average TTOP values were ~-

1°C. Mackay (1981) stated that bi-directional freezeback should occur only in cold permafrost below -3°C.

Thawing Season

Air TDD were almost the same at the north-facing burned and unburned sites and slightly higher at the south-facing burned than the corresponding unburned site. These differences were accentuated at the ground surface, and ground TDD were 14% higher at the north-facing burned site and 36% higher at the south-facing unburned site than their respective unburned counterparts. The degree of difference is less than the doubling of TDD found in a black spruce forest after fire by Van Cleve & Viereck (1983). Thaw depth increases in Bishop and Steele Creek were similar to (although at the lower end of the scale) others in the literature for forested regions of the Yukon, Alaska and the N.W.T. (Table 6.4).

Table 6.4: Thaw Depth Increases after Fire in Boreal Forest Locations.

	Area	Thaw Increase (cm)	Thaw Increase (%)
Mackay, 1971	Inuvik, N.W.T.	24.1 (1st year), 34.8 (2nd year)	49%, 71%
Lotspeich et al., 1970	Eastern Alaska	0	
Wein, 1971	Interior Alaska		15-20%
Brown et al., 1969	Alaska		40-60%
Heginbottom, 1971	Northwest Canada	9	
Viereck, 1982	Fairbanks, Alaska		61% (2a)
Bishop Creek	Yukon	20 (2a)	21-36% (2a)

The freeze-back of the north-facing burned site was later and thawing more rapid than that of the north-facing unburned site, similar to observations by Burn (1998) near Whitehorse, Yukon. Viereck (1982) noted that burned active layers froze completely up to a month after corresponding unburned active layers. In Steele Creek the north-facing burned active layer became cryotic at the same time as the north-facing unburned active layer. However, there was a delay of three weeks between when the unburned north-facing active layer became entirely cryotic and when the 0°C isotherm reached 100 cm in the burned south-facing active layer.

The lowest temperatures, nt values and TDD were all found at the north-facing unburned site. Shading by vegetation and insulation by moss and organic material lower surface temperatures, nt values and ground TDD (Taylor 1995; Walker et al., 1994). Conversely, the highest temperatures, ground TDD and nt values were at the south-facing burned site, where no vegetation or organic material was left on the blackened mineral soil. This is in agreement with findings in Alaska (Klene et al., 2001), Mackenzie Valley (Taylor, 1995) and central Yukon (Karunaratne & Burn, 2003) that low thermal diffusivity organic soil thickness is inversely correlated with nt. High nt values (>0.85) were observed at all of the burned sites in Steele Creek where this material had been removed.

Conclusions

The average annual air and ground temperatures were roughly ordered in accordance with their aspect and burn status, with north-facing/unburned sites cooler, south-facing/burned sites

warmer, and east- and west-facing sites in between. The order of processes (thawing direction) was SB, SU, W, NB, E, NU, and (freezing direction) NU, W, NB, E, SU, SB. In general northerly-facing and unburned sites began to thaw later, refreeze earlier and were cooler throughout the soil profile than southerly-facing and burned sites. There was a three-week plus gap between the earliest and latest sites to thaw, begin freezing up and became completely cryotic. Mean surface temperatures were warmer than air temperatures at all sites and much warmer at burned sites in comparison with unburned sites of the same aspect. Burned permafrost sites had similar thaw and freezing processes regardless of aspect. Thaw was deeper in 2006 than 2005 at all sites with permafrost. The thermal difference between burned and unburned sites was greater at the north-facing than south-facing sites. Vegetation at unburned sites reduced thawing and maintained cool surface temperatures. Air temperatures varied little in comparison with ground temperatures. Small variations in air temperatures between burned and unburned sites were likely the result of sensible heat transfer from the surface during the thaw season. Ground thawing varied more between sites than freezing and was greater at burned than unburned sites.

Snow accumulation may have reduced freezing at the north-facing unburned site and west-facing site, resulting in lower ground freezing at these sites than would be expected from air freezing. Bi-directional freezing was observed at all sites with permafrost, except the east-facing burned site, despite TTOP values as high as ~-1°C. This permafrost can be classified as climate-driven, ecosystem-protected (Shur & Jorgensen 2007). Thaw in burned areas may continue indefinitely, or surface temperatures may stabilize once sufficient vegetation has colonized the sites to provide shade and cool the ground surface.

The thaw of permafrost beneath burned terrain by up to several decimeters would have resulted in the release of water from transient layer ice, providing the high porewater pressures necessary for the landslides examined in Chapter 5. The detached organic mat observed in Chapter 5 may have been the result of a combination of ground subsidence due to permafrost thaw and destruction of root structures. A supra-permafrost talik may be in the process of development at the east-facing site. Resistivity imaging data shows a similar talik beneath a detachment failure approximately 50 m from the site. (Chapter 7). Concentrated groundwater flowing through supra-permafrost taliks contributed to slope instability and elevated porewater pressures.

Chapter 7: Resistivity Investigation of Steele Creek

The locations of resistivity transects are shown in Figure 4.2.

North-South Transect

The north-south transect ran across the tributary creek valley from the south-facing burned logger to the north-facing burned logger (Figure 7.1). The raw resistivity inversion from the transect is displayed in Figure 7.2. The interpretation of the image data is presented in Figure 7.3. The measurements were carried out on June 5, 2006 when the thaw plane had reached depths of 40 cm on the north-facing burned slope and greater than 100 cm on the south-facing burned slope (or possibly seasonal frost had been completely eliminated).

Figure 7.1: North-South Transect. Looking up north-facing slope.

In interpreting resistivity data, low resistivity values are generally associated with thawed soils while high values can represent ice-rich permafrost (Etzelmüller et al., 2006). However, high resistivity values may also indicate bedrock. Intermediate values may be either thawed ground or ice-poor permafrost (less than or equal to saturation). Ground truthing is required to verify the resistivity image interpretations. There was no ground truthing done at Steele Creek, but extensive excavations in adjoining similar valleys provided an indication of general conditions for the area. An additional complication is that gradation is present in the resistivity image between high and low resistivity regions and some of this could represent artifacts of the inversion process. These factors must be taken into account when interpreting resistivity inversion images.

There are four zones with resistivity values exceeding 5 kΩm. A surface layer generally less than 1 kΩm extends across most of the transect with the exception of the channel and parts of the southern end. The resistivity information suggests variable frozen ground conditions along the transect. All distances mentioned in the text refer to the slope surface distances shown on the resistivity profiles and not the true horizontal distances. The resistivity image does not include the uppermost 1 m of material, which encompasses most of the active layer, as well as any surficial icings. Across the entire transect the near-surface low resistivity (<1 kΩm) indicated surficial materials, which may be unfrozen colluvium (i). Approximately 5 m below the surface from 0-60 m along the transect, the high resistivity region (>5 kΩm) was likely fractured schist bedrock (j). This appeared similar to permafrost, but such a possibility appears unlikely, for two reasons. First, an excavation at 60 m on July 1, 2006, found unfrozen shattered schist bedrock at 1.4 meters below the surface, beyond which further excavation was impossible. Second, the av-

erage ground temperature at 100 cm at the south-facing burned site (32 m along transect, directly above the high resistivity area) was greater than 1˚C, which suggests that permafrost is absent. The positive temperatures at 100 cm do not completely eliminate the possibility of degrading permafrost with a supra-permafrost talik, either developed post-fire or post-atmospheric warming since the 1970s on the south-facing slope. The intermediate resistivity region (k) (~1 kΩm) may be frozen, ice-poor valley bottom gravels. This interpretation is supported by a verbal communication from Tom Morgan (Dawson resident) who described an exploration borehole within 30 m which encountered gravel near the valley bottom (personal communication Nov. 2006). Deposits interpreted as ice-rich frozen gravels beneath frozen silt in the Indian River valley had resistivities of 6.5 to 10 kΩm. The lower values in Steele Creek suggest that the gravels are ice-poor. The location of the division between k and j is likely a gradient created by the inversion software, rather than the exact location of a defined boundary. Detailed borehole data would be required to confirm the interpretation of these deep sections.

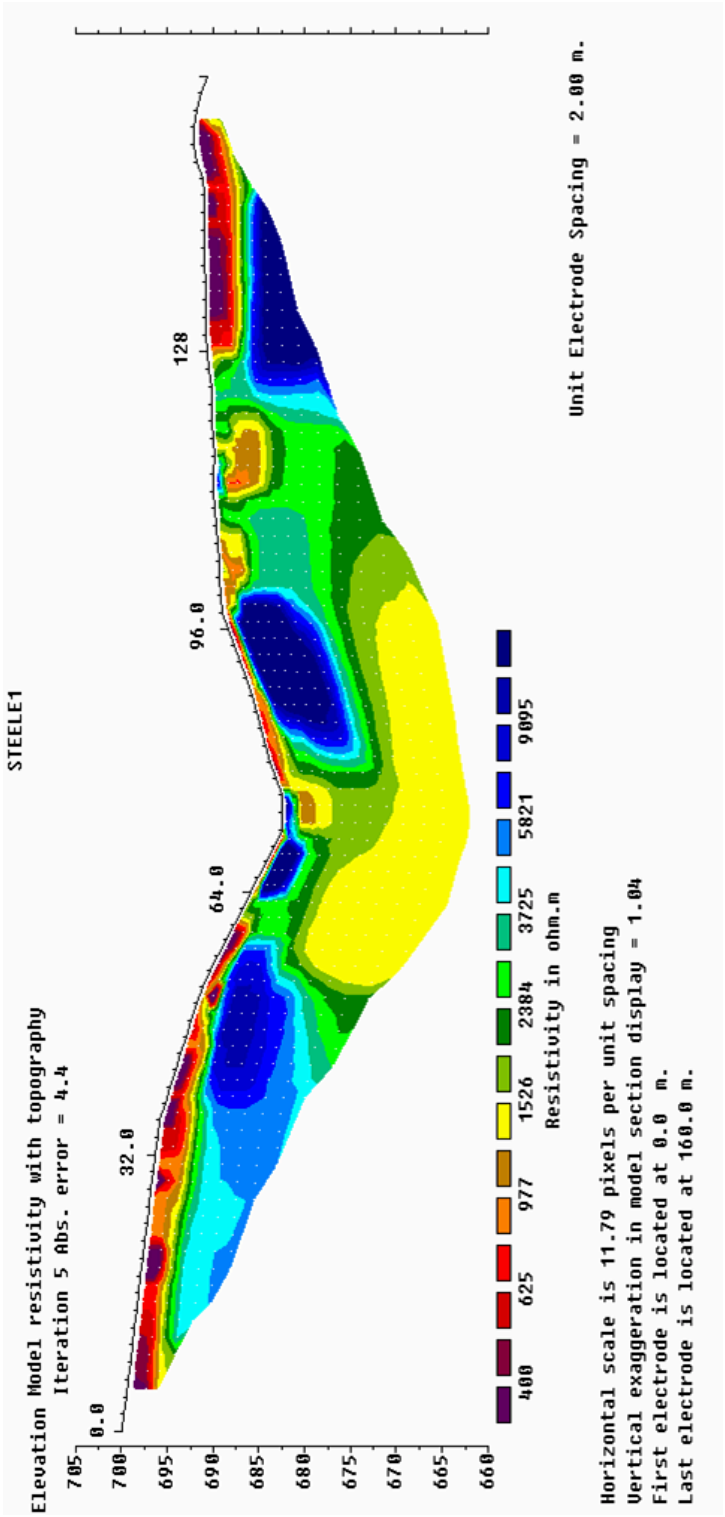

Figure 7.2: North-South Transect Raw Resistivity Inversion Image. The south-facing burned and north-facing burned logger sites are at 32 m and 98 m respectively along the transect.

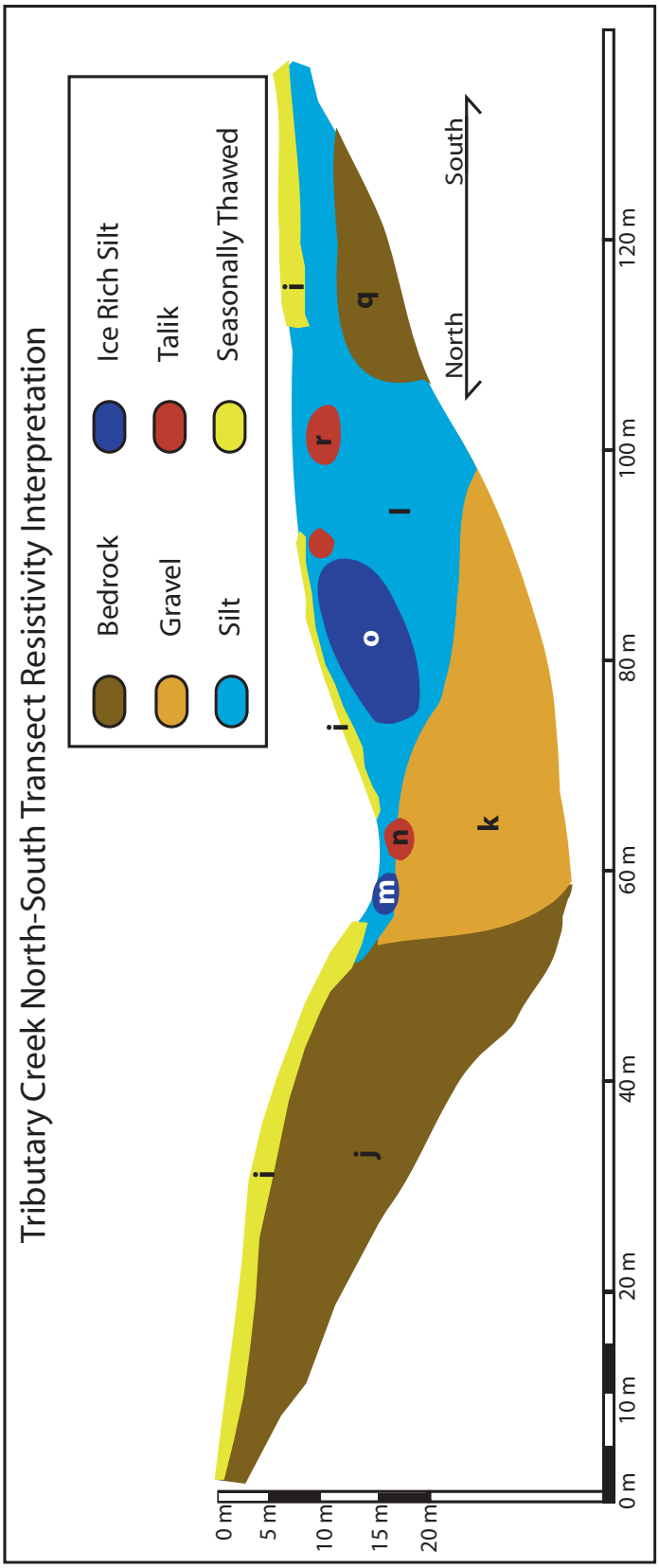

Figure 7.3: North-South Resistivity Transect Image Interpretation.

The highly resistivity region (>5 kΩm) near the base of the south-facing slope from 64 to 72 m and 0 to 5 m depth is interpreted to be ice-rich permafrost (m), likely caused by shading from the opposite bank and possibly affected by late-lying icings which were present at the time of the survey. The section of (m) that extends across the valley floor may be seasonally frozen ground. The region from 72 to 78 m extending from the 2 m to 5 m below the surface near the gully bottom (1-1.5 kΩm) was interpreted as unfrozen fluvial gravels (n) and which may constitute a suprapermafrost talik. Frozen silt deposits (1.6-3.7 kΩm) (l) extend beneath the north-facing slope and within which there is a particularly ice rich section (o) extending with resistivities greater than 5 kΩm. Two potential taliks (r) exist from the surface to 5 m (<.7 kΩm). The region beneath (>5 kΩm) was probably resistant schist bedrock or possibly ice-rich loess permafrost (q).

East-West Transect

The east-west transect ran across Steele Creek from the west-facing to east-facing slope directly west from the west-facing thermal logger (Figure 7.5). The raw resistivity image from the is presented in Figure 7.6. The interpretation of that image is displayed in Figure 7.7.

Figure 7.4: East-West Transect. View is towards east-facing slope. Failure SC03A is visible in the background.

The east-west transect revealed subsurface conditions which differed from those along the north-south transect. On the east side of the valley there are two high resistivity regions which are interpreted as being ice-rich (>3 kΩm) colluvium (a) and either ice-rich colluvium or resistant bedrock (b). However, the interpretation of ice-rich colluvium at the latter is favored due to the presence of thermokarst on the surface. Directly beneath Steele Creek is a very low resistivity area (>.2 kΩm) which may be saturated, thawed fluvial gravels (c). Higher up the west slope is

an irregular area of permafrost (>1 kΩm) which extends to approximately 10 m below the surface (d). The rest of the transect showed low resistivity material (<1 kΩm) which may be thawed, saturated colluvium or thawed, saturated decomposed bedrock (e). Where this material extends beneath the permafrost (f), it forms either a sub- or intrapermafrost talik. This talik could provide a conduit for groundwater moving downslope. The water could have emerged from the ground near the headscarp of failure SC03A (g), thus providing the high porewater pressures which initiated the failure.

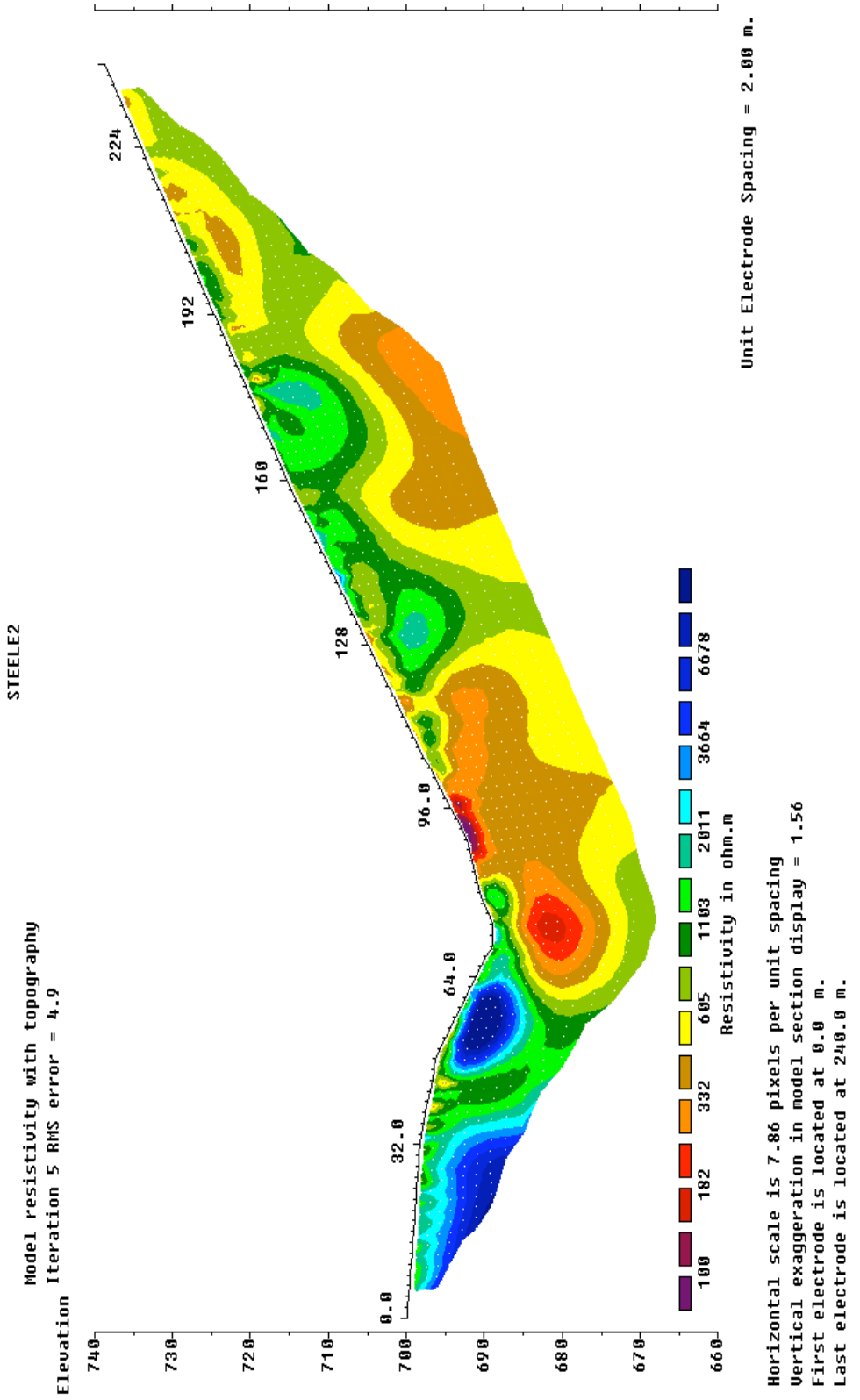

Figure 7.5: East-West Transect Raw Resistivity Inversion Image.

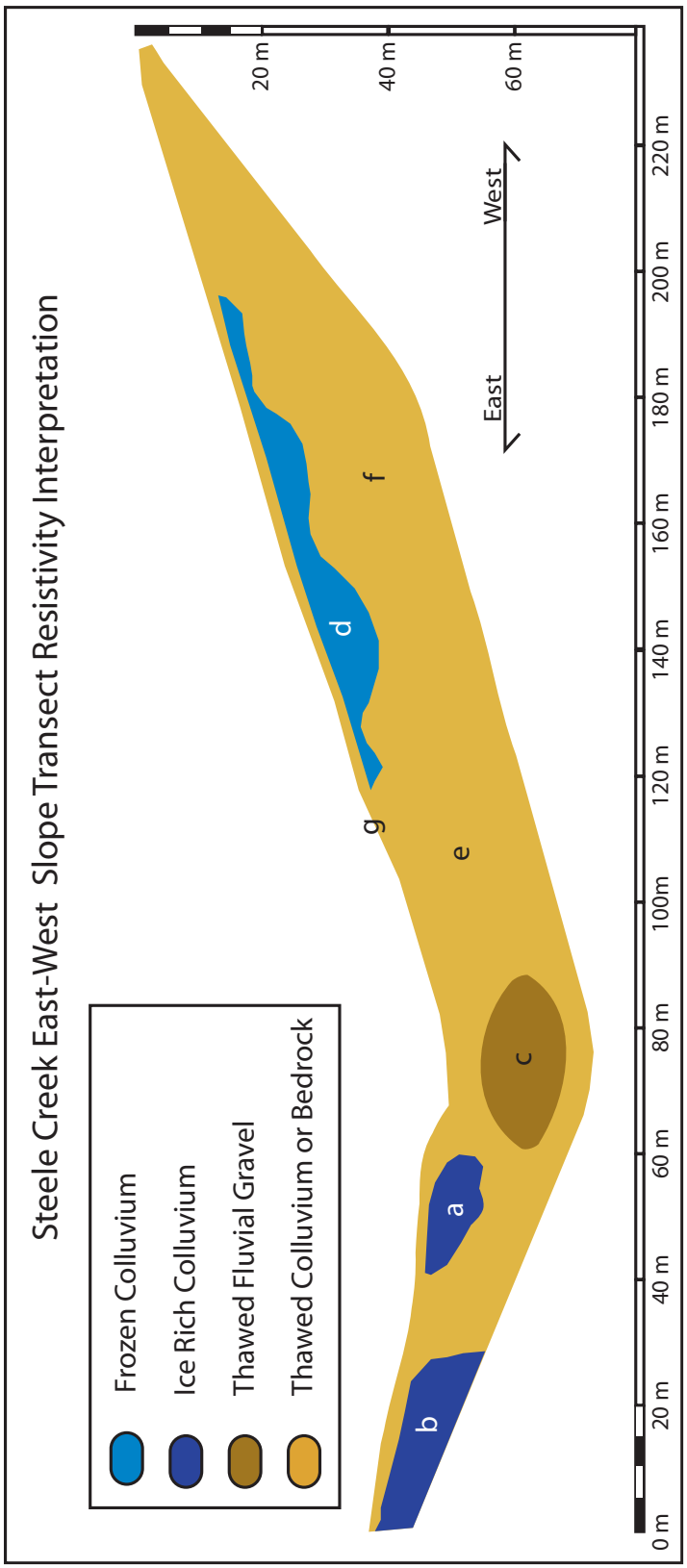

Figure 7.6: East-West Transect Image Interpretation.

The interpretation of ice-rich soils on the west-facing side of the valley is supported by thermokarst collapse observed along shallow ephemeral stream channels. These features were over 1 m deep and showed evidence of progressive development throughout the summer. Tension cracks developed into block toppling events, and muddy water was observed in the pits later in the summer (Figure 7.7).

Figure 7.7: Thermokarst Collapse. ~50 m upslope of west-facing thermal logger.

Summary

1. A possible talik beneath the failure scar on the east-facing slope may indicate that slope failures occurred over pre-existing supra-permafrost taliks downslope of permafrost. The potential for high resistivity bedrock and the paucity of ground truthing information make it difficult to reach definitive conclusions regarding the resistivity results. However, thermal data and other observations broadly fit with the resistivity results and indicate a complex distribution of permafrost in the area.

2. South-facing slopes may have permafrost where they are shaded by vegetation on the north-facing slopes and creek bottom icings.

3. There was evidence of ice-rich permafrost beneath the west-facing and north-facing slopes.

Chapter 8: Conclusions

Areas of boreal forest which had been burned by forest fire had active layers up to 20 cm (+31%) deeper than adjacent unburned areas two years after fire. Thermal profiles and freezing or thawing processes were roughly distributed in accordance with aspect and burn status. The order of processes (thawing direction) was south-facing burned, south-facing unburned, east-facing, west-facing, north-facing burned, north-facing unburned. In general northerly-facing and unburned sites began to thaw later, refreeze earlier and were cooler throughout the soil profile than southerly-facing and burned sites. However, burned permafrost sites had similar thaw and freezing processes regardless of aspect. Surface temperatures were warmer than air and active layer temperatures at all sites and much warmer at burned sites in comparison with unburned sites of the same aspect. Thermal differences between burned and unburned sites were greater at north-facing than south-facing sites. On north- and west-facing slopes freeze-up was two-sided, despite warm permafrost temperatures ranging from -0.9°C to -3.1°C, so that ice lenses can be expected to form near the base of the active layer. When active layer depths increased in burned areas these ice lenses thawed, raising soil porewater pressures over the permafrost aquiclude.

Mean annual air temperatures in the area were below 0˚C but surface offsets were sufficiently large to produce positive mean annual ground surface temperatures at some of the burned sites. Without significant thermal offsets, as may be the case in unvegetated coarse soils, these ground surface temperatures would be replicated at depth and would lead to long-term thaw of permafrost. This thaw can be expected to continue, depending on climatic conditions, until sufficient revegetation occurs to shade the surface and rebuild the insulating organic mat.

The detachment failures which were observed in Steele Creek occurred from a few weeks to two years after forest fire, and only on slopes where permafrost was extensive. They were not similar to others in the literature in that almost all occurred in coarse-gained soils and had failure planes elevated above the permafrost table. These landslides were flow-type failures that rafted portions of the organic mat on top of deforming, non-cohesive sediment. They occurred in areas of deeper thaw but their distribution and the resistivity data suggest that they were associated with taliks which concentrated groundwater flow from upslope.

Factors contributing to post-fire instability included the destruction of the organic mat, reducing shear strength, and high porewater pressures from thawed ice-rich permafrost. High soil porewater pressures created instability in soils below a suspended organic layer. Mobilization of this thawed saturated mineral material placed strain on the overlying weakened organic layer, which tore at zones of stress concentration. The organic mat was then rafted downhill on top of the liquefied mass of saturated soil. Once the slope gradient decreased or sufficient water was expelled, the mass stopped moving and the organic material was deposited in highly distorted debris piles. At some of the larger failures, the moving mass acquired sufficient weight and momentum to scour down to the permafrost table.

Fossil failures in the Steele Creek Valley and other Yukon locations indicate that detachment failure is an episodic process controlled by fire. In unglaciated areas, such as Steele Creek, given a fire recurrence interval in the order of 100 years, this process has likely occurred thousands of

times during the Pleistocene and may be responsible for elements of the form of the region's slopes. These include permafrost slopes having a generally gentler gradient and more defined mid-slope break of slope than non-permafrost slopes. Predicted increases in the frequency and magnitude of forest fire in the boreal forest due to warming climates may increase incidence of these types of failures.

Chapter 9: References

ACGR. 1988. *Glossary of Permafrost and Related Ground-Ice Terms.* National Research of Canada, Technical Memorandum No. 142. pp. 64.

Anderson, DM, Reynolds RC, Brown J. 1969. Bentonite debris flows in northern Alaska. *Science,* **164**. pp. 173-174.

Arenson L & Springman S. 2000. Slope stability and related problems of alpine permafrost. *In: Proceedings of the International Workshop on Permafrost Engineering*, Longyearbyen, Svalbard, Norway, 18–21 June 2000. pp.183–196.

ASTM. 2007. ASTM D6913-04e1 Standard Test Methods for Particle-Size Distribution (Gradation) of Soils Using Sieve Analysis. ASTM International.

Aylsworth JM, Duk-Rodkin A, Robertson T, Traynor J.A. 2000b. Landslides of the Mackenzie valley and adjacent mountainous and coastal regions. *In: The Physical Environment of the Mackenzie Valley, Northwest Territories: a Base Line for the Assessment of Environmental Change*, (ed.) L.D. Dyke and G.R. Brooks; Geological Survey of Canada, Bulletin 547, pp. 167-176.

Beltrami H, Kellman L. 2003. An examination of short- and long-term air-ground temperature coupling. *Global and Planetary Change*, **38**: pp. 291–303.

Bond J, Sanborn P. 2006. Using geochemistry to characterize colluvial dispersion in unglaciated terrain. Poster. *Yukon Geoscience Forum,* Whitehorse, Yukon, November 25-28, 2006.

Bostock, H.S. 1948. Physiography of the Canadian Cordillera, with Special Reference to the Area North of the Fifty-fifth Parallel. Geol. Surv. Can. Mem. 247. 106 pp.

Burn CR. 1993. Permafrost degradation following forest fire, Takhini Valley, southern Yukon Territory. *In Programme with Abstracts, 3rd International Geomorphology Conference, McMaster University, Hamilton, August 1993*. Compiled by D. Ford, B. McCann, and S. Vajoczki. pp.116.

Burn CR. 1998. The response (1958-1997) of permafrost and near-surface ground temperatures to forest fire, Takhini River valley, southern Yukon Territory. *Canadian Journal of Earth Sciences*. **35**: pp. 184-199.

Burn CR. 2000. The thermal regime of a retrogressive thaw slump near Mayo, Yukon Territory. *Canadian Journal of Earth Science.* **37**. pp. 967-981.

Carlson H. 1952. Calculation of Depth of Thaw in Frozen Ground. Frost Action in Soils: A Symposium. *In Highway Research Board Special Report 2*. National Research Council, Washington, D.C., pp. 192–223.

Carter LD & Galloway JP. 1981. Earthflows along Henry Creek, northern Alaska. *Arctic*. **34:** pp. 325-328.

Cogley JG & McCann SB. 1976. An exceptional storm and its effects in the Canadian High Arctic. *Arctic, Antarctic, and Alpine Research*, Vol. **8**, pp. 105-110.

Code JA. 1973. The stability of natural slopes in the Mackenzie Valley (18 pages No. 73-9) *Environmental-Social Committee, Northern Pipelines*, Task Force on Northern Oil Development.

Crozier, M.J., 1973. Techniques for the morphometric analysis of landslides. *Zeitschrift fur Geomorphologie* N.F. **17** pp. 78-101.

Duk-Rodkin A. 1996. Surficial Geology, Dawson, Yukon Territory. *Geological Survey of Canada*, Open File 3288, scale 1:250 000.

Dyke LD. 2000. Stability of permafrost slopes in the Mackenzie Valley. *In The Physical Environment of the Mackenzie Valley, Northwest Territories: A Base Line for the Assessment of Environmental Change*, Dyke LD, Brooks GR (eds). Geological Survey of Canada Bulletin 547: pp. 177–186. Canada, Energy Mines and Resources Canada: Ottawa.

Dyke L. 2004. Stability of frozen and thawing slopes in the Mackenzie Valley, Northwest Territories. Géo Quebec 2004, *57th Canadian Geotechnical Society Conference*, pp. 31-38.

Dyrness CT, Viereck LA, Van Cleve K. 1986. Fire in taiga communities of interior Alaska. In K. Van Cleve, F.S.. Chapin III, P.W. Flanagan, L.A. Viereck and C.T. Dyrness, editors. *Ecological series vol. 57: Forest Ecosystems in the Alaskan Taiga.* Springer-Verlag, New York, USA, pp. 74-86.

Eaton AK, Rouse, Lafleur WR, Marsh PM, Blanken PD. 2001. Surface energy balance of the Western and Central Canadian Subarctic: Variations in the Energy Balance among Five Major Terrain Types. *Journal of Climate,* **14**: pp. 3692–3703.

Etzelmüller B, Heggem ESF, Sharkhuu N, Frauenfelder R, Kaab A. et al. 2006. Mountain distribution modelling using a multi-criteria approach in the Hovsgol area, northern Mongolia. *Permafrost and Periglacial Processes.* **17:2**. pp. 91-104.

Fraser T. 1995. On the nature and origin of muck deposits, Klondike District, Yukon Territory. M.A. thesis, Carleton University, Ottawa.

Fraser, TA & Burn CR. 1997. On the nature and origin of "muck" deposits, Klondike area, Yukon Territory. *Canadian Journal of Earth Sciences.* vol. **34**, p. 1333-1344.

French HM. 1996. The periglacial environment. Addison Wesley Longman, Harlow 1996 (341pp).

French HM, Harris SA, van Everdingen RO. 1983. The Klondike and Dawson. *In: Northern Yukon Territory and Mackenzie Delta, Canada: Guidebook to Permafrost and Related Features.* Fairbanks, Alaska: Division of Geological & Geophysical Surveys, Dept. of Natural Resources, State of Alaska.

Froese DG, Barendregt RW, Enkin RJ, Baker J. 2000. Paleomagnetic evidence for multiple late Pliocene–early Pleistocene glaciations in the Klondike area, Yukon Territory. Canadian *Journal of Earth Sciences*. **37**, pp. 863 – 877.

Geertsema, M. 2005. Influence of landslides on biophysical diversity – a perspective from British Columbia. *36th International Binghamton Geomorphology Symposium (BGS 2005) on 'Geomorphology and Ecosystems.* October 7-9, 2005. Department of Geography, University at Buffalo (SUNY). Buffalo, New York, USA. pp. 12.

Gordy SP, Makepeace AJ, (compilers). 2000. Yukon Digital Geology; 2 CD-ROM set. Geological Survey of Canada, Open File D3826 or Exploration and Geological Services Division (EGSD), Yukon Region, Indian and Northern Affairs Canada (DIAND) (EGSD) EGSD Open File 1999-1(D).

Grechishchev S. 2003. Ice segregation and slope stability in permafrost layers. *In M. Phillips, S.H. Springman and L.U. Arenson (Eds) Proceedings- 8th International Conference on Permafrost,* Zurich, Switzerland, July 20-25, 2003. pp. 313-317.

Hanna AJ & McRoberts EC. 1988. Permafrost slope design for a buried oil pipeline. *In Proceedings, Fifth International Conference on Permafrost.* August 2-5, 1988. Trondheim, Norway. Tapir Publishers. pp. 1247-1252

Hanna A.J., McNeill D., Tchekhovski A., Fridel T., Babkirk, Leibman M.O. 1995. Cryogenic landslides on the Yamal Peninsula, Russia: preliminary observations. *Permafrost and Periglacial Processes* **6**: pp. 259–264.

Hanna AJ, McNeill D, Tchekhovski A, Fridel T, Babkirk C. 1998. The effects of the 1994 and 1995 forest fires on the slopes of the Norman Wells pipeline. *In Proceedings, Seventh International Conference on Permafrost*, Yellowknife, 23–27 June 1998, Lewkowicz AG, Allard M (eds). Nordicana, Centre d'etudes nordiques: Quebec City; 421–426. LU (eds). Swets and Zeitlinger: Lisse; pp. 651–656.

Harada K, Wada K, Fukada M. 2000. Permafrost mapping by transient electromagnetic method. Permafrost and Periglacial Processes. **11** pp. 71-84.

Hardy RM & Morrison HL. 1972. Slope stability and drainage considerations for arctic pipelines. *in Proceedings of the Canadian Northern Pipeline Research Conference.* National Research Council of Canada. Technical Memo 104. pp. 249-265.

Harris, C. 1981. Periglacial Mass-Wasting: A Review of Research. *British Geomorphological Research Group*, Research Monograph Series, 4. Geo Abstracts, Norwich, England. 203 p.

Harris, C. 1987. Mechanisms of mass movement in periglacial environments. *In Slope Stability: Geotechnical engineering and geomorphology.* Edited by M.G. Anderson and K.S. Richards. John Wiley and Sons Ltd., Chichchester, UK pp. 531-559

Harris C, Lewkowicz AG. 1993a. Form and internal structure of active-layer detachment slides, Fosheim Peninsula, Ellesmere Island, N.W.T., Canada. *Canadian Journal of Earth Sciences* **30**: pp. 1708–1714.

Harris C, Lewkowicz AG. 1993b. Micromorphological investigations of active-layer detachment slides, Ellesmere Island, Canadian Arctic. *In Sixth International Conference on Permafrost,* Beijing, China. South China University of Technology Press: Wushan, Guangzhou; pp. 232–237.

Harris SA & Gustafson CA. 1988. Retrogressive slumps, debris flows and river valley development in icy, unconsolidated sediments on hills and mountains. *Zeitschrift für Geomorphologie*. **32**. pp. 441-455.

Harris SA & Gustafson CA. 1993. Debris flow characteristics in an area of continuous permafrost, St. Elias Range, Yukon Territory. *Zeitschrift für Geomorphologie*, **37**: pp. 41-56.

Harris C, Davies MCR. 1998. Pressures recorded during laboratory freezing and thawing of natural silt-rich soil. *In Proceedings of the 7th International Conference on Permafrost, Lewkowicz AG, Allard M. (eds).* Collection Nordicana. **57**: pp. 433–439.

Harris C, Lewkowicz AG. 2000. An analysis of the stability of thawing slopes, Ellesmere Island, Nunavut, Canada. *Canadian Geotechnical Journal.* **37**: 449–462.

Harris C, Vonder Muhll D. 2001. Permafrost and climate in Europe: climate change, mountain permafrost degradation and geotechnical hazard. *In Global Change and Protected Areas*, Visconti D. (ed.). Kluwer: Dordrecht. **9**: pp. 71-82.

Harris C, Davies MCR, Coutard JP. 1995. Laboratory simulation of periglacial solifluction: significance of porewater pressure, moisture contents and undrained shear strength during thawing. *Permafrost and Periglacial Processes.* **6**: pp. 293–312.

Harris C, Rea B, Davies MCR. 2001. Scaled physical modeling of mass movement processes on thawing slopes. *Permafrost and Periglacial Processes.* **12**: pp. 125-135.

Harris C, Smith JS, Davies MCR, Rea B. 2008. An investigation of periglacial slope stability in relation to soil properties based on physical modeling in the geotechnical centrifuge. *Geomorphology.* **93**: pp. 437-459.

Harry DG & MacInnes KL. 1988. The effect of forest fires on permafrost terrain stability, Little Chicago-Travaillant Lake Area, MacKenzie Valley, N.W.T. *Current Research, Part D, Geological Survey of Canada Paper,* 88-ID, Ottawa, Ontario: pp. 91-94.

Hauck C & Vonder Muhll D. 2003. Inversion and interpretation of two-dimensional geo-electric measurements for detecting permafrost in mountainous regions. *Permafrost and Periglacial Processes*. **14**: pp. 305-318.

Hauck C & Kneisel C. 2006. Application of Capacitively-coupled and DC Electrical Resistivity Imaging for Mountain Permafrost Studies. *Permafrost and Periglacial Processes,* 17 (2), 169-177.

Hauck C, Guglielmin M, Isaksen K, Vonder Muhll D. 2001. Applicability of frequency-domain and time-domain electromagnetic methods for mountain permafrost studies. *Permafrost and Periglacial Processes*. **12**: pp. 39-52.

Hauck C, Isaksen K, Vonder Muhll D, Sollid JL. 2004. Geophysical surveys designed to delineate the altitudinal limit of mountain permafrost: an example from Jotunheimen, Norway. *Permafrost and Periglacial Processes*. **15**: pp. 191-205.

Haugen RK, Slaughter CW, Howe KE, Dingman SL. 1982. Hydrology and climatology of the

Caribou-Poker Creeks Research Watershed, Alaska, *CRREL Rep*. *82-26*, 42 p.

Heginbottom A. 1971. Some effects of a forest fire on the permafrost active layer at Inuvik, N.W.T. *in Proceedings of a Seminar on the Permafrost Active Layer*, May 4 – 5, 1971, edited by R. J. E. Brown, Tech. Memo., 103, pp. 31 – 36, NRCC, Ottawa, Ontario.

Heginbottom JA. 1978. An Active Retrogressive Thaw Flow Slide on Eastern Melville Island, District of Franklin. *Scientific and Technical Notes in Current Research Part A,* Geological Survey of Canada, Paper 78-1A. pp. 525-526.

Heginbottom JA. 1989. A survey of geomorphic processes in Canada. In R.J. Fulton, (Eds), *Quaternary Geology of Canada and Greenland*. Trondheim, Norway; Tapir Publishers. pp. 573-644.

Heginbottom JA, Radburn LK. 1992. Permafrost and ground ice conditions of Northwestern Canada. Geological Survey of Canada, Map 1691A.

Heginbottom JA, Dubreuil MA, Harker PA. 1995. Canada – Permafrost. *In: National Atlas of Canada, 5th ed.*, Natural Resources Canada, Ottawa, Plate 2.1: MCR 4177.

Henry KA & Smith MW. 2001. A model-based map of ground temperatures for the permafrost regions of Canada. *Permafrost and Periglacial Processes.* **12**: pp. 389–398.

Hodgson DA. 1977. A preliminary account of surficial materials, geomorphological processes, terrain sensitivity and quaternary history of King Christian and southern Ellef Ringnes Islands, District of Franklin. *Report of Activities, Part A, Geological Survey of Canada Paper*, 77-1A . pp. 485-493.

Hughes OL, Veillette JJ, Pilon J, Hanley PT, van Everington RO. 1973. Terrain evaluation with respect to pipeline construction, Mackenzie Transportation Corridor, Central Part, Lat 64 top 68N. No. 73-37. *Environmental-Social Committee, Northern Pipelines, Task Force on Northern Oil Development.*

Huscroft CA, Lipovsky PS, Bond JD. 2004a. A regional characterization of landslides in the Alaska Highway corridor, Yukon. *Yukon Geological Survey, Open File* 2004-18, 65 p., report and CD-ROM.

Huscroft CA, Lipovsky PS, Bond JD. 2004b. Permafrost and landslide activity: Case studies from southwestern Yukon Territory. *In: Yukon Exploration and Geology* 2003, D.S. Emond and L.L. Lewis (eds.), Yukon Geological Survey, pp. 107-119.

Jackson LE Jr. 2005. Surficial Geology, Reindeer Mountain, Yukon Territory. *Geological Survey of Canada, Open File 4588*, scale 1:50 000.

Johnson L & Viereck L. 1983. Recovery and active layer changes following a tundra fire in

northwestern Alaska. in *Proceedings, Permafrost Fourth International Conference*. July 17-22, 1983, Fairbanks, AK. pp. 543-547.

Karunaratne KC & Burn CR. 2003. Freezing n-factors in discontinuous permafrost terrain, Takhini River valley, Yukon Territory, Canada. *Proceedings, Eighth International Conference on Permafrost,* , 21-25 July, 2003. Zurich, Switzerland. Balkema, Lisse. **1**: pp. 519-524.

Karunaratne KC & Burn CR. 2004. Relations between air and surface temperature in discontinuous permafrost terrain near Mayo, Yukon Territory. *Canadian Journal of Earth Sciences*, **41**: pp. 1437-1451.

Klene AE, Nelson FE, Shiklomanov NI. 2001. The N-factor in natural landscapes: variability of air and soil-surface temperatures, Kuparuk River basin, Alaska, USA. Arctic, Antarctic and Alpine Research, **33**: pp. 140–148.

Klock GO, Helvey JD. 1976. Debris flows following wildfires in north central Washington. *In Proceedings of the Third Federal Inter-Agency Sedimentation Conference,* Denver, Colorado; pp. 91–96.

Kneisel C, Hauck C, Vonder Muhll D. 2000. Permafrost below the timberline confirmed and characterized by geoelectric resistivity measurements, Bever Valley , eastern Swiss Alps. *Permafrost and Periglacial Processes,* **11**, pp 295 –304.

Kokelj SV, Lewkowicz AG. 1998. Long-term influence of active-layer detachment sliding on permafrost slope hydrology, Hot Weather Creek, Ellsmere Island, Canada. *Seventh Annual Conference on Permafrost*. pp 583-589.

LeBarge WP & Coates J (compiled). 2005. Yukon Placer Database 2005 - Geology and mining activity of placer occurrences, 2005. Database in Microsoft Access 2000 format, and accompanying maps in Portable Document Format (PDF) CD-Rom.

Liang L-H, Zhou Y-W, Wang JC. 1991. Changes to the permafrost environment after forest fire, Da Xi'an Ridge, Gu Lian Mining Area, China, *Permafrost and Periglacial Processes.* **2**: pp. 253–257.

Leibman MO. 1995. Cryogenic Landslides on the Yamal Penninsula, Russia: Preliminary observations. *Permafrost and Periglacial Processes.* **6**: pp. 259-264

Leibman MO, Erogov IP. 1996. Climatic and environmental controls of cryogenic landslides, Yamal, Russia. *In Senneset, K. (Ed.) Proceedings of the Seventh International Symposium on Landslides,* Trondhiem. A.A. Balkema, Rotterdam. pp. 1941-1946.

Leibman MO, Rivkin FM, Saveliev VS. 1993. Hydrogeological aspects of cryogenic slides on the Yamal Peninsula. In *Sixth International Conference on Permafrost*, Beijing, China. South China University of Technology Press: Wushan, Guangzhou; pp. 380–382.

Leibman MO, Kizakov AI, Sulerzhitsky LD, Zaretskaia NE. 2003. Dynamics of landslide slopes and their development on Yamal Peninsula. *In Permafrost, Proceedings of the Eighth International Conference on Permafrost,* Phillips M., Springman S.M., Arenson L.U. (eds). Swets and Zeitlinger: Lisse; pp. 651–656.

Lewkowicz AG. 1987. Nature and Importance of thermokarst processes, Sand Hills Moraine, Banks Island, Canada. *Geographica Annuliska.* **69**A: pp. 321-327.

Lewkowicz AG. 1988. Slope processes. *In Advances in Periglacial Geomorphology,* Clark MJ (eds), Wiley: Chichester; pp. 325–368.

Lewkowicz AG. 1990. Morphology, frequency and magnitude of active-layer detachment slides, Fosheim Peninsula, Ellesmere Island, N.W.T. *In Permafrost— Canada: Proceedings of the Fifth Canadian Permafrost Conference*. Universite Laval: Quebec City; pp. 111-118.

Lewkowicz AG. 1992. Factors influencing the distribution and initiation of active-layer detachment slides on Ellesmere Island, Arctic Canada. *In Periglacial Geomorphology, Proceedings of the 22nd Annual Binghamton Symposium in Geomorphology, Dixon JC, Abrahams AD (eds).* John Wiley and Sons: Chichester; pp. 223–250.

Lewkowicz AG. 2004. Permafrost and Landslide Initiation in Northern Canada: Changing Cli-

mates, Changing Roles. In: T. Kulkarni,\ and A. Blais-Stevens (eds.). *Vulnerability of Landslide Risk to Climate Change.* Proceedings from C-CIARN Landscape Hazards Workshop 2003, Vancouver, BC. C-CIARN Landscape Hazards Report 04-01. p.8.

Lewkowicz AG. 2007. Dynamics of active layer detachment failures, Foshiem Peninsula, Ellsmere Island, Nunavut, Canada. *Permafrost and Periglacial Processes.* **18**: pp.1-15.

Lewkowicz AG & Hartshorn J. 1998. Terrestrial record of rapid mass movements in the Sawtooth Range, Ellesmere Island, NT, Canada. *Canadian Journal of Earth Sciences.* **35**: pp. 55–64.

Lewkowicz AG & Kokelj SV. 2002. Slope sediment yield in arid lowland continuous permafrost environments, Canadian Arctic Archipelago. *Catena*. **46:** pp. 261-283.

Lewkowicz AG & Harris C. 2005a. Morphology and geotechnique of active-layer detachment failures in discontinuous and continuous permafrost, northern Canada. *Geomorphology,* **69**: pp. 275-297.

Lewkowicz AG & Harris C. 2005b. Frequency and magnitude of active-layer detachment failures in discontinuous and continuous permafrost, northern Canada. *Permafrost and Periglacial Processes*. **16**: pp. 115-130.

Lipovsky PS, Coates J, Lewkowicz AG, Trochim E. 2006. Active layer detachments following

the summer 2004 forest fires near Dawson City, Yukon. *In: Yukon Exploration and Geology 2005*, D.S. Edmond, G.D. Bradshaw, L.L. Lewis and L.H. Weston (eds.), Yukon Geological Survey, pp. 175-194.

Loke MH, Barker RD. 1995. Rapid least-squares inversion of apparent resistivity pseudosections using a quasi-Newton method. *Geophysical Prospecting* **44**: pp. 131-152.

Lowey GW. 2004. Placer geology of the Stewart River (115N&O) and part of the Dawson (116B&C) map areas, west-central Yukon, Canada. *Yukon Geological Survey, Bulletin 14*, 275 p.

Lunardini VJ. 1978. Theory of n-factors and correlation of data. *In Proceedings of the 3rd International Conference on Permafrost*, 10–13 July 1978, Edmonton, Alta. National Research Council of Canada, Ottawa, Ont., Vol. **1**, pp. 40–46.

Lotspeich FB. 1973. Permafrost and the Environment in Alaska. *U.S. Environmental Protection Agency, Arctic Environmental Research Laboratory.* Working Paper 18.

Lyle, R.R., 2006. Landslide susceptibility mapping in discontinuous permafrost: Little Salmon Lake, central Yukon. Unpublished MSc thesis. Queen's University, Ontario. 351 p.

Mackay JR. 1977. Changes in the active layer from 1968 to 1976 as a result of the Inuvik fire. *In Report of activities, part B. Geological Survey of Canada*, Paper 77-1B, pp. 273-275.

Mackay JR. 1981. Active layer slope movement in a continuous permafrost environment, Garry Island, Northwest Territories, Canada. *Canadian Journal of Earth Sciences* **18**: pp. 1666–1680.

Mackay JR. 1983. Downward water movement into frozen ground, western Arctic coast, Canada. *Canadian Journal of Earth Sciences*, **20**: pp. 120-134.

Mackay JR. 1995. Active layer changes (1968 to 1993) following the forest-tundra fire near Inuvik, N.W.T., *Canada. Arctic and Alpine Research.* **27**: pp. 323-336.

Mackay JR, Matthews JV. 1973. Geomorphology and Quaternary history of the Mackenzie River Valley near Fort Good Hope, N.W.T., Canada. Canadian Journal of Earth Sciences **10**: pp. 26-41.

Mathewson CC, Mayer-Cole TA. 1984. Development and run-out of a detachment slide, Bracebridge Inlet, Bathurst Island, Northwest Territories, Canada. *Bulletin of the Association of Engineering Geologists*. **21**: pp. 407-424.

McCoy VM & Burn CR. 2005. Potential alteration by climate change of the forest-fire regime in the boreal forest of central Yukon Territory. *Arctic*, **58**: pp. 276-285.

McRoberts EC. 1978. Slope Stability in Cold Regions. In: Andersland, O.B. and D.M. Anderson (eds.). 1978. *Geotechnical Engineering for Cold Regions*. New York: McGraw-Hill Inc. pp. 363-404.

*McRoberts EC, Morgenstern NR. 1973. A study of landslides in the vicinity of the Mackenzie River, Mile 205 to 660. Ottawa: *Environmental-social Committee, Northern Pipelines, Task Force on Northern Oil Development*, Information Canada, Ottawa, Ontario.

McRoberts EC, Morgenstern NR. 1974a. The stability of thawing slopes. *Canadian Geotechnical Journal* **11**: pp. 447–469.

McRoberts EC & Morgenstern NR. 1974b. Stability of slopes in frozen soil, Mackenzie Valley, N.W.T. *Canadian Geotechnical Journal*, **11**: pp. 554-573.

Morgenstern NR & Nixon JF. 1971. One-dimensional consolidation of thawing soils. *Canadian Geotechnical Journal* **11**: pp. 447–469.

Mortensen JK. 1996. Geological compilation maps of the northern Stewart River map area, Klondike and Sixtymile districts (115N/15, 16; 115O/13, 14 and parts of 115O/15, 16). *Exploration and Geological Services, Yukon, Indian and Northern Affairs Canada*, Open File 1996-1(G), 43 p., 1:50 000 scale.

Morton DM. 1989. Distribution and frequency of storm-generated soil slips on burned and unburned slopes, San Timoteo Badlands, Southern California. *In Landslides in a Semi-Arid Environment with Emphasis on the Inland Valleys of Southern California* , Sadler PM, Morton DM

(eds). Publications of the Inland Geological Society, **2**: pp. 279 – 284.

Muhll DV, Hauck C, Gubler H, McDonald R, Russill N. 2001. New geophysical methods of investigating the nature and distribution of mountain permafrost with special reference to radiometry techniques. *Permafrost and Periglacial Processes.* **12**: pp. 27-38

Naldrett DL. 1981. Aspects of the surficial geology and permafrost conditions, Klondike Goldfields and Dawson City, Yukon Territory. Unpublished M.Sc. Thesis, University of Ottawa, Ontario.

Niu F, Cheng G, Ni W, Jin D. 2005. Engineering-related slope failure in permafrost regions of the Qinghai-Tibet Plateau. *Cold Regions Science and Technology*. **42**: pp. 215-225.

Oke TR. 1978. Boundary Layer Climates. Routledge, New York. 435 p.

Osterkamp TE, Viereck L, Shur Y, Jorgenson MT, Racine C, Doyle A., Boone RD. 2000. Observations of thermokarst and its impact on boreal forests in Alaska, USA, *Arctic, Antarctic and Alpine Research*. **32**: 303 –315.

Pufahl DE & Morgenstern NR. 1979. Stabilization of Planar Landslides in Permafrost. *Canadian Geotechnical Journal*. **16**: pp. 734-747.

Racine CH, Patterson III WA, Dennis JG. 1983. Permafrost thaw associated with tundra fires in northwest Alaska. In *Permafrost, Fourth International Conference, Proceedings*, 17-22 July 1983, University of Alaska, Fairbanks, Alaska, pp. 1024-1029. National Academy Press, Washington, D.C.

Reynolds JM. 1997: An introduction to applied and environmental geophysics. John Wiley & Sons: Chichester, UK.

Riseborough DW. 2002. The mean annual temperature at the top of permafrost, the TTOP model, and the effect of unfrozen water. *Permafrost and Periglacial Processes*, **13**: pp. 137–143.

Riseborough DW & Burn CR. 1988. Influence of an organic mat on the active layer. In *Permafrost, Proceedings of the 5th International Conference,* Trondheim, Norway, August 1988. Tapir, Trondheim, **1**: 633-638.

Riseborough DW & Smith MW. 1998. Exploring the limits of permafrost. *In Proceedings, Seventh International Conference on Permafrost*, Yellowknife, NWT. pp. 935-942.

Romanovsky VE & Osterkamp TE. 1995. Interannual variations of the thermal regime of the active layer and near surface permafrost in Northern Alaska. *Permafrost and Periglacial Processes*, **6**: pp. 313–335.

Rouse WR. 1976. Microclimatic changes accompanying burning in subarctic lichen woodland. *Arctic and Alpine Research*, **8**: pp. 357-376.

*Rouse WR & Mills MP. 1977. A classification of fire effects on the micro- climate of forest and tundra ecosystems: Final report, R71-19/2, 21 pp., Indian and North. Affairs, Ottawa, Ontario.

Sanborn PT, Smith CAS, Froese DG, Zazula GD, Westgate JA. 2006. Full-glacial paleosols in perennially frozen loess sequences, Klondike goldfields, Yukon Territory, Canada. *Quaternary Research*, **66**: pp. 147-157.

*Savigny W, Logue C, MacInnes K. 1995. Forest fire effects on slopes formed in ice-rich permafrost soils Mackenzie Valley, Northwest Territories. *In 48th Canadian Geotechnical Conference*, 25–27 September 1995, Vancouver, B.C. Canadian Geotechnical Society: pp. 989–998.

Shur YL & Jorgensen MT. 2007. Patterns of permafrost formation and degradation in relation to climate and ecosystems. *Permafrost and Periglacial Processes.* **10**: pp. 1-13.

Shur Y, Hinkel K, Nelson F. 2005. The Transient Layer: Implications for Geocryology and Climate-Change Science. *Permafrost and Periglacial Processes.* **16**: pp. 5–17.

*Sigafoos RS & Hopkins DM. 1952. Soil instability on slopes in regions of perennially frozen ground. In *Frost Action in Soils: A Symposium*. pp. 176-192. Highway Research Board Special

Report No.2 (National Research Council Publication 213).

Smith CAS, Meikle JC, Roots CF. (eds.), 2004. Ecoregions of the Yukon Territory: Biophysical Properties of Yukon Landscapes. Agriculture and Agri-Food Canada, *PARC Technical Bulletin* No. 04-01, Summerland, British Columbia, 313 p.

Smith MW. 1975. Microclimatic influences on ground temperatures and permafrost distribution, Mackenzie Delta, Northwest Territories. *Canadian Journal of Earth Sciences*, **12**: pp. 1421–1438.

Smith MW & Riseborough DW. 2002. Climate and the limits of permafrost: a zonal analysis. *Permafrost and Periglacial Processes*. **13**: pp.1-15.

Stangl KO, Roggensack WD, Hayley DW. 1982. Engineering geology of surficial soils, eastern Melville Island. *In H.M. French (eds) The Roger J.E. Brown Memorial Volume, Proceedings of the Fourth International Conference on Permafrost.* Calgary, Alberta, March 2-6, 1981. (pp. 136-147). Ottawa: National Research Council of Canada.

Swanson FJ. 1981. Fire and geomorphic processes. *In: Gen. Tech. Rep. USDA Forest Service.* WO-26. Washington, DC, pp. 401–420.

Swanson DK 1996. Susceptibility of permafrost soils to deep thaw after forest fires in interior

Alaska, U.S.A., and some ecologic implications. *Arctic and Alpine Research*, **28**: pp. 217-227.

Taylor AE. 1995. Field measurements of n-factors for natural forest areas, Mackenzie Valley, Northwest Territories. *Geological Survey of Canada, Current Research 1995-B,* pp. 89–98.

Thie J. 1974. Distribution and Thawing of Permafrost in the Southern Part of the Discontinuous Zone in Manitoba. *Arctic* **27**: pp. 189–200.

Van Cleve K & Viereck LA. 1983. A comparison of successional sequences following fire on permafrost-dominated and permafrost-free sites in Interior Alaska, *In Permafrost: Proceeding of the 4th International Conference*, pp. 1286 – 1291, Natl. Acad. Press, Washington, D.C.

Viereck LA. 1973. Ecological effects of river flooding and forest fires on permafrost on the taiga of Alaska. *In North American Contribution, 2nd International Conference on Permafrost*, Yakutsk, U.S.S.R., July 13-28, 1973. National Academy of Sciences, Washington, D.C., pp. 60-67.

Viereck LA. 1982. Effects of fire and firelines on active layer thickness and soil temperatures in interior Alaska. *In Proceedings of the 4th Canadian Permafrost Conference, The Roger J. E. Brown Memorial Volume*, pp. 123– 134, Natl. Res. Council of Can., Ottawa, Ont., Canada, 1982.

Viereck LA. 1983. The effects of fire in black spruce ecosystems of Alaska and northern Canada. *In The Role of Fire in Northern Circumpolar Ecosystems.* pp. 201-220. Edited by R.W. Wein and D.A. MacLean. Wiley and Sons, New York.

Vallejo LE. 1980. A new approach to the stability analysis of thawing slopes. *Canadian Geotechnical Journal* **17:** pp. 607-612.

Vallejo LE & Edil TB. 1981. Stability of thawing slopes; Field and theoretical investigations. *In A.A. Balkema (Eds), Soil Mechanics and foundation. Proceedings 10th International Conference*, June 1981 (pp. 545-548). Stockholm.

Walker MD, Walker DA, Auerbach NA. 1994. Plant communities of a tussock tundra landscape in the Brooks Range foothills, Alaska. *Journal of Vegetation Science.* **5**; pp. 843-866.

*Wahl HE, Fraser DB, Harvey RC, Maxwell JB. 1987. Climate of Yukon. Ottawa, Ontario, Supply and Services Canada, 323p.

Williams DJ & Burn CR. 1996. Surficial Characteristics Associated with the Occurrence of Permafrost near Mayo, Central Yukon Territory, Canada. *Permafrost and Periglacial Processes*, **7**: pp. 193-206.

Woo MK & Steer P. 1983. Slope hydrology as influenced by thawing of the active layer, Resolute, N.W.T. *Canadian Journal of Earth Sciences*. **20**: pp. 978-986.

Yarie, J. 1981. Forest fire cycles and life tables: a case study from interior Alaska. *Canadian Journal of Forest Research*. **11**: pp. 554–562.

*Yoshikawa K, Hinzman LD, Ishikawa N, Collins CM, Lunardini VJ. 1998. Air and ground temperature models at Caribou-Poker Creeks Research Watershed, *paper presented at 49th AAAS Arctic Science Conference,* American Association for the Advancement Of Science. Fairbanks, Alaska, 25 – 28 October 1998.

Yoshikawa K, Bolton WR, Romanovsky VE, Fukuda M, Hinzman LD. 2003. Impacts of Wildfire on the Permafrost in the Boreal Forests of Interior Alaska. *Journal of Geophysical Research,* **107**, 8148

*Yukon Wildland Fire Review Panel. 2004. Wildland Fire Review Final Report
Prepared for: Minister Glenn Hart Minister of Community Services Yukon Government
May 2005.

Yukon Ecoregions Working Group, 2004. Klondike Plateau Ecoregion. In: Ecoregions of the Yukon Territory: Biophysical properties of Yukon landscapes, C.A.S. Smith, J.C. Meikle and C.F. Roots (eds.), Agriculture and Agri-Food Canada, PARC Technical Bulletin No. 04-01, Summerland, British Columbia, p. 159-168.

*Zhou Y, Liang L, Gu Z, Liang F, Zhang Q. 1993. Effects of forest fire on the hydro-thermal regime of frozen ground, the northern part of Da Hinggan Ling, China. In *Proceedings, 6th International Conference on Permafrost, Beijing, China,* July 5-9,1993. South China University of Technology Press, Wushan Guangzhou, China, pp. 819-825.

Zoltai SC. 1993. Cyclic development of permafrost in the peatlands of northwestern Alberta, Canada. *Arctic and Alpine Research.* **25**: pp. 240-246.

Appendix A: Thermal Data Logger Locations

	North	West	Altitude
North-facing Unburned	0600011	7053500	624 m
North-facing Burned	0599798	7053433	612 m
South-facing Unburned	0599978	7053529	616 m
South-facing Burned	0599788	7053497	605 m
East-facing Burned	0599766	7053135	608 m
West-facing Burned	0599818	7053097	598 m

*WGS 84 Datum

Appendix B: Failure Parameters

Failure	SC 01A	SC 02A	SC 03AB	SC 04A	SC 05A
Initiation Year	2004	2004	2004, 2005	2004	2004
UTM N*	599749	599754	599702	599894	599702
UTM E*	7053086	7053070	7052955	70599894	7052955
Slope	19	19	19	32	24
Aspect	55	58	51	73	56
Elevation (m a.s.l.)			653	635	635
Depth (cm)	30	50	80	17	35
Length (m)	22	55	80	6	9
Width (m)	5	10	20	2	3
Scar (m)	8	50	60	4	8
Volume Material (m3)	12	250	960	1	7
Horizontal Distance (m)	21	52	76	5	8
Vertical Distance (m)	7	18	26	3	4
Length/Width Ratio	4.4	5.5	4.0	3.0	3.6
Scar/Length %	36	91	75	67	89

* WGS 84 Datum

Failure	SC 06A	SC 07A	SC 08A	SC 09A	SC 10A
Initiation Year	2004	2004	2004	2004	2004
UTM N*	599868	599765	599787	599818	599860
UTM E*	7052589	7052554	7052456	7052280	7052315
Slope	21	19	21	21	30
Aspect	69	49	54	67	56
Elevation (m a.s.l.)	641	671	670	672	654
Depth (cm)	20	60	35	22	60
Length (m)	10	90	49	28	10
Width (m)	3	9	7	5	5
Scar (m)	7	65	33	18	7
Volume Material (m3)	4	332	74	18	19
Horizontal Distance (m)	9	85	46	26	9
Vertical Distance (m)	4	29	18	10	5
Length/Width Ratio	3.3	10.6	7.5	6.2	2.2
Scar/Length %	65	72	66	65	70

* WGS 84 Datum

Failure	SC 11A	SC 12A	SC 13A	SC 14A	SC 15P
Initiation Year	2004	2004	2004	2004	pre-fire
UTM N*	599874	599889	600039	600048	600067
UTM E*	7052087	7052026	7052008	7052001	7052030
Slope	31	26	24	26	24
Aspect	74	75	275	275	332
Elevation (m a.s.l.)	664	666	663	667	670
Depth (cm)	27	32	35	160	20
Length (m)	6	24	22	16	
Width (m)	2	7	6	4	
Scar (m)	3	18	21	12	
Volume Material (m3)	2	37	44	77	0
Horizontal Distance (m)	5	22	20	14	0
Vertical Distance (m)	3	11	9	7	0
Length/Width Ratio	3.2	3.7	3.7	4.0	
Scar/Length %	44	75	95	75	

* WGS 84 Datum

Failure	SC 16A	SC 17A	SC 18A	SC 19A	SC 20A
Initiation Year	2004	2004	2004	2004	2004
UTM N*	600059	600052	600043	600039	600019
UTM E*	7052064	7052138	7052143	7052166	7052188
Slope	27	25	29	30	30
Aspect	270	265	275	275	275
Elevation (m a.s.l.)	669	664	663	661	660
Depth (cm)	24	20	17	20	22
Length (m)	5	12	6	5	12
Width (m)	2	4	2	2	2
Scar (m)	3	8	2	5	3
Volume Material (m3)	1	6	1	2	1
Horizontal Distance (m)	4	11	5	4	10
Vertical Distance (m)	2	5	3	2	6
Length/Width Ratio	2.5	3.4	3.8	2.5	6.0
Scar/Length %	60	67	33	100	21

* WGS 84 Datum

Failure	SC 21A	SC 22A	SC 23A	SC 24A	SC 25A
Initiation Year	2004	2004	2004	2004	2004
UTM N*	600019	600064	600048	600043	600109
UTM E*	7052187	7052234	7052221	7051757	7051601
Slope	23	14	13	22	19
Aspect	275	290	290	285	270
Elevation (m a.s.l.)	650	665	662	679	688
Depth (cm)	32	40	30	25	60
Length (m)	11	70	13	35	106
Width (m)	3	12	5	6	14
Scar (m)	10	30	11	27	89
Volume Material (m3)	9	144	16	39	717
Horizontal Distance (m)	10	68	13	33	100
Vertical Distance (m)	4	17	3	13	34
Length/Width Ratio	3.8	5.8	2.5	6.0	7.8
Scar/Length %	87	43	81	77	84

* WGS 84 Datum

Failure	SC 26A	SC 27A	SC 28A	SC 29A	SC 30A
Initiation Year	2004	2004	2004	2004	2004
UTM N*	600097	600079	600093	600109	600328
UTM E*	7051572	7051558	7051522	7051507	7050634
Slope	23	22	21	19	22
Aspect	282	281	235	228	280
Elevation (m a.s.l.)	684	683	683	684	702
Depth (cm)	80	75	90	80	60
Length (m)	22	43	49	51	42
Width (m)	5	9	23	11	8
Scar (m)	13	25	35	29	32
Volume Material (m3)	52	169	725	264	154
Horizontal Distance (m)	20	40	46	48	39
Vertical Distance (m)	8	16	18	17	16
Length/Width Ratio	4.3	4.8	2.1	4.5	5.3
Scar/Length %	60	58	71	57	76

* WGS 84 Datum

Failure	SC 31A	SC 32A	SC 33B	SC 34A	SC 35P
Initiation Year	2004	2004	2005	2005	?
UTM N*	600359	599794	600014	599801	599821
UTM E*	7050491	7053404	7052587	7052893	7052836
Slope	21	21	23	27	27
Aspect	279	331	323	80	80
Elevation (m a.s.l.)	713	632	642	642	643
Depth (cm)	50	30	72	30	20
Length (m)	55		25		5
Width (m)	11		9		4
Scar (m)	43		16		4
Volume Material (m3)	223	0	104	0	3
Horizontal Distance (m)	51	0	23	0	4
Vertical Distance (m)	20	0	10	0	2
Length/Width Ratio	5.2		2.8		1.3
Scar/Length %	77		64		80

* WGS 84 Datum

Failure	SC 36A	SC 37A	SC 38B	SC 39B	SC 40B
Initiation Year	2004	2004	2005	2005	2005
UTM N*	600755	600741	600375	599646	599870
UTM E*	7049917	7049956	7050466	7053325	7053483
Slope	12	15	22	25	23
Aspect	250	254	270	55	343
Elevation (m a.s.l.)	727	736	715	609	636
Depth (cm)	70	60	80	80	50
Length (m)	31	46	43	34	26
Width (m)	7	8	8	14	22
Scar (m)	26	36	43	25	16
Volume Material (m3)	134	170	268	280	176
Horizontal Distance (m)	30	44	40	31	24
Vertical Distance (m)	6	12	16	14	10
Length/Width Ratio	4.2	5.8	5.5	2.4	1.2
Scar/Length %	85	77	100	74	62

* WGS 84 Datum

Appendix C. Grain Size Analysis

EBA ENGINEERING CONSULTANTS LTD.

PARTICLE SIZE ANALYSIS REPORT

PROJECT:	JC Thesis
SITE:	SC 39B
	Steele Creek Valley
PROJECT NO:	JC Thesis
CLIENT:	University of Ottawa
SAMPLE NO:	L2
DATE TESTED:	Aug 01/06 BY: PO
USC CLASSIFICATION:	CL
NATURAL MOISTURE CONTENT:	6.1%
REMARKS:	Sample obtained from test pit.

%Gravel = 39 %Sand = 52 %Silt = 5 %Clay = 4

LL = 40 PL = 20.1 PI = 19.9

PARTICLE SIZE	PERCENT PASSING
50	100
25	91
19	86
12.5	78
9.5	72
4.75	61
2.0	49
0.850	41
0.425	32
0.250	25
0.150	17
0.075	9

CLAY	SILT	SAND			GRAVEL	
		FINE	MEDIUM	COARSE	FINE	COARSE

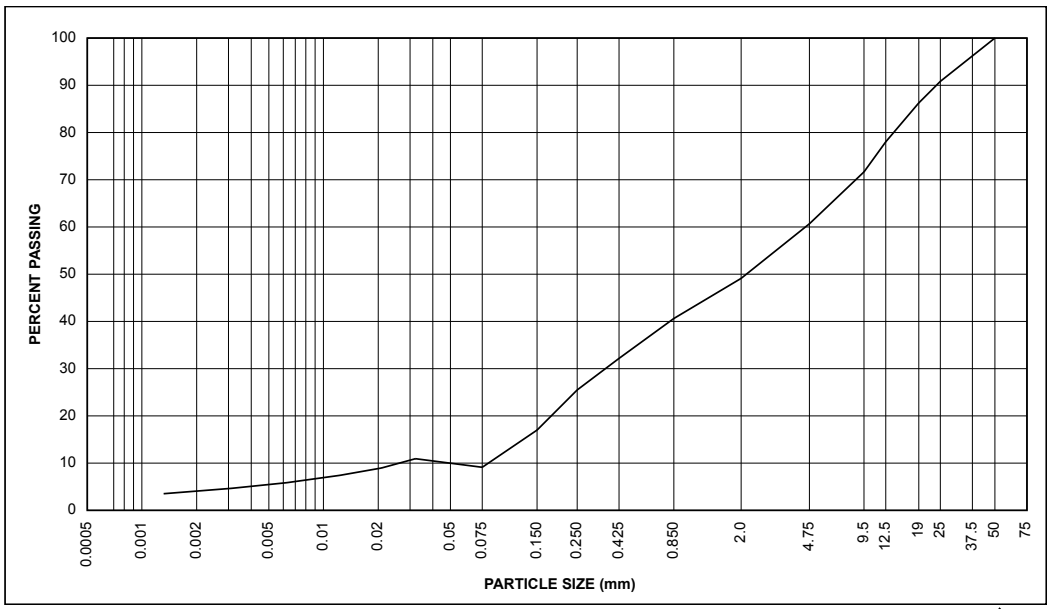

EBA ENGINEERING CONSULTANTS LTD.

PARTICLE SIZE ANALYSIS REPORT

PROJECT:	**JC Thesis**
SITE:	**SC 03AB**
	Steele Creek Valley
PROJECT NO:	**JC Thesis**
CLIENT:	**University of Ottawa**
SAMPLE NO:	**LA 3**
DATE TESTED:	**Apr 13/05** **BY: PO**
USC CLASSIFICATION:	**CL**
NATURAL MOISTURE CONTENT:	**5.0%**
REMARKS:	**Sample obtained from test pit.**

%Gravel = 28 %Sand = 68 %Silt = 2 %Clay = 2

LL = 40 PL = 20.1 PI = 19.9

PARTICLE SIZE	PERCENT PASSING
50	100
25	100
19	94
12.5	90
9.5	86
4.75	72
2.0	49
0.850	33
0.425	23
0.250	17
0.150	11
0.075	4

CLAY	SILT	SAND			GRAVEL	
		FINE	MEDIUM	COARSE	FINE	COARSE

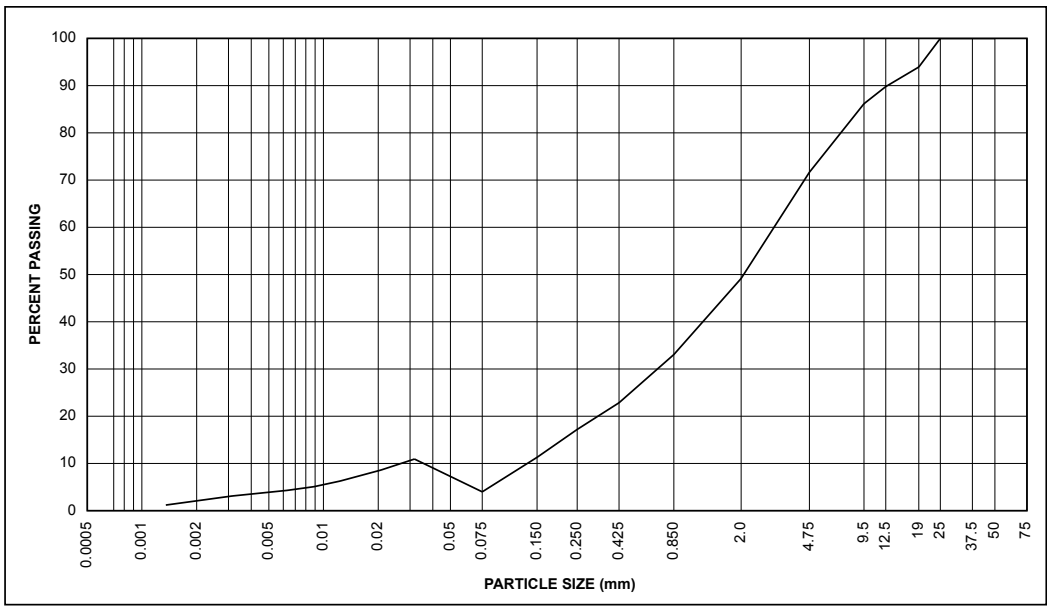

EBA ENGINEERING CONSULTANTS LTD.

PARTICLE SIZE ANALYSIS REPORT

PROJECT: JC Thesis
SITE: SC 03AB
Steele Creek Valley
PROJECT NO: JC Thesis
CLIENT: University of Ottawa
SAMPLE NO: LA4
DATE TESTED: Apr 13/05 **BY:** PO
USC CLASSIFICATION: CL
NATURAL MOISTURE CONTENT: 3.3%
REMARKS: Sample obtained from test pit.
%Gravel = 37 %Sand = 129 %Silt/Clay = -66
LL = 40 PL = 20.1 PI = 19.9

PARTICLE SIZE	PERCENT PASSING
50	100
25	80
19	74
12.5	71
9.5	70
4.75	63
2.0	-18
0.850	-39
0.425	-51
0.250	-56
0.150	-61
0.075	-66

CLAY	SILT	SAND			GRAVEL	
		FINE	MEDIUM	COARSE	FINE	COARSE

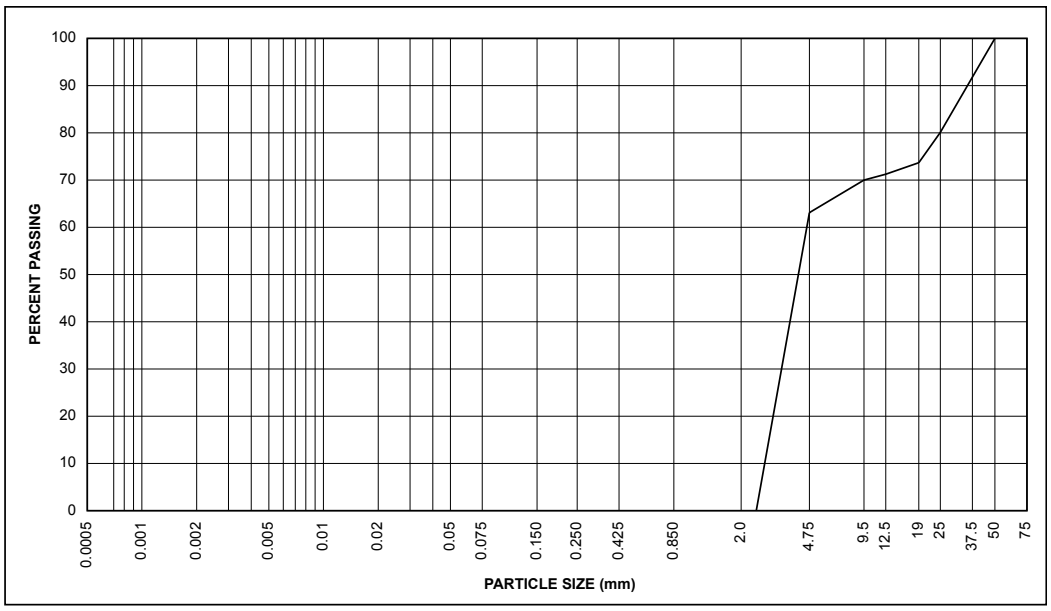

EBA ENGINEERING CONSULTANTS LTD.

PARTICLE SIZE ANALYSIS REPORT

PROJECT:	JC Thesis
SITE:	Steele Creek Valley
	SC 13A
PROJECT NO:	JC Thesis
CLIENT:	University of Ottawa
SAMPLE NO:	L0
DATE TESTED:	Apr 13/05 **BY:** PO
USC CLASSIFICATION:	CL
NATURAL MOISTURE CONTENT:	9.2%
REMARKS:	Sample obtained from test pit.
%Gravel = 31	%Sand = 51 %Silt/Clay = 18
LL = 40	PL = 20.1 PI = 19.9

PARTICLE SIZE	PERCENT PASSING
50	100
25	75
19	75
12.5	73
9.5	73
4.75	69
2.0	56
0.850	49
0.425	40
0.250	33
0.150	25
0.075	18

CLAY	SILT	SAND			GRAVEL	
		FINE	MEDIUM	COARSE	FINE	COARSE

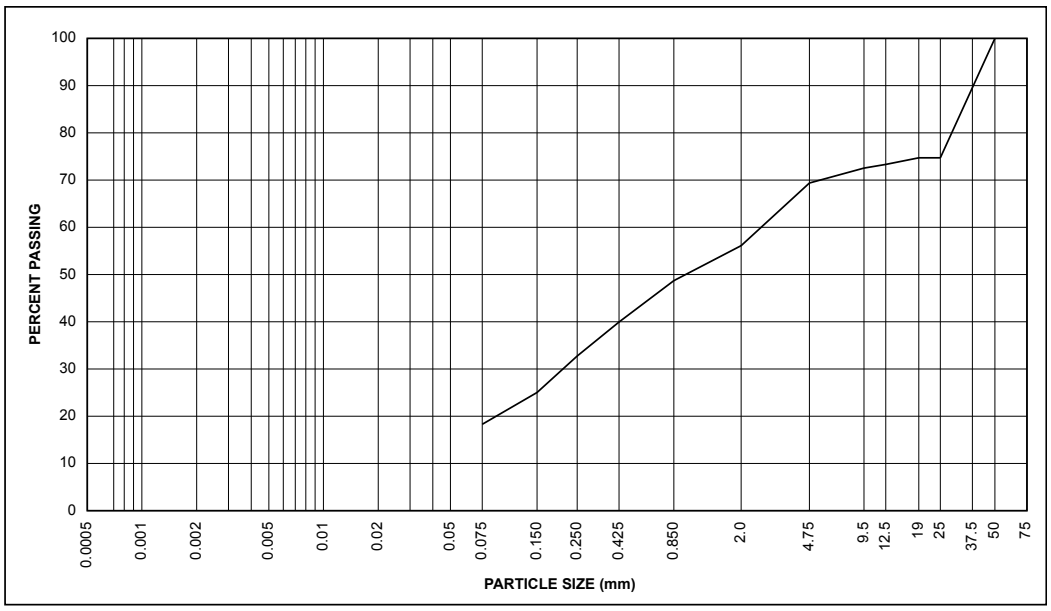

EBA ENGINEERING CONSULTANTS LTD.

PARTICLE SIZE ANALYSIS REPORT

PROJECT: JC Thesis
SITE: SC 13A
Steele Creek Valley
PROJECT NO: JC Thesis
CLIENT: University of Ottawa
SAMPLE NO: Y2
DATE TESTED: Apr 13/05 **BY:** PO
USC CLASSIFICATION: CL
NATURAL MOISTURE CONTENT: 4.1%
REMARKS: Sample obtained from test pit.
%Gravel = 42 %Sand = 37 %Silt = 17 %Clay = 4
LL = 40 PL = 20.1 PI = 19.9

PARTICLE SIZE	PERCENT PASSING
50	100
25	78
19	74
12.5	67
9.5	65
4.75	58
2.0	49
0.850	41
0.425	36
0.250	31
0.150	26
0.075	21

CLAY	SILT	SAND			GRAVEL	
		FINE	MEDIUM	COARSE	FINE	COARSE

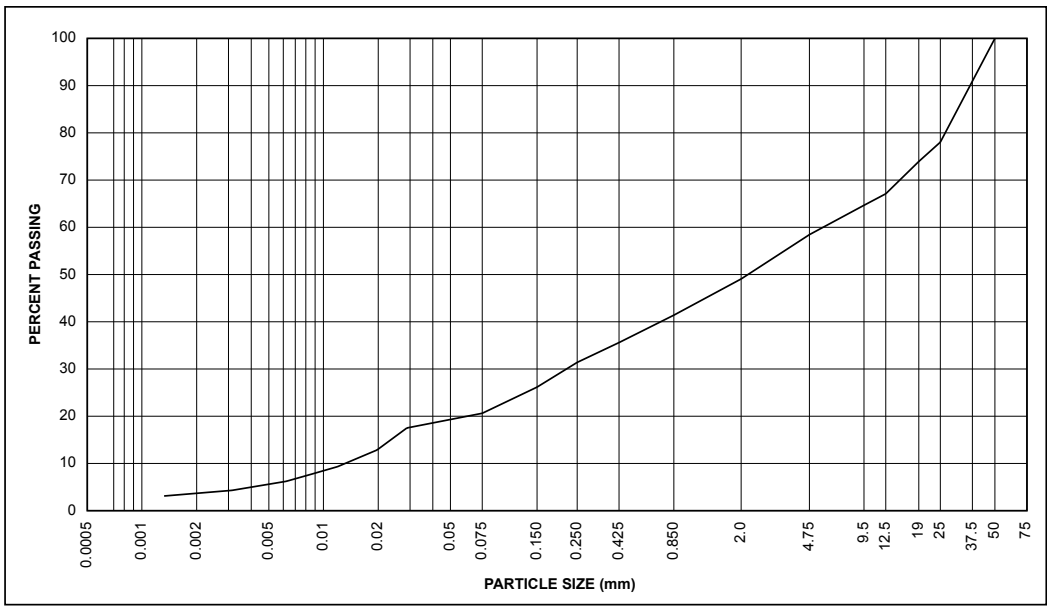

EBA ENGINEERING CONSULTANTS LTD.

PARTICLE SIZE ANALYSIS REPORT

PROJECT: JC Thesis
SITE: SC 13A
Steele Creek Valley
PROJECT NO: JC Thesis
CLIENT: University of Ottawa
SAMPLE NO: Y3
DATE TESTED: Apr 13/05 **BY:** PO
USC CLASSIFICATION: CL
NATURAL MOISTURE CONTENT: 4.4%
REMARKS: Sample obtained from test pit.
%Gravel = 24 %Sand = 57 %Silt = 15 %Clay = 4
LL = 40 PL = 20.1 PI = 19.9

PARTICLE SIZE	PERCENT PASSING
50	100
25	100
19	98
12.5	92
9.5	89
4.75	76
2.0	62
0.850	52
0.425	43
0.250	36
0.150	28
0.075	19

CLAY	SILT	SAND			GRAVEL	
		FINE	MEDIUM	COARSE	FINE	COARSE

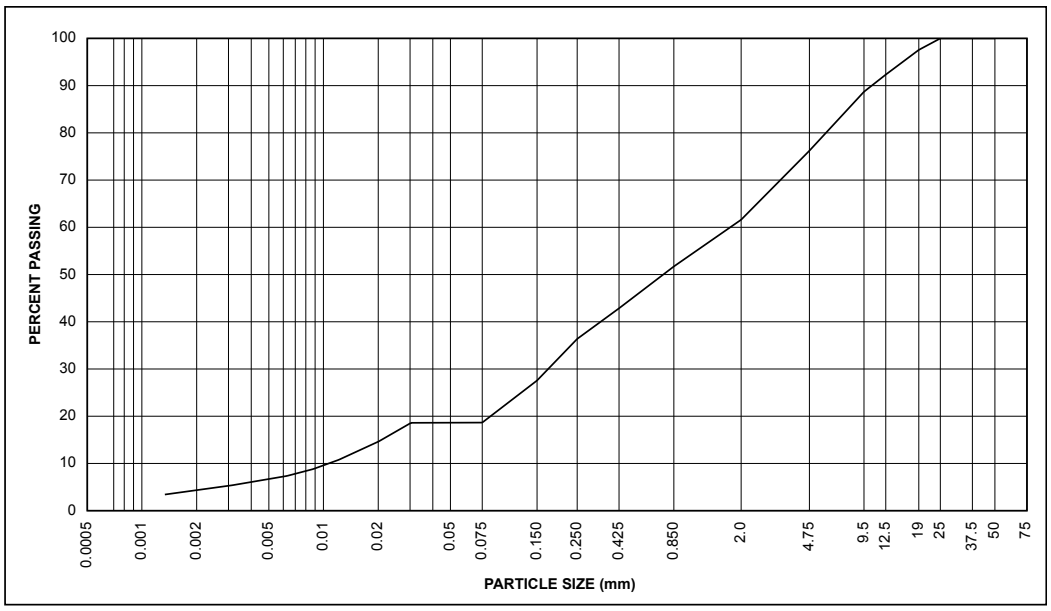

EBA ENGINEERING CONSULTANTS LTD.

PARTICLE SIZE ANALYSIS REPORT

PROJECT: JC Thesis
SITE: SC 13A
Steele Creek Valley
PROJECT NO: JC Thesis
CLIENT: University of Ottawa
SAMPLE NO: Y 4
DATE TESTED: Apr 13/05 **BY:** PO
USC CLASSIFICATION: CL
NATURAL MOISTURE CONTENT: 3.0%
REMARKS: Sample obtained from test pit.
%Gravel = 34 %Sand = 54 %Silt = 11 %Clay = 2
LL = 40 PL = 20.1 PI = 19.9

PARTICLE SIZE	PERCENT PASSING
50	100
25	100
19	88
12.5	82
9.5	76
4.75	66
2.0	53
0.850	41
0.425	32
0.250	26
0.150	19
0.075	12

CLAY	SILT	SAND			GRAVEL	
		FINE	MEDIUM	COARSE	FINE	COARSE

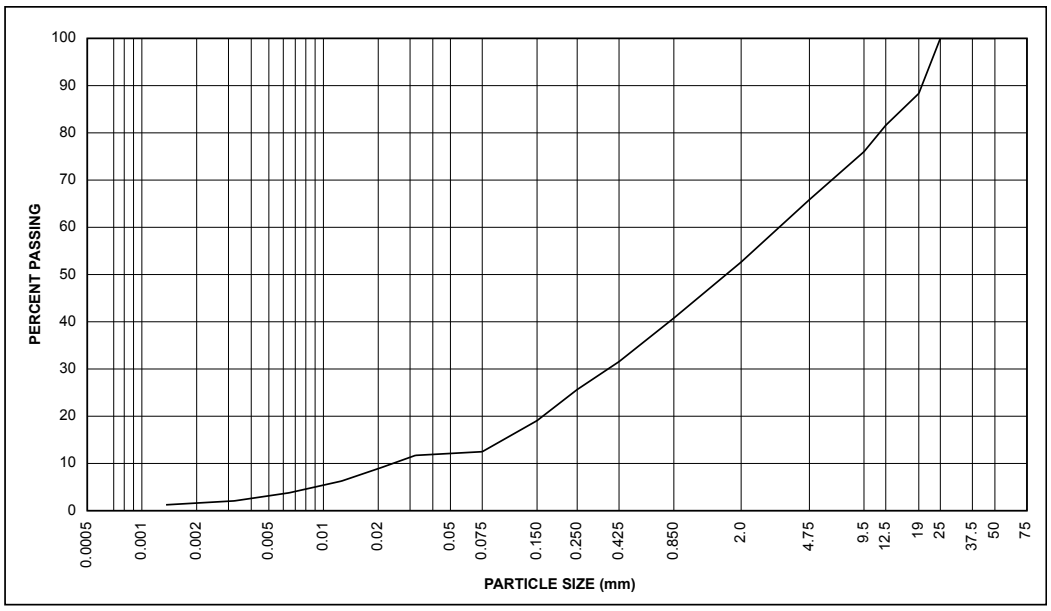

EBA ENGINEERING CONSULTANTS LTD.

PARTICLE SIZE ANALYSIS REPORT

PROJECT: JC Thesis
SITE: SC 13A
Steele Creek Valley
PROJECT NO: JC Thesis
CLIENT: University of Ottawa
SAMPLE NO: Y 5
DATE TESTED: Apr 13/05 **BY:** PO
USC CLASSIFICATION: CL
NATURAL MOISTURE CONTENT: 1.8%
REMARKS: Sample obtained from test pit.
%Gravel = 65 %Sand = 32 %Silt = 2 %Clay = 1
LL = 40 PL = 20.1 PI = 19.9

PARTICLE SIZE	PERCENT PASSING
50	100
25	58
19	55
12.5	49
9.5	44
4.75	35
2.0	25
0.850	19
0.425	13
0.250	10
0.150	7
0.075	3

CLAY	SILT	SAND			GRAVEL	
		FINE	MEDIUM	COARSE	FINE	COARSE

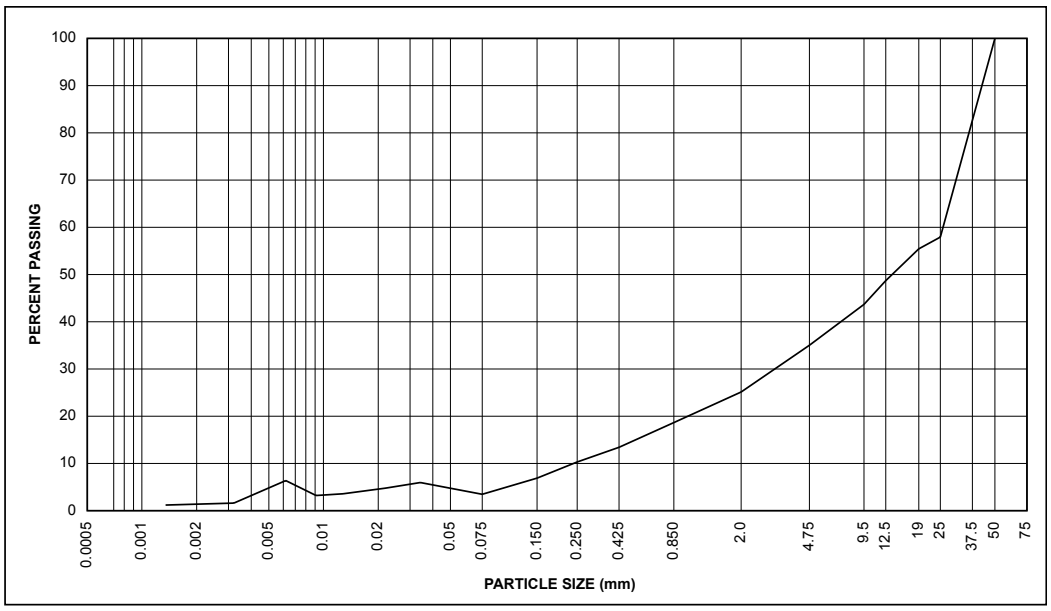

EBA ENGINEERING CONSULTANTS LTD.

PARTICLE SIZE ANALYSIS REPORT

PROJECT: JC Thesis
SITE: SC 13A
Steele Creek Valley
PROJECT NO: JC Thesis
CLIENT: University of Ottawa
SAMPLE NO: Y 6
DATE TESTED: Apr 13/05 **BY:** PO
USC CLASSIFICATION: CL
NATURAL MOISTURE CONTENT: 3.2%
REMARKS: Sample obtained from test pit.
%Gravel = 28 %Sand = 50 %Silt/Clay = 22
LL = 40 PL = 20.1 PI = 19.9

PARTICLE SIZE	PERCENT PASSING
50	100
25	100
19	96
12.5	88
9.5	83
4.75	72
2.0	25
0.850	25
0.425	24
0.250	23
0.150	23
0.075	22

CLAY	SILT	SAND			GRAVEL	
		FINE	MEDIUM	COARSE	FINE	COARSE

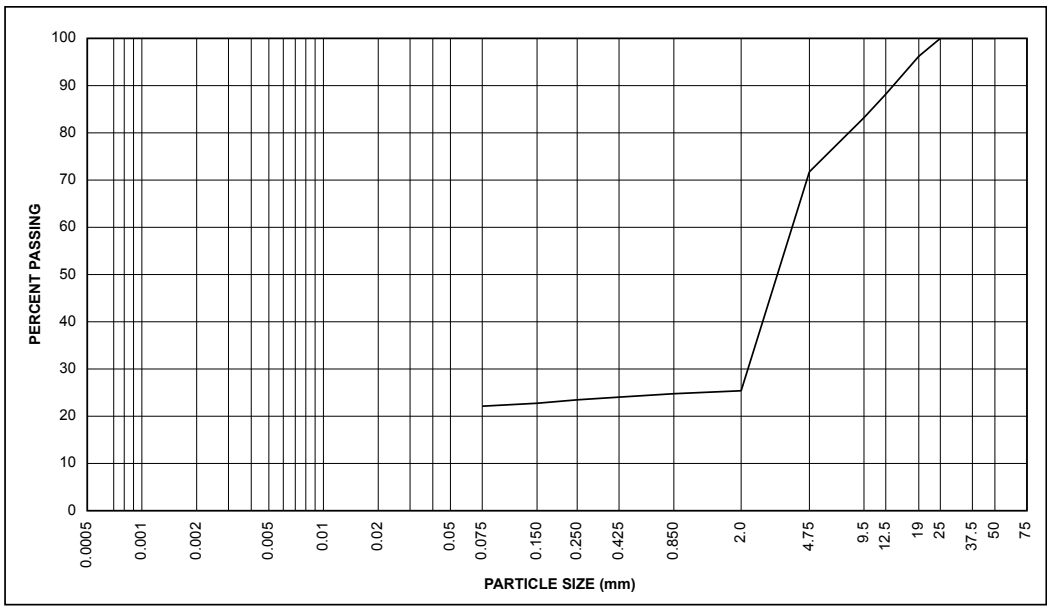

EBA ENGINEERING CONSULTANTS LTD.

PARTICLE SIZE ANALYSIS REPORT

PROJECT:	**JC Thesis**
SITE:	**SC 13A**
	Steele Creek Valley
PROJECT NO:	**JC Thesis**
CLIENT:	**University of Ottawa**
SAMPLE NO:	**Y 7**
DATE TESTED:	**Apr 13/05** **BY:** **PO**
USC CLASSIFICATION:	**CL**
NATURAL MOISTURE CONTENT:	**1.8%**
REMARKS:	**Sample obtained from test pit.**
%Gravel = 51	**%Sand = 65** **%Silt/Clay = -16**
LL = 40	**PL = 20.1** **PI = 19.9**

PARTICLE SIZE	PERCENT PASSING
50	100
25	81
19	77
12.5	66
9.5	61
4.75	49
2.0	8
0.850	2
0.425	-3
0.250	-7
0.150	-11
0.075	-16

CLAY	SILT	SAND			GRAVEL	
		FINE	MEDIUM	COARSE	FINE	COARSE

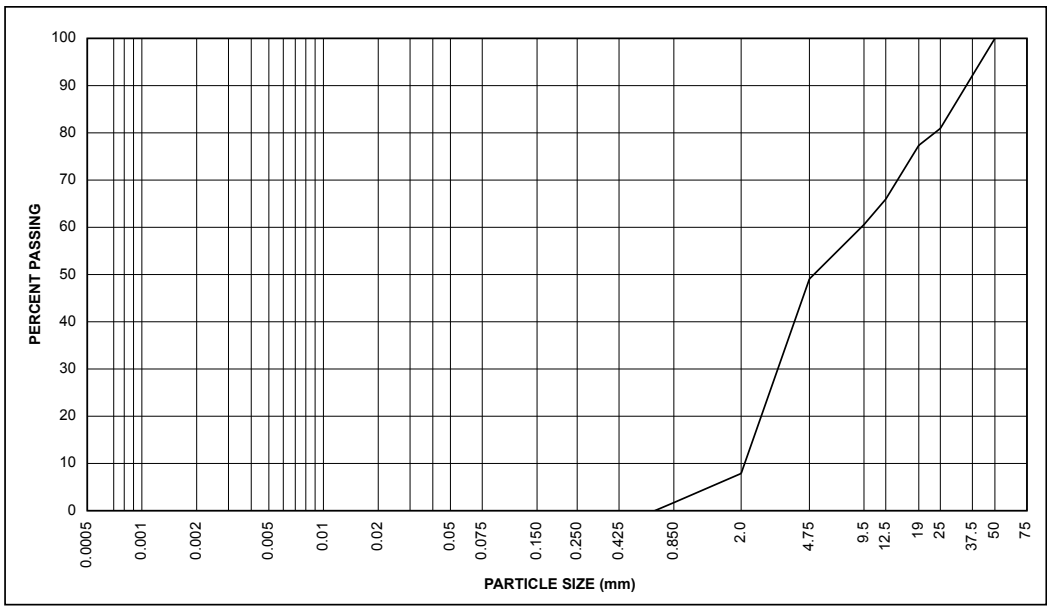

EBA ENGINEERING CONSULTANTS LTD.

PARTICLE SIZE ANALYSIS REPORT

PROJECT: JC Thesis
SITE: SC 33B
Steele Creek Valley
PROJECT NO: JC Thesis
CLIENT: University of Ottawa
SAMPLE NO: L1
DATE TESTED: Apr 13/05 **BY:** PO
USC CLASSIFICATION: CL
NATURAL MOISTURE CONTENT: 5.4%
REMARKS: Sample obtained from test pit.
%Gravel = 48 %Sand = 48 %Silt = 1 %Clay = 3
LL = 40 PL = 20.1 PI = 19.9

PARTICLE SIZE	PERCENT PASSING
50	100
25	80
19	77
12.5	65
9.5	61
4.75	52
2.0	42
0.850	32
0.425	24
0.250	19
0.150	12
0.075	4

CLAY	SILT	SAND			GRAVEL	
		FINE	MEDIUM	COARSE	FINE	COARSE

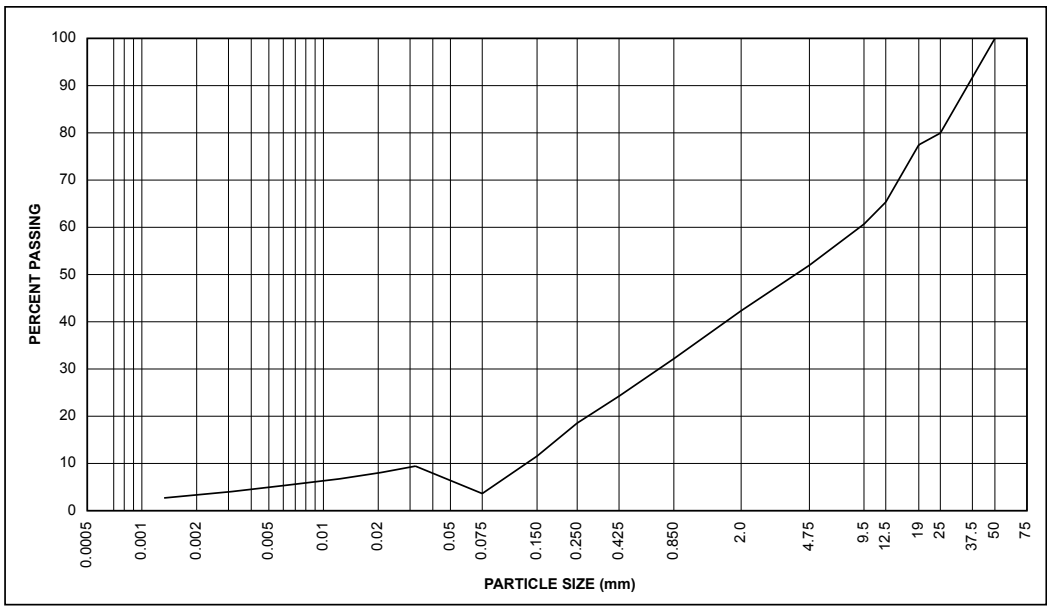

EBA ENGINEERING CONSULTANTS LTD.

PARTICLE SIZE ANALYSIS REPORT

PROJECT: JC Thesis
SITE: SC 33B
Steele Creek Valley
PROJECT NO: JC Thesis
CLIENT: University of Ottawa
SAMPLE NO: L 2
DATE TESTED: Apr 13/05 **BY:** PO
USC CLASSIFICATION: CL
NATURAL MOISTURE CONTENT: 4.7%
REMARKS: Sample obtained from test pit.
%Gravel = 43 %Sand = 37 %Silt = 17 %Clay = 3
LL = 40 PL = 20.1 PI = 19.9

PARTICLE SIZE	PERCENT PASSING
50	100
25	95
19	81
12.5	77
9.5	69
4.75	57
2.0	46
0.850	39
0.425	34
0.250	31
0.150	26
0.075	20

CLAY	SILT	SAND			GRAVEL	
		FINE	MEDIUM	COARSE	FINE	COARSE

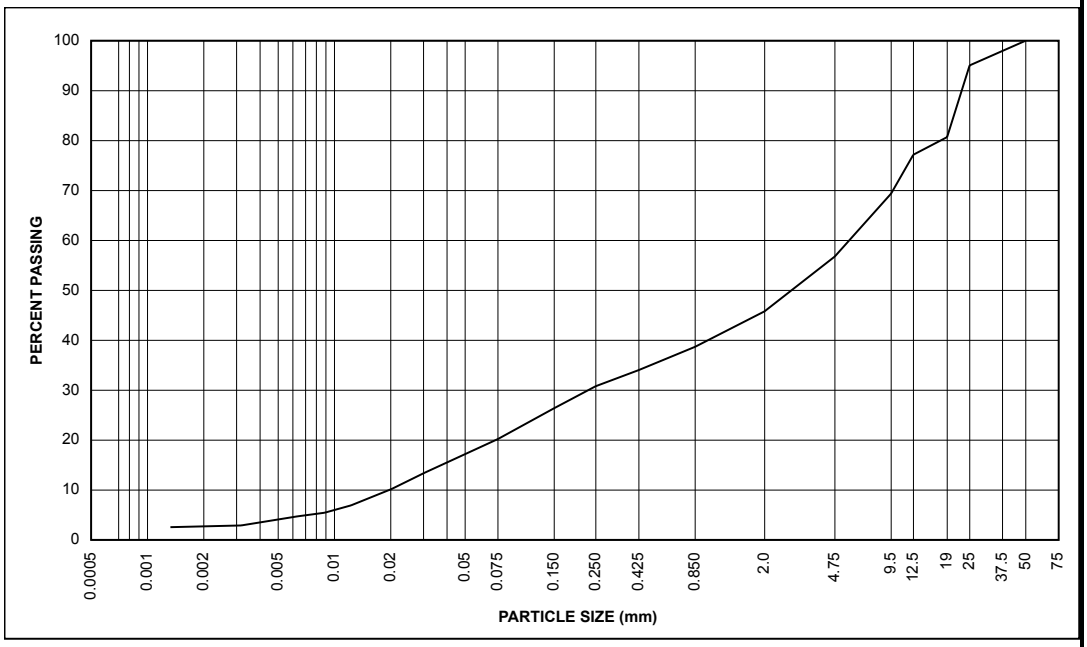

EBA ENGINEERING CONSULTANTS LTD.

PARTICLE SIZE ANALYSIS REPORT

PROJECT: JC Thesis
SITE: Steele Creek Valley
SC 33B
PROJECT NO: JC Thesis
CLIENT: University of Ottawa
SAMPLE NO: L 3
DATE TESTED: Apr 13/05 **BY:** PO
USC CLASSIFICATION: CL
NATURAL MOISTURE CONTENT: 4.3%
REMARKS: Sample obtained from test pit.
%Gravel = 35 %Sand = 68 %Silt/Clay = -3
LL = 40 PL = 20.1 PI = 19.9

PARTICLE SIZE	PERCENT PASSING
50	100
25	92
19	85
12.5	80
9.5	75
4.75	65
2.0	42
0.850	30
0.425	22
0.250	16
0.150	8
0.075	-3

CLAY	SILT	SAND			GRAVEL	
		FINE	MEDIUM	COARSE	FINE	COARSE

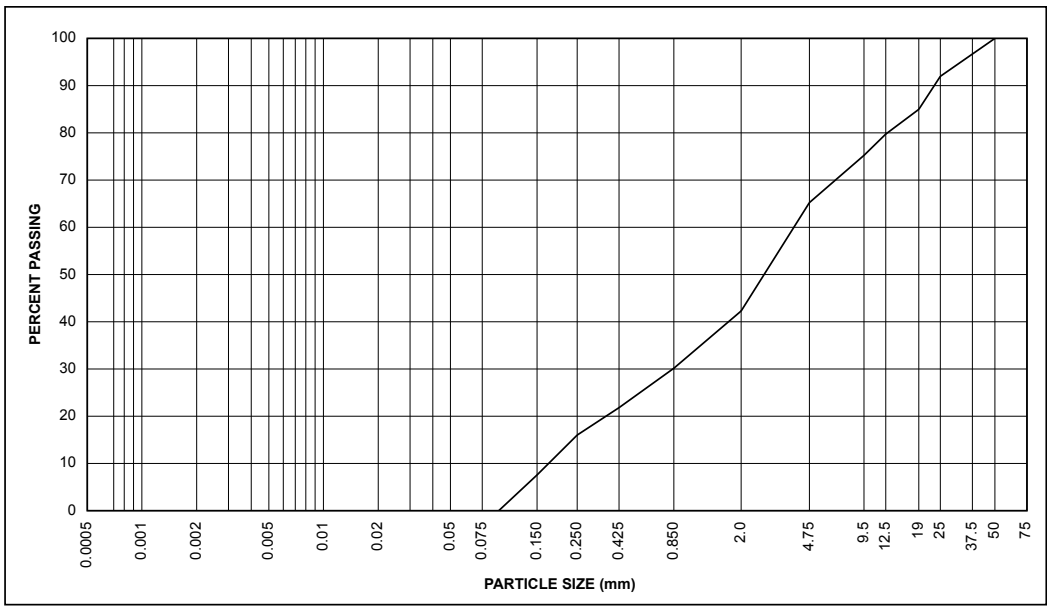

EBA ENGINEERING CONSULTANTS LTD.

PARTICLE SIZE ANALYSIS REPORT

PROJECT: JC Thesis
SITE: SC 33B
Steele Creek Valley
PROJECT NO: JC Thesis
CLIENT: University of Ottawa
SAMPLE NO: L 2
DATE TESTED: Apr 13/05 **BY:** PO
USC CLASSIFICATION: CL
NATURAL MOISTURE CONTENT: 4.7%
REMARKS: Sample obtained from test pit.
%Gravel = 43 %Sand = 37 %Silt = 17 %Clay = 3
LL = 40 PL = 20.1 PI = 19.9

PARTICLE SIZE	PERCENT PASSING
50	100
25	95
19	81
12.5	77
9.5	69
4.75	57
2.0	46
0.850	39
0.425	34
0.250	31
0.150	26
0.075	20

CLAY	SILT	SAND			GRAVEL	
		FINE	MEDIUM	COARSE	FINE	COARSE

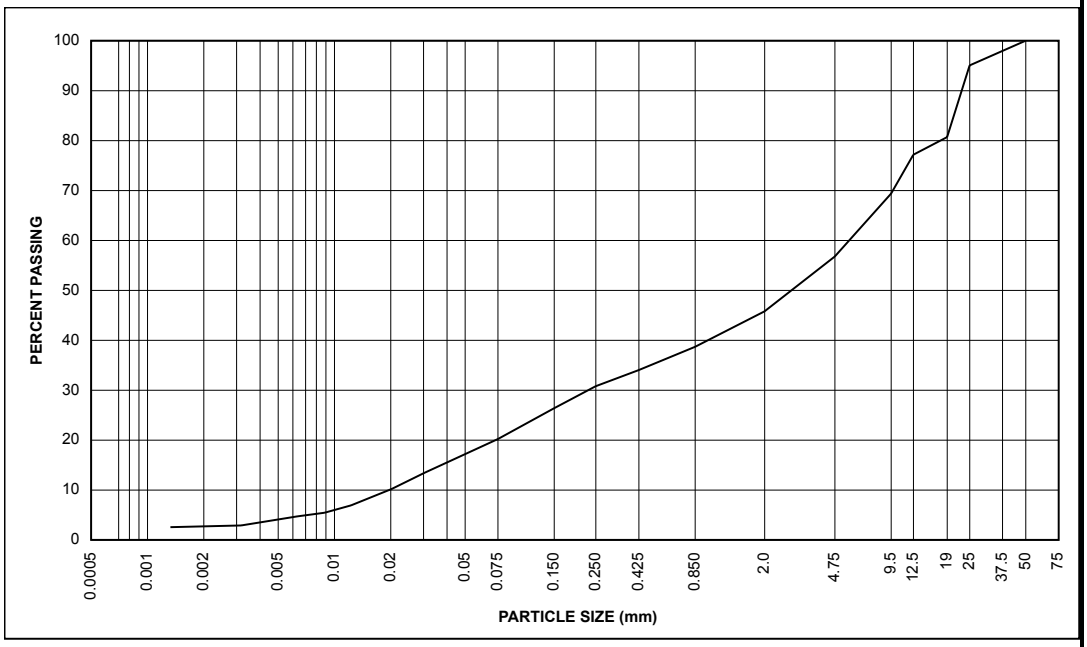

EBA ENGINEERING CONSULTANTS LTD.

PARTICLE SIZE ANALYSIS REPORT

PROJECT: JC Thesis
SITE: SC 39B
Steele Creek Valley
PROJECT NO: JC Thesis
CLIENT: University of Ottawa
SAMPLE NO: L2
DATE TESTED: Aug 01/06 **BY:** PO
USC CLASSIFICATION: CL
NATURAL MOISTURE CONTENT: 6.1%
REMARKS: Sample obtained from test pit.
%Gravel = 39 %Sand = 52 %Silt = 5 %Clay = 4
LL = 40 PL = 20.1 PI = 19.9

PARTICLE SIZE	PERCENT PASSING
50	100
25	91
19	86
12.5	78
9.5	72
4.75	61
2.0	49
0.850	41
0.425	32
0.250	25
0.150	17
0.075	9

CLAY	SILT	SAND			GRAVEL	
		FINE	MEDIUM	COARSE	FINE	COARSE

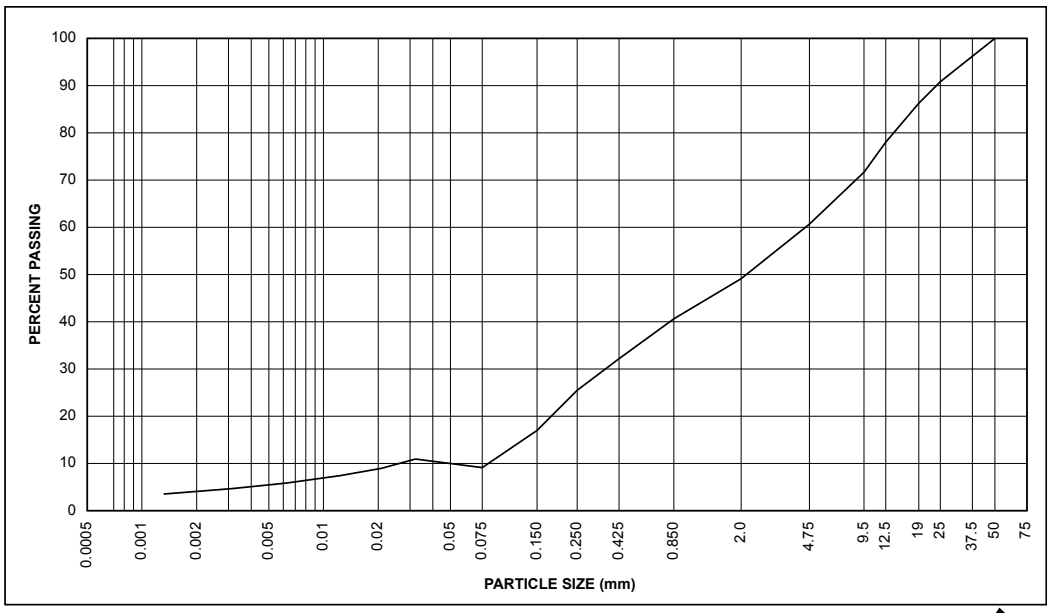

EBA ENGINEERING CONSULTANTS LTD.

PARTICLE SIZE ANALYSIS REPORT

PROJECT: JC Thesis
SITE: SC 40B
Steele Creek Valley
PROJECT NO: JC Thesis
CLIENT: University of Ottawa
SAMPLE NO: T 01
DATE TESTED: Apr 13/05 **BY:** PO
USC CLASSIFICATION: CL
NATURAL MOISTURE CONTENT: 3.3%
REMARKS: Sample obtained from test pit.
%Gravel = 0 %Sand = 7 %Silt = 87 %Clay = 6
LL = 40 PL = 20.1 PI = 19.9

PARTICLE SIZE	PERCENT PASSING
50	100
2.0	100
0.850	100
0.425	100
0.250	99
0.150	98
0.075	93

CLAY	SILT	SAND			GRAVEL	
		FINE	MEDIUM	COARSE	FINE	COARSE